NASA CR-54155
AVCO RAD SR 64-290

First Quarterly Progress Report

RESISTOJET RESEARCH AND DEVELOPMENT - PHASE II

by

Richard R. John and Stewart Bennett

perpared for

NATIONAL AERONAUTICS AND SPACE ADMINISTRATION

November 25, 1964

CONTRACT NAS 3-5908

Technical Management
NASA Lewis Research Center
Cleveland, Ohio
Electric Propulsion Office
Henry Hunczak

RESEARCH AND ADVANCED DEVELOPMENT DIVISION
AVCO CORPORATION
Wilmington, Massachusetts

NASA CR-54155
AVCO RAD SR 64-290

First Quarterly Progress Report

RESISTOJET RESEARCH AND DEVELOPMENT - PHASE II

by

Richard R. John and Stewart Bennett

perpared for

NATIONAL AERONAUTICS AND SPACE ADMINISTRATION

November 25, 1964

CONTRACT NAS 3-5908

Technical Management
NASA Lewis Research Center
Cleveland, Ohio
Electric Propulsion Office
Henry Hunczak

RESEARCH AND ADVANCED DEVELOPMENT DIVISION
AVCO CORPORATION
Wilmington, Massachusetts

NOTICE

This report was prepared as an account of Government sponsored work. Neither the United States, nor the National Aeronautics and Space Administration (NASA), nor any person acting on behalf of NASA:

A.) Makes any warranty or representation, expressed or implied, with respect to the accuracy, completeness, or usefulness of the information contained in this report, or that the use of any information, apparatus, method, or process disclosed in this report may not infringe privately owned rights; or

B.) Assumes any liabilities with respect to the use of, or for damages resulting from the use of any information, apparatus, method or process disclosed in this report.

As used above, "person acting on behalf of NASA" includes any employee or contractor of NASA, or employee of such contractor, to the extent that such employee or contractor of NASA, or employee of such contractor prepares, disseminates, or provides access to, any information pursuant to his employment or contract with NASA, or his employment with such contractor.

Requests for copies of this report should be referred to

National Aeronautics and Space Administration
Office of Scientific and Technical Information
Attention: AFSS-A
Washington, D.C. 20546

ABSTRACT

Experimental results are presented on a fast-heatup low-power (5 to 20 watts) resistojet suitable for the attitude control and station keeping of a 500-pound synchronous satellite. Propulsion performance measurements obtained with a stainless steel heater tube indicate thrust levels of the order of 0.70×10^{-3} pounds at 200 seconds specific impulse with an electrical input power of 12 watts and an ammonia flow rate of 3.2×10^{-6} lb/sec. It is anticipated that operation with a tungsten tube heater element with ammonia as a working fluid will lead to specific impulses close to 300 seconds at the 0.10 to 1×10^{3} - pound thrust level, and at energy conversion efficiencies of about 20 percent. A preliminary weight analysis on an ammonia resistojet (specific impuse $\sim$ 270 seconds) attitude and orbit control system for a 3-year mission of a 500-pound satellite indicates a total system weight of 85 pounds compared to nearly 200 pounds for a low thrust (specific impulse $\sim$ 75 seconds) chemical system.

CONTENTS

CONTENTS (Concl'd)

ILLUSTRATIONS

ILLUSTRATIONS (Cont'd)

ILLUSTRATIONS (Concl'd)

TABLES

SUMMARY

The overall objective of this program is to carry out research and development on both pulsed and continuous resistojet thrustors for operation from 5 to 5000 watts. Work is presently being concentrated on the development of 5- to 50-watt thrustors suitable for the attitude and orbit control of sattellites in the 500- to 1000-pound class. Preliminary system studies have indicated that thrustors for this application should have characteristic thrust levels from 0.10 to 1 x 10^{-3} pounds and characteristic impulse bits from 10^{-4} to 10^{-3} lb-sec.

There are two basic concepts for the low-power resistojet thrustor. These are thermal storage and fast heatup. In the thermal storage resistojet, thrustor power is continuously supplied to the heater element and only the propellant flow is pulsed. The heat capacity of the thermal storage unit is sufficiently great that the temperature of the heater element remains essentially constant during short propellant pulses. In the fast-heatup resistojet thrustor both the power and the propellant flow are pulsed. In contrast to the thermal storage device, the heat capacity of the fast-heatup device is held to a minimum. The advantages of the thermal storage device include no thermal cycling, minimum time delay between input signal and resulting impulse bit, and constant power input, which reduces system complexity; the main disadvantage of the thermal storage unit is the high average power consumption, and the resulting large system weight. The primary advantage of the fast-heatup unit is low average power consumption; disadvantages include the necessity for frequent thermal cycling and the existence of a delay time between the input signal and the time that the thrustor is at operating temperature.

Experiments have been carried out with both thermal storage and fast-heatup units operated at power levels between 10 and 50 watts. The prototype thermal storage unit consisted of a composite tungsten/zirconia heater element with axial gas flow passages. The heater was surrounded by radiation shields. The unit weighed approximately 10 grams, and at 2000°K, had a heat content of 6000 joules. The prototype, fast-heatup resistojet consisted of a thin-walled, high-temperature metal tube which had a 0.38 mm (15 mil) inside diameter, a 0.70 mm (28 mil) outside diameter, and was 2 cm long. The fast-heatup thrustor weighed approximately 50 x 10^{-3} grams and had a heat content of only about 30 joules at 1500°K. The minimum average power input to maintain the thermal storage unit at an operating temperature of 2000°K was established to be at least of the order of 10 watts. The average power level for the fast-heatup thrustor operated at a 5-percent duty cycle, which is typical of the 500-pound satellite application, was an order of magnitude lower. Based on these results the experimental effort is currently directed to the design and development of the fast-heatup device.

A critical problem in the development of any propulsion system is accurate thrust measurements. A simple thrust stand has been developed, capable of measuring thrusts down to 10^{-4} pounds, and at a frequency response of approximately 100 cps. The thrust stand consists of a horizontal plate supported by four horizontal wires in tension. The thrust axis of the engine is vertical. The vertical displacement of the platform, resulting from the applied engine thrust, is measured by a linear differential transformer, which has an ultimate sensitivity of 0.3×10^{-6} inch.

Typical thrustor performance for the fast-heatup resistojet using a stainless steel heater element and ammonia is characterized by thrust levels from 10^{-4} to 10^{-3} pounds, specific impulses up to 225 seconds, and power inputs from 5 to 20 watts. The overall electric-to-thrust power efficiency is about 20 percent. It is anticipated that operation with a tungsten heater element which would allow operating temperatures of 2000°K will result in specific impulses up to 300 seconds.

A single-axis resistojet attitude control system package is being designed and constructed for evaluation on the air bearing at the NASA Lewis Electric Propulsion Test Facility. The attitude control package will include the resistojet thrustors, ammonia tankage, control and power conditioning system, and sensors for the determination of the position of the position of the test vehicle.

Preliminary estimates, based on the thrustor performance results, have been made of the weight of a three-axis attitude control and station keeping system for a 500-pound satellite. The total system weight is about 85 pounds for a 3-year mission; the 85-pounds includes allowances for tankage, controls, structure, solar cells, valves, and thrustors. In is interesting to note that a state of the art chemical control system, which operates at a thrust level of 10^{-3} pound, would require 175 pounds of propellant alone for the same 3-year mission. Thus, although questions are still open on thrustor reliability, the low-power (5 to 50 watts) fast-heatup resistojet holds considerable promise for attitude and orbit control of satellites in the 500- to 1000-pound class.

I. INTRODUCTION

This is the first Quarterly Progress Report submitted under contract NAS 3-5908, entitled Resistojet Research and Development - Phase II: this report covers the period 6 July through 30 September, 1964.

A. PROGRAM OBJECTIVES

The objectives of this program are to pursue research and development of electrothermal thrustors of the resistance type in the power range from 5 watts to 5 kw. Both pulsed and continuous operation of the thrustors are to be explored. During this first quarter, attention has been focussed on the 10-to 50-watt input power level, with possible application to attitude control and station keeping of a 500-pound synchronous satellite. An objective of this portion of the program is to demonstrate control about a single axis using the air bearing facility at the NASA Lewis Research Center.

B. PROGRAM ORGANIZATION

This program originates from the Electric Propulsion Office of the NASA Lewis Research Center. Mr. Henry Hunczak is Project Manager for the NASA Lewis Research Center. The Project Director at Avco RAD is Dr. R. R. John. Other participants in this research and their areas of principle contribution are: Messrs. W. Huss and K. Clark and Drs. S. Bennett, A. Tuchman and H. Noeske, Thrustor and Test System Design and Development; Mr. C. Stewart, Thrustor Heat Transfer; Mr. J. T. Smith, Materials Development; Messrs. R. Coulombre, P. Bergstrom, and J. Vullo, System Design.

C. PROGRAM SCHEDULING

This is the first Quarterly Progress Report, and summarizes technical progress under contract NAS 3-5908. Data on contract costs and manpower have been previously submitted in Monthly Letter Reports 1 (10 August), 2 (10 September) and 3 (10 October).

II. RESISTOJET ENGINE DEVELOPMENT

A. REQUIRED ENGINE PROPULSION PERFORMANCE CHARACTERISTICS

1. Minimum Propellant Requirements

In the evaluation of electric or other propulsion devices for the attitude control and station keeping of satellites, the main criteria to be considered are system reliability and weight. Further, the relative weights and reliability of the different systems can be compared only within the constraints established by a particular mission. The operating principles of a thrustor can be generalized; however, the propulsion performance required of an attitude control and station keeping thrustor system must be associated with a particular mission.

The major portion of the overall program effort is currently being concentrated on the development of resistojets suitable for the attitude control and station keeping of a satellite with specifications similar to those shown in table I.

TABLE I

SATELLITE MISSION AND DESIGN REQUIREMENTS

Satellite type	Synchronous
Satellite size	
Configuration	Right circular cylinder
Weight	500 pounds
Roll moment of inertia	41.2 slug-ft^2
Pitch and yaw moment of inertia	32.7 slug-ft^2
Moment arm	2 feet
Attitude and station tolerances	
Attitude	±0.5 degree
Station	±0.1 degree
Attitude disturbance torques	
Disturbance torques	0 to 500 dyne-cm
Lifetime	1 to 3 years

The major vehicle attitude disturbance torque at the 24-hour altitude is due to solar radiation pressure[1]; other torques result from gravity gradient, interaction of onboard electromagnetic fields with external fields, etc. If the assumed 500 dyne-cm disturbance torque acts for 1 year (3.15×10^7 seconds) the minimum required correction angular impulse for a single axis is (500 dyne-cm) x (3.15×10^7 seconds) = 15.7×10^9 dyne-cm-sec/year/axis or 1170 lb-ft-sec/year/axis. Assuming a 2-foot moment arm for the attitude control thrustors, the minimum required impulse for attitude control is 585 lb-sec/year/axis.

The minimum possible value for the control thrust is given by (500 dyne-cm)/(2 feet) (30.4 cm/ft) = 8.24 dynes or (8.24 dynes) x 2.248×10^{-6} lb/dyne) = 0.0185×10^{-3} pounds. The reliable operation of a thrustor at this thrust level does not appear to be within the state of the art. The vehicle must thus be controlled by a series of impulse bits each of which has a greater amplitude than the 1.85×10^{-5} pounds required for minimal control of the 500-pound satellite.

The major perturbations on the vehicle orbit are due to Earth triaxiality and the sun/moon perturbation.[2] Correction for the sun/moon gravitational perturbations is 163 feet/sec/year, assuming an optimum thrust mode of two nodal firings per day [3]; the Earth's triaxiality requires[3] a correction of 7 feet/sec/year.* Thus, the minimum required velocity correction for station keeping is about 170 feet/sec/year. For nonoptimum applied thrust modes, this value might increase to 270 feet/sec/year.[2] The minimum impulse to maintain the 500-pound satellite on station for 1 year is ΔVM = (170 feet/sec) (500 lb/32.2 feet/sec^2) = 2640 lb-sec/year. This value of impulse required for station keeping is to be compared to the 1755 lb-sec/year required for 3-axis attitude control. The minimum impulse requirement for the 500-pound satellite is then 4395 lb-sec/year.

The fuel required to produce a given impulse $\int F dt$ is, of course, a function of the specific impulse and is given by $\int F dt / I_{sp}$. Values of the minimum amount of propellant required during a 3-year time period for the attitude control and station keeping of the design satellite are presented in table II and figure 1. The total effective impulse is 4395 lb-sec/year or 13,200 lb-sec for 3 years.

*See appendix A.

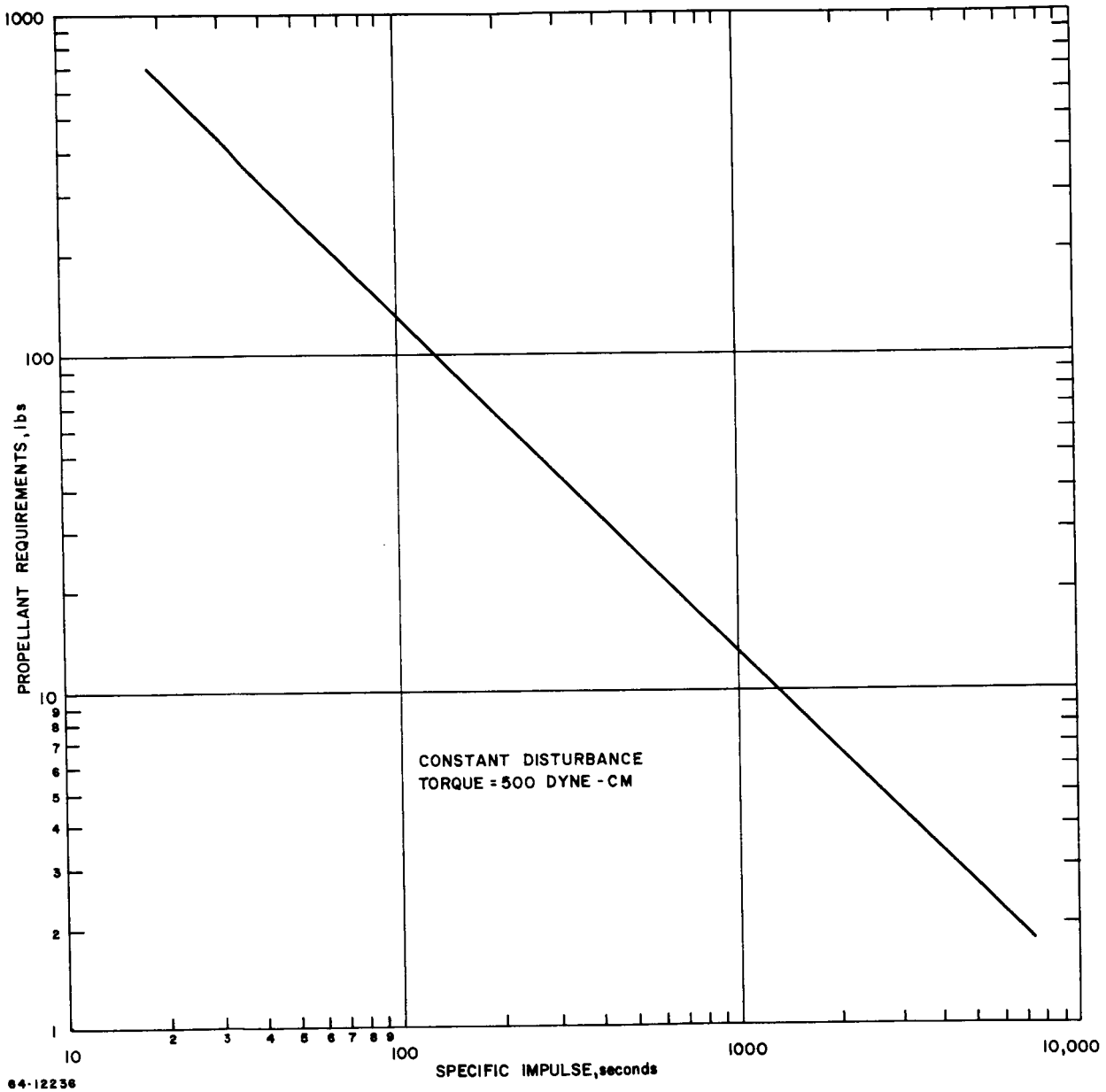

Figure 1 MINIMUM PROPELLANT REQUIREMENT FOR A 3-YEAR ATTITUDE AND ORBIT CONTROL OF A 500-POUND SATELLITE

TABLE II

SATELLITE PROPELLANT REQUIREMENTS-MINIMUM
(TOTAL REQUIRED IMPULSE, 13,200 SECONDS)

Specific Impulse I_{sp} (seconds)	Propellant Weight for Attitude Control $W_{prop\ AC}$ (pounds)	Propellant Weight for Station Keeping $W_{prop\ SK}$ (pounds)	Total Propellant Weight $W_{prop.,\ total}$ (pounds)
50	105	159	264
100	52.5	79.5	132
200	26.3	39.7	66
300	17.5	26.5	44
500	10.5	15.9	26.4
1000	5.3	7.9	13.2
5000	1.05	1.59	2.64
10000	0.53	0.79	1.32

It is to be stressed that the preceding propellant requirements are "ideal" values. The "actual" propellant requirements depend on the type of control logic, and the nature and frequency of the applied impulse bits. It is unlikely, however, that the actual propellant requirements will be more than a factor of 2 or 3 greater than the values shown in table II and figure 1. In the idealized case it is noted that the absolute weight saving in propellant obtained by increasing the specific impulse from 50 to 300 seconds is 220 pounds; this is a considerable fraction of the total 500-pound weight of the satellite. If the weight of the power supply and other equipment required to attain 300 seconds in the attitude control and station keeping thrustors is considerably less than 220 pounds there will, of course, be considerable motivation to use the 300-second system.

Thus far attention has been focused on idealized attitude control and station keeping systems. No mention has been made of the size, i.e., thrust and duration, and the frequency of the impulse bits required for actual satellite control. The following sections present a highly simplified discussion of satellite control logic with the purpose of establishing the width, amplitude, and frequency of the applied impulse bits required for satellite attitude and orbit control

2. Soft Versus Hard Cycle Operation

For a given disturbance torque on the satellite, τ_d, there are two basic control cycles for applying the control impulse bit, K_c; these are the soft

cycle and the hard cycle. In the soft cycle, the disturbance torque, τ_d, pushes the vehicle in one direction, and the control impulse bit, K_c, pushes it back the other way. The control impulse bits are scheduled such that all the control impulse goes into countering the disturbance impulse. All the propellant is used to counterbalance the disturbance torque. In the hard cycle, on the other hand, some of the delivered impulse counters impulse delivered at the other end of the cycle as well as the applied disturbance impulse. As a result, the propellant consumption in the hard cycle is greater than that for soft cycle operation at a given disturbance torque level. It is therefore advantageous to control the attitude of a satellite by means of soft as opposed to hard cycle operation.

In order that soft cycle operation be attained, it is sufficient that the control impulse bit be equal to or less than the impulse bit given by the equation[1]

$$FT_{thrust)_{max}} = K_{c)_{max}} = \frac{2}{l} [\theta^* I \tau_d]^{1/2} \qquad (1)$$

where, l is the thrustor moment arm, θ^* is the attitude angular accuracy, I is the vehicle inertia, and τ_d is the disturbance torque. Thus, the maximum impulse bit which can be used and still have soft cycle operation increases with increase in the attitude angular accuracy, with increase in vehicle inertia and increase in disturbance torque. Values of the maximum impulse bit which can be tolerated for soft cycle operation of the design satellite as a function of disturbance torque are presented in figure 2.

Refering to figure 2, assuming a maximum disturbance torque of 500 dyne-cm the control impulse bit must be less than about 5×10^{-3} lb-sec. On the other hand if the disturbance torque is only 5 dyne-cm, the control impulse bit must be reduced a factor of ten to 5×10^{-4} lb-sec in order to assure soft cycle operation.

From equation (1) it immediately follows that, for a given impulse bit and vehicle, the disturbance torque must be greater than a critical value in order to establish a soft limit cycle. The minimum value of the disturbance torque required to establish soft cycle is given by equation (2).

$$\tau_{d)_{min}} = \frac{K_c^2 \, l^2}{4} \, \frac{1}{\theta^* I} \qquad (2)$$

As might be expected, the larger the applied control impulse bit the larger the applied disturbance torque sufficient to bring about a soft limit cycle.

3. Soft and Hard Cycle Propellant Requirements

As indicated, in the soft limit cycle the input disturbance, τ_d, is exactly counterbalanced by the average torque introduced by the attitude control

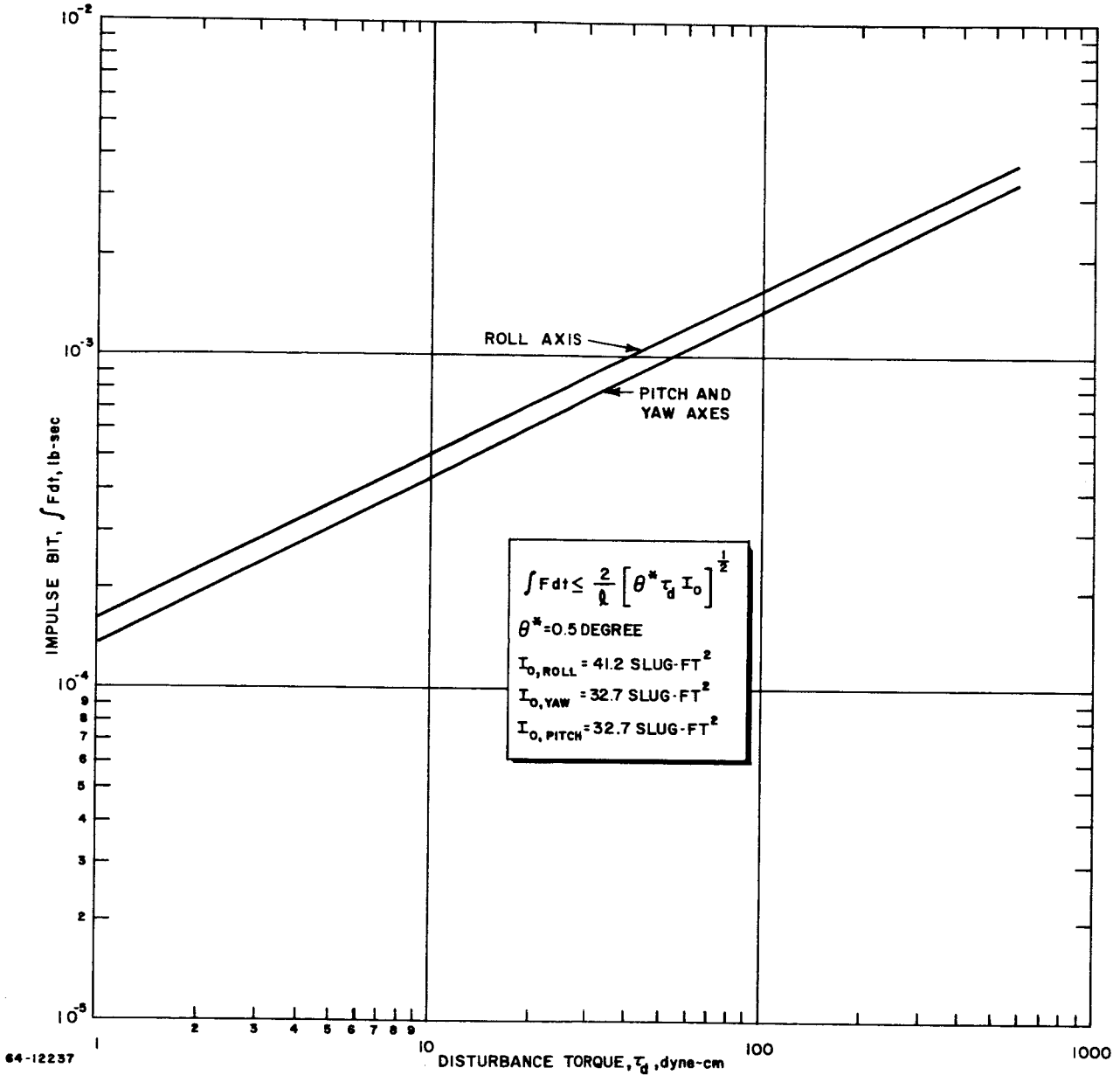

Figure 2 MAXIMUM IMPULSE BIT FOR A SOFT LIMIT CYCLE AS A FUNCTION OF DISTURBANCE TORQUE

thrustors. The basic equation for the total impulse required for soft limit cycle operation is given by

$$\int_{\text{mission}} \tau_d \, dt = \sum_{\substack{\text{all} \\ \text{pulses}}} l \int F \, dt = N l K_c \tag{3}$$

where, N, is the total number of impulse bits per mission and F is the amplitude of the thrust pulse. The propellant flow during an impulse bit is given by F/I_{sp} ; the total propellant used during an impulse bit is $\int F dt/I_{sp} = K_c/I_{sp}$. The propellant used during a mission is NK/I_{sp} . Therefore, the propellant weight is given by

$$W_{prop} = \frac{NK_c}{I_{sp}} = \frac{\int_{\text{mission}} \tau_d \, dt}{l I_{sp}} = \frac{\tau_d T_m}{l I_{sp}} \tag{4}$$

where, T_m, is the total mission time.

The number of cycles is immediately given by

$$N = \frac{\tau_d T_m}{l K_c} \tag{5}$$

Referring to equation (4), the required weight of propellant for soft cycle operation increases linearly with the disturbance torque and mission time and is inversely proportional to the specific impulse. Values of the fuel consumption per axis for a 3-year mission, as a function of disturbance torque and engine specific impulse, are shown in figure 3. It is noted that the propellant consumption for soft cycle operation is independent of the absolute magnitude, length, or amplitude of the impulse bit; propellant consumption is only a function of the total value of the disturbance impulse, $\tau_d T_m$, and not of the individual values of the disturbance torque or mission time. This is not the case, as will be discussed below, for hard limit cycle operation.

In the hard limit cycle, the time averaged applied control torque is much greater than the disturbance torque, τ_d. The limiting case, of course, occurs when the disturbing torque is zero; in this situation there will always be a hard limit cycle. For the case of zero disturbance it can be shown that the required propellant weight is given by

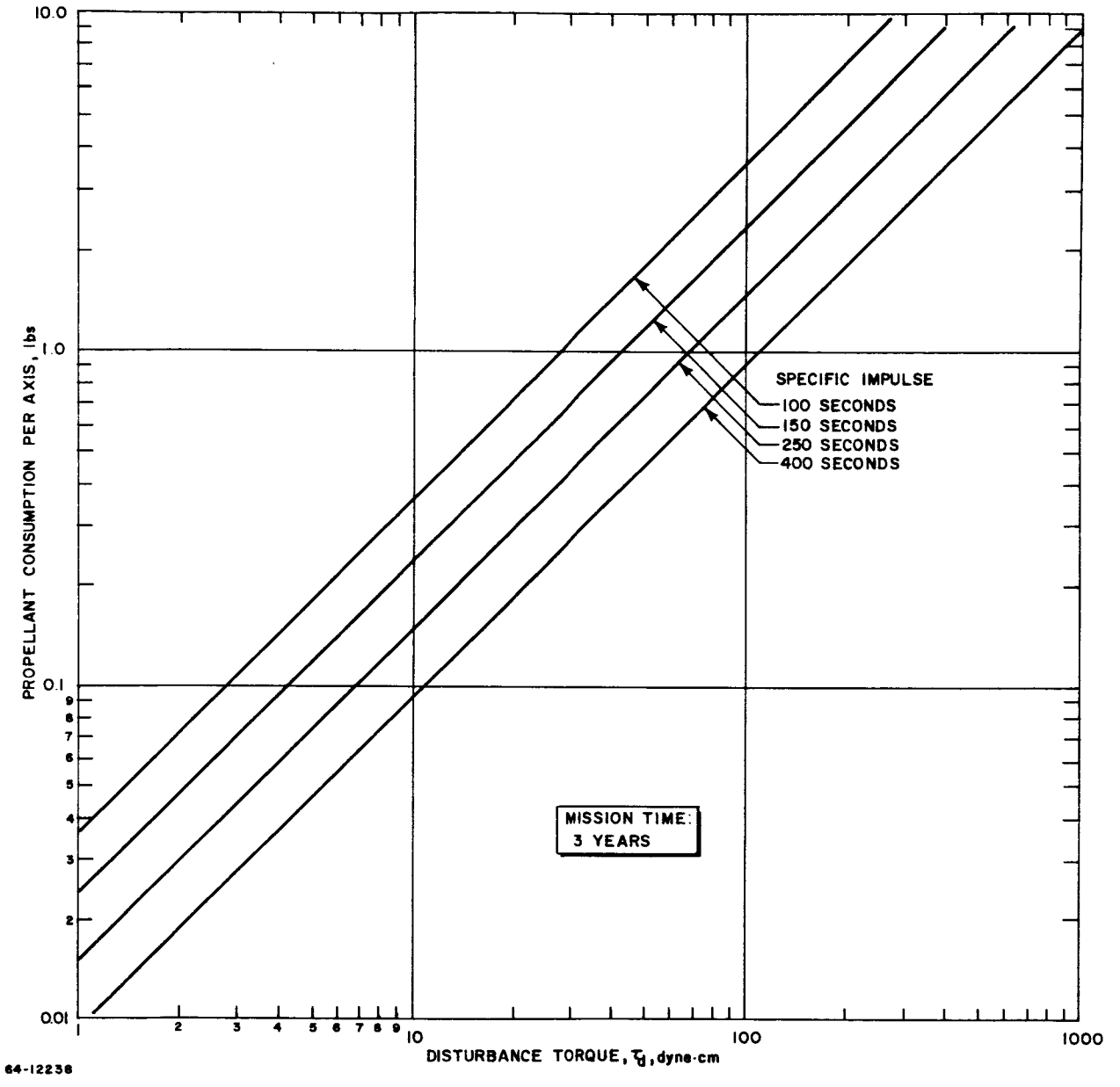

Figure 3 PROPELLANT CONSUMPTION VERSUS DISTURBANCE TORQUE AND THRUSTOR SPECIFIC IMPULSE

$$W_{prop} = \frac{l K_c^2 T_m}{4 I\theta^* I_{sp}} \tag{6}$$

and the number of cycles/mission is given by

$$N = \frac{l K_c T_m}{4 I\theta^*} \quad . \tag{7}$$

The hard limit cycle fuel consumption ($r_d = 0$) is thus proportional to the square of the control impulse bit and inversely proportional to the attitude angular accuracy and vehicle inertia. Clearly, to reduce the hard limit cycle fuel consumption the applied control impulse bit must be kept small. An increase in the control impulse bit by a factor of 10 will increase the fuel consumption by a factor of 100.

For example, if l = 2 feet, $K_c = 10^{-3}$ lb-sec, $T_m = 9.45 \times 10^7$ seconds (3 years), I = 41.2 slug-ft^2, θ^* = 0.5 degree (0.00875 radians) and I_{sp} = 300 seconds, the required propellant weight for zero disturbance torque is 0.44 lb/axis. If the control impulse torque were increased to 10^{-2} lb-sec, the propellant weight would rise to 44 pounds.

It is difficult to write a general relation for propellant consumption in the hard limit cycle when $r_d \neq 0$; however, equation (6) gives a reasonable estimate of the fuel consumption between the disturbance torque at which the system goes into a hard limit cycle and zero disturbance torque.

4. Duty Cycle Requirements (no warmup period)

The duty cycle is of interest since it affects the demands on the power supply. The duty cycle is defined as the ratio of the time when power is being delivered to the engine to the total mission time. In the case of the resistojet it is possible that the engine will be heated close to operating temperature before the gas is turned on; in this situation the thrust time is less than the power-on time. The present section contains an analysis of the case in which the power-on and thrust times are equal ($t_{warmup} = 0$); in the following section the power-on time is assumed to be greater than the thrust time ($t_{warmup} \neq 0$).

In the soft limit cycle the total impulse delivered in the course of the mission exactly counterbalances the disturbance impulse. From equation (5) the duty cycle, η, is given by

$$\eta = \frac{N t_{thrust}}{T_m} \quad \frac{r_d}{l F} \quad . \tag{8}$$

The duty cycle is independent of the width of the impulse bit, t_{thrust}, and only depends on the amplitude, F. If the applied torque, F, is large the duty cycle is small.

In the hard limit cycle with $\tau_d = 0$ the duty cycle becomes, from equations (6) and (7),

$$\eta = \frac{F\ t^2_{thrust}}{4\ I\theta^*} \quad . \tag{9}$$

The duty cycle thus increases with the thrust level and with the square of the thrusting time.

The power input to an electric propulsion thrustor is given by

$$P_{input} = \frac{2.18 \times 10^{-2}\ T\ I_{sp}\ \text{watts}}{\epsilon_o} \tag{10}$$

where, T is the thrust in millipounds and ϵ_o is the ratio of thrust power to electric input power. For example, at a thrust of 1 mlp (millipound), a specific impulse of 300 seconds, and an overall efficiency of 25 percent the required input electrical power is 26 watts.

In the attitude control thrustor system for a satellite there may be at least nine thrustors. If the duty cycle for each of the individual thrustors is greater than 100/9 or 11.1 percent the basic power supply output must be increased beyond that required for a single thrustor.

5. Duty Cycle Requirements (warmup period)

When the thrustor warmup time is not negligible, the duty cycle becomes

$$\eta = \frac{N(T_{thrust} + T_{warmup})}{T_m} \quad . \tag{11}$$

Therefore, for the soft limit cycle, from equations (8) and (11) the duty cycle becomes

$$\eta = \frac{\tau_d}{l\,F} + \frac{\tau_d}{l\,K_c}\ T_{warmup} \tag{12}$$

or

$$\eta = \frac{\tau_d}{l\,F}\left(1 + \frac{T_{warmup}}{T_{thrust}}\right) \quad . \tag{13}$$

If T_{warmup} is small compared to T_{thrust} the duty cycle is unchanged. However, if T_{thrust} is increased to make this the case, then either F must be decreased or the impulse bit increases. If F is decreased too much η will become large at large τ_d. If the impulse bit is increased too much the hard cycle will occur for larger τ_d and propellant consumption will increase.

In the case of $\tau_d = 0$ with a hard limit cycle equation (9) becomes

$$\eta = \frac{lF\ T^2_{thrust}}{4I\theta^*} \left(1 + \frac{T_{warmup}}{T_{thrust}}\right) \tag{14}$$

Thus, for the hard duty cycle, if the warmup time is equal to the thrust time the duty cycle is increased by a factor of 2.

6. Impulse Bit Length and Thrust Amplitude Requirements for Satellite Attitude Control

From the relations presented in the preceding sections, it is possible to bracket the values of the thrust amplitude and impulse bit length required for satellite attitude control. The satellite under consideration will be that described in table I.

a. The minimum tolerable thrust level is a function of duty cycle and disturbance torque and can be determined from equation (8) for zero warmup time and equation (13) for positive warmup time. The required duty cycle for any individual thrustor is assumed to be equal to or less than 5 percent, i.e. ≤ 0.05. The maximum disturbance torque is 500 dyne-cm.

b. At the other extreme, one upper thrust limit is fixed by the duty cycle for hard cycle operation at zero disturbance torque; this limit can be determined from equation (14) for a positive warmup period.

c. Finally, another upper thrust limit is fixed by the requirement that it is advisable, from the viewpoint of propellant consumption, to hold soft cycle operation to as low a disturbance torque level as possible. The minimum thrust requirement is given by equation (1); for purposes of calculation it is assumed that the soft cycle is to be held to a disturbance torque of 50 dyne-cm.

Results of calculations from the preceding relations are presented in figures 4 through 8. Figure 4 presents a curve of thrust amplitude, F versus impulse bit length, T_{thrust}, for zero warmup time. The lowest horizontal line corresponds to the minimum thrust (0.37×10^{-3} pound) compatible with a 5-percent duty cycle and a 500 dyne-cm disturbance torque. A lower

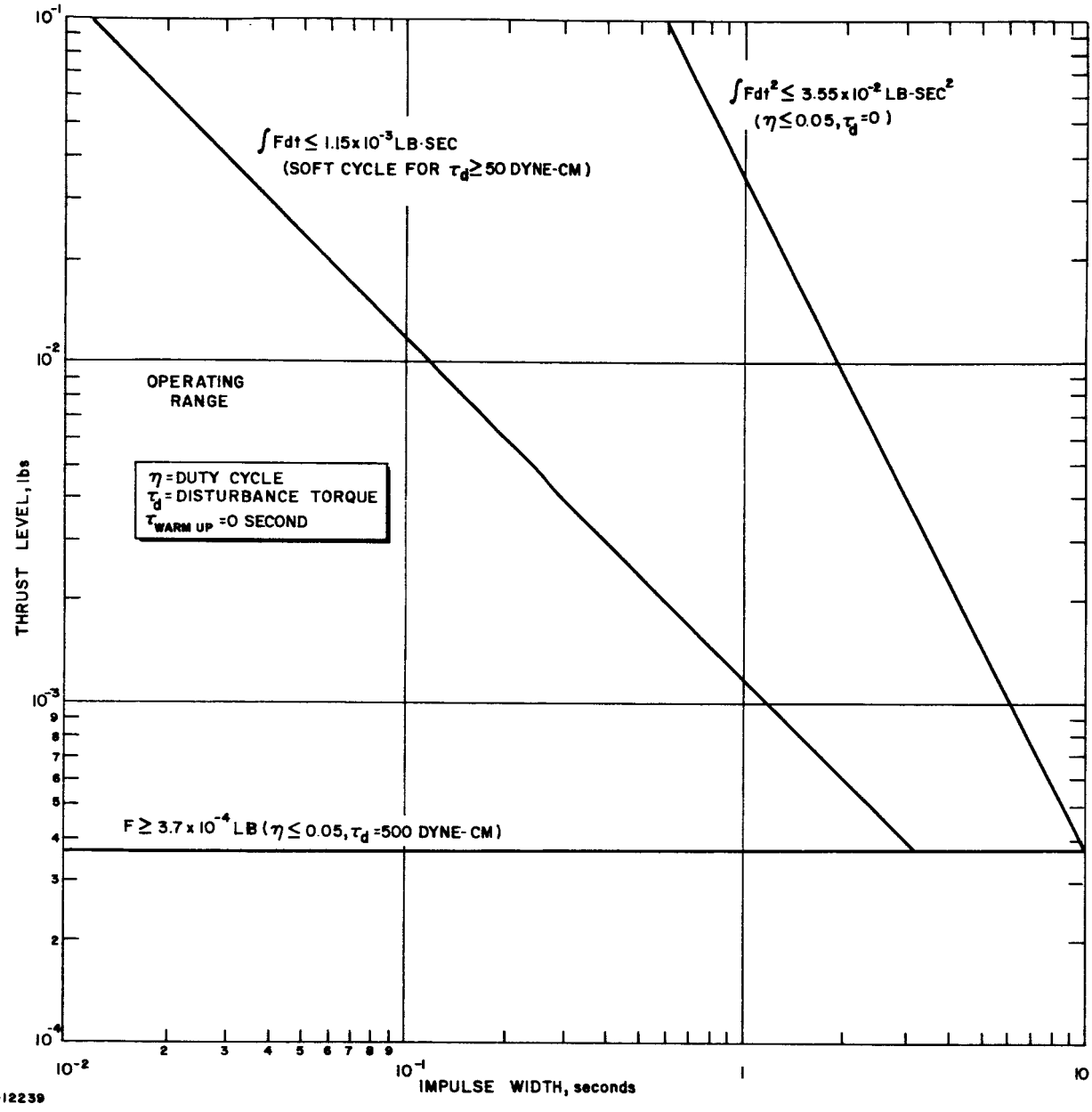

Figure 4 THRUST LEVEL VERSUS IMPULSE BIT WIDTH FOR 0-SECOND WARMUP TIME

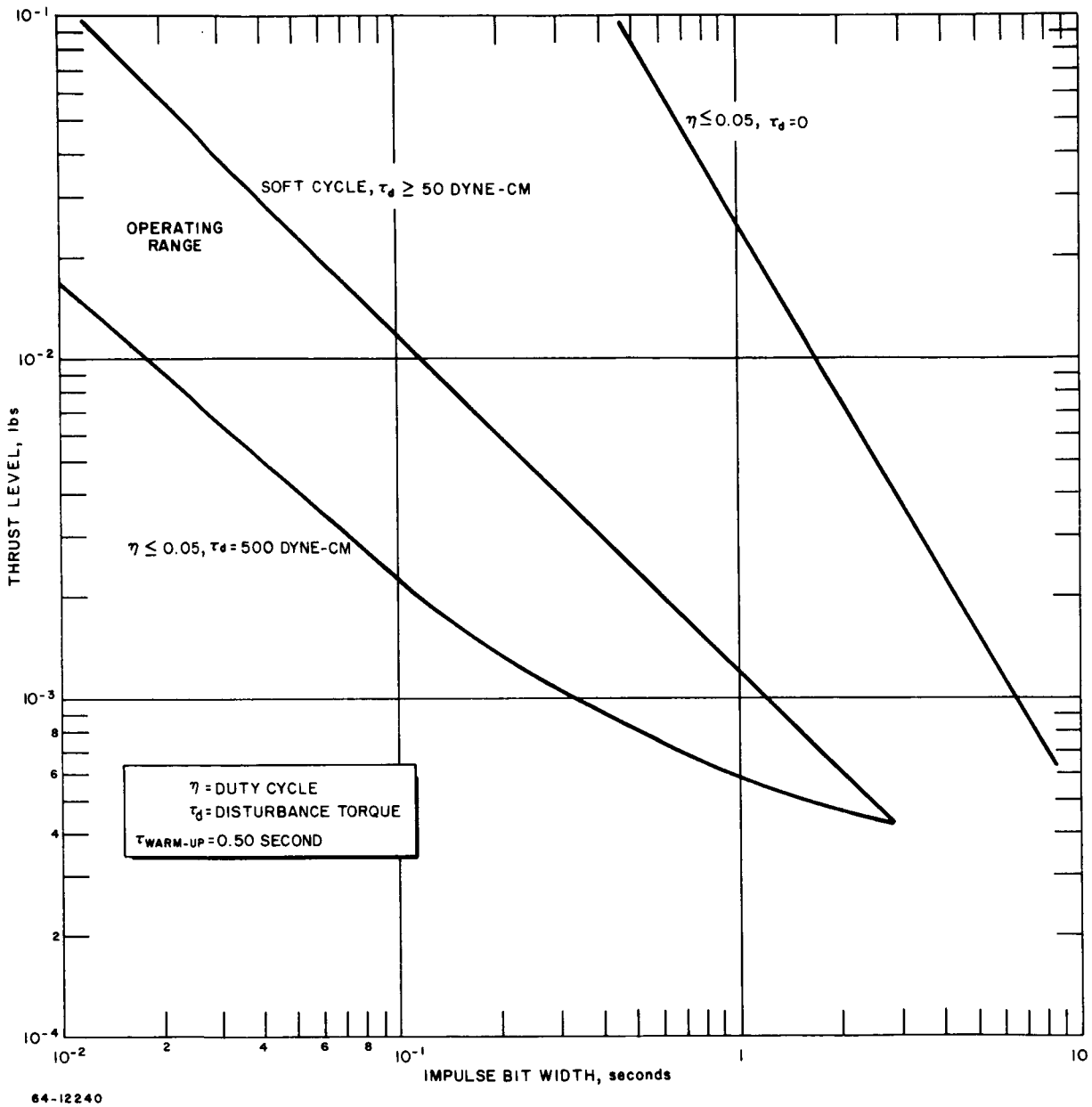

Figure 5 THRUST LEVEL VERSUS IMPULSE BIT WIDTH FOR 0.50-SECOND WARMUP TIME

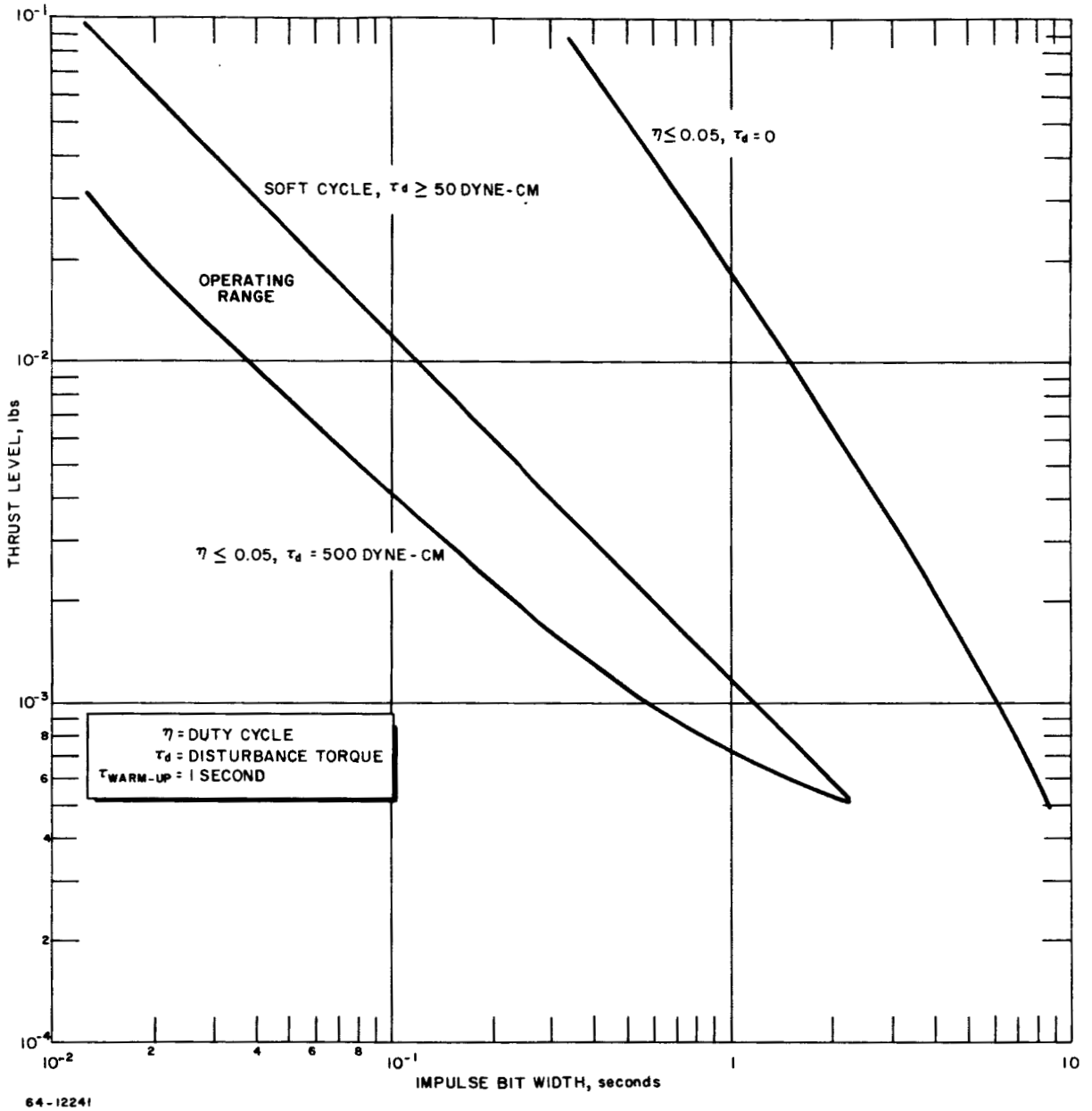

Figure 6 THRUST LEVEL VERSUS IMPULSE BIT FOR 2-SECOND WARMUP TIME

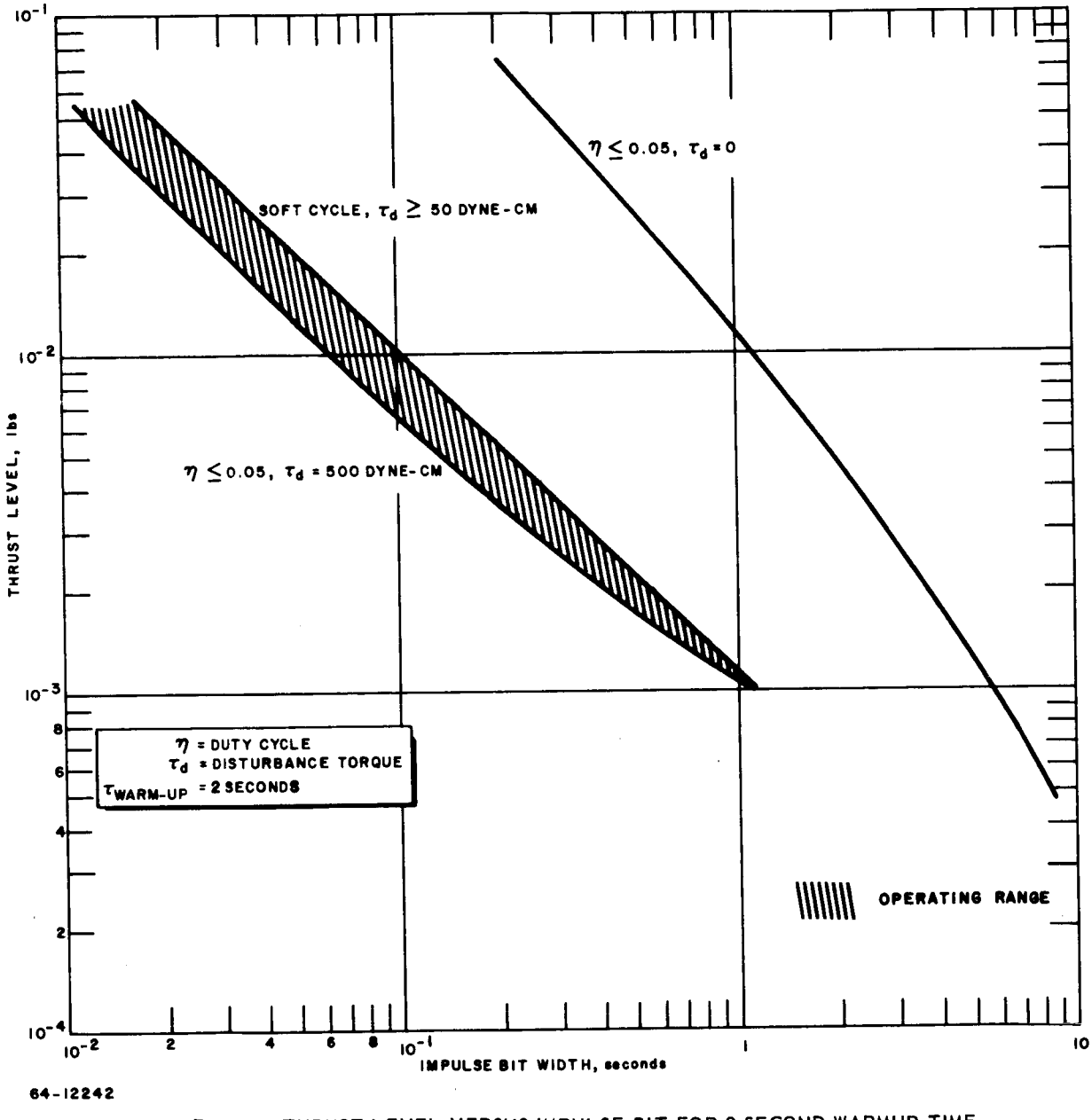

Figure 7 THRUST LEVEL VERSUS IMPULSE BIT FOR 2-SECOND WARMUP TIME

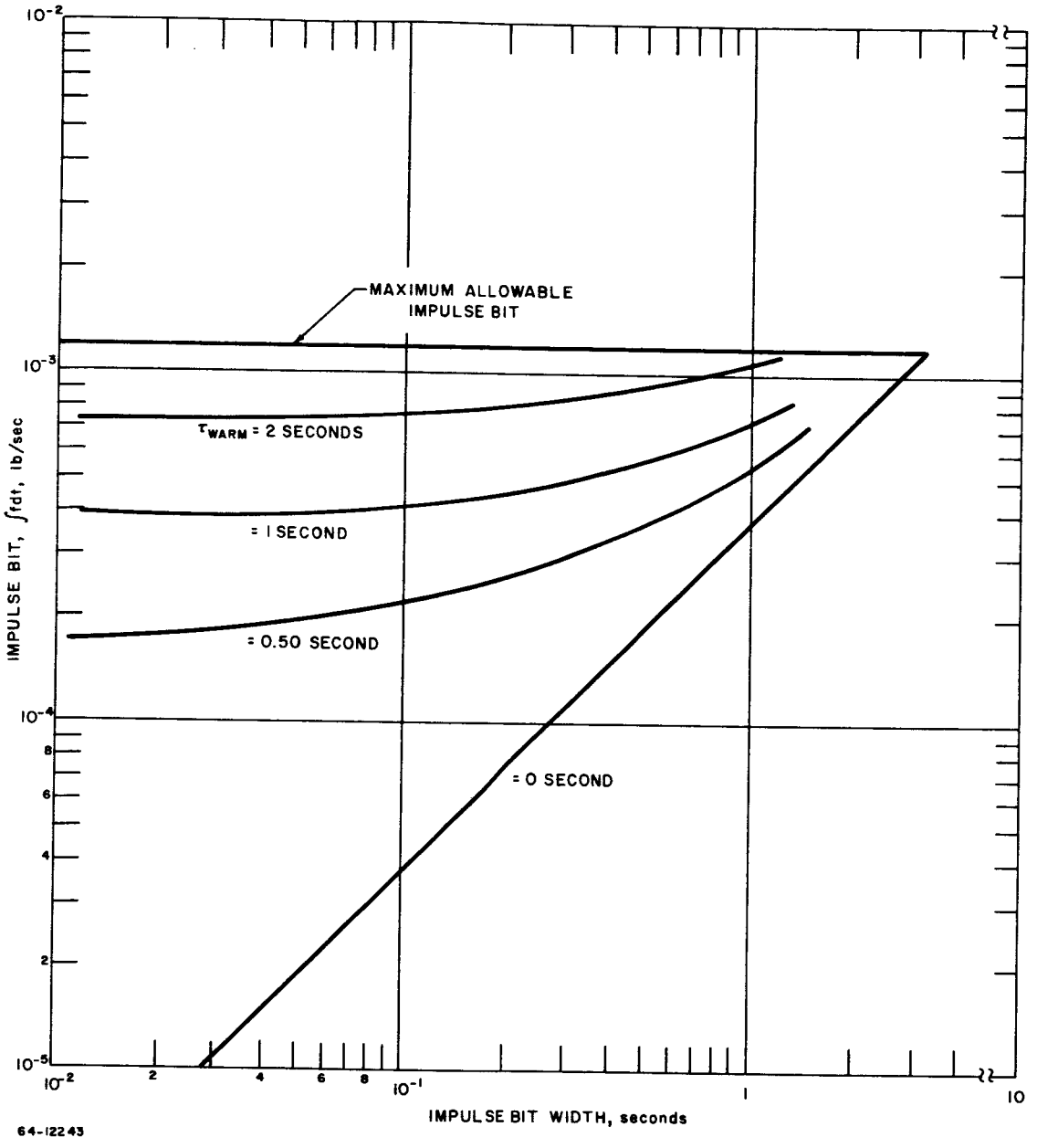

Figure 8 MINIMUM ALLOWABLE IMPULSE BIT VERSUS IMPULSE BIT WIDTH AND WARMUP TIME

value of the applied thrust will result in duty cycle greater than 5 percent per thrustor. The upper value of the applied thrust is fixed either by the requirement for a soft limit cycle or a 5-percent duty cycle at zero disturbance torque. This situation is illustrated in figure 4. In order to hold a soft limit cycle down to 50 dyne-cm disturbance, the applied thrust must be below values given on the curve $F\,T_{thrust} = 1.15 \times 10^{-3}$ lb-sec. The requirement for a 5-percent duty cycle at zero disturbance torque is less severe and can be established by having the control thrusts below values on the curve given by $F\,T_{thrust} = 3.55 \times 10^{-2}$ lb-sec^2. The useful operating area is given by the shaded area in figure 4. For zero warmup time the thrust should be of the order of 1 mlb, the thrust time of the order of 1 second, and the impulse bit about 10^{-3} lb-sec. At 300 seconds and 25 percent overall energy conversion efficiency, the power input would be 26 watts.

Figures 5 through 7 present values of thrust amplitude versus impulse bit length for thrustor warmup times of 0.50, 1.0, and 2.0 seconds. In comparison with the results shown in figure 3 for zero warmup time, the operating range is greatly reduced with increase in warmup time. In particular the very small impulse bits have been eliminated since they would result in excessive duty cycles at the larger disturbance torques. In all cases, up to 2-second warmup time, the allowable operating range is determined by the requirements that a soft cycle can be maintained for $\tau_d \geq 50$ dyne-cm and a duty cycle smaller than 5 percent at a disturbance torque of 500 dyne-cm.

The results are summarized in figure 8. Impulse bit size is plotted as a function of thrust time. The horizontal line gives the maximum allowable impulse bit in order to maintain a soft limit cycle for $\tau_d \geq 50$ dyne-cm. The other lines indicate for warmup times of 0, 0.5, 1 and 2 seconds the minimum impulse bit to keep the duty cycle of each thrustor less than 5 percent at a disturbance torque level of 500 dyne-cm. The following conclusions can be reached from figure 8.

1. Increase in warmup time increases the minimum allowable values of the control impulse bits. Since small input bits are desirable to maintain a soft cycle at the lowest values of the disturbance torque, τ_d, and to reduce the propellant consumption, it is desirable to minimize the warmup time.

2. At a given warmup time some reduction in impulse bit can be achieved by reduction in the thrust time. For warmup times in excess of 0.50 second, however, little reduction can be achieved in the size of the minimum impulse bit by reduction in the thrust time below 500 msec.

3. Thrust times in excess of 3 seconds and warmup times much greater than 2 seconds will violate either the duty or soft cycle boundary conditions. The maximum allowable power on time will thus be about 5 seconds per pulse. Assuming an upper power limit of 100 watts per thrustor, an operating temperature of 2000°K, and a tungsten thrustor, the thrustor will have to weigh much less than 250 x 10^{-3} gram to permit it to come up to operating temperature in the allowable time.

4. It appears clear that with anticipated warmup times of the order of 1-second duty cycles substantially less than 5 percent will be hard to achieve.

7. Impulse Bit Length and Thrust Amplitude Requirements for Satellite Station Keeping

The station keeping system operates in a substantially different mode than the attitude control system. The major contribution to the total impulse required to maintain the orbit of a stationary satellite is the effect of solar-lunar attraction. The total impulse required each day to correct the solar lunar-perturbations is 7.2 lb-sec/day ($M\Delta V$ = 15.6 slugs x 0.461 ft/sec/day) assuming two nodal firings per day. If the thrust is applied continuously, the total impulse required to correct the solar lunar perturbations can be as much as 11.7 lb-sec/day. At a specific impulse of 300 seconds, 7.2 lb-sec of impulse/day requires 26.2 pounds of propellant for a 3-year mission, while 11.7 lb-sec/day of impulse requires 42.6 pounds of propellant. Including a tankage factor the propellant weight penalty for continuous rather than impulsive thrusting can be as much as 20 pounds.

Table III presents values of the total thrusting time per day as a function of thrust level to obtain the required 7.2 lb-sec of impulse. Also included in table III are values of the required thrustor power assuming a 300-second specific impulse level and an overall energy conversion efficiency of 25 percent.

TABLE III

REQUIRED THRUST TIME VERSUS THRUST LEVEL
(total impulse = 7.2 lb-sec)

Thrust Level (mlb)	Total Thrust Time (hours)	Nodal Thrust Time (hours)	Thrustor Power (watts)
0.50	4.00	2.00	13.1
1.00	2.00	1.00	26.2
5.00	0.40	0.20	131
10.00	0.20	0.10	262

Referring to table III, it is likely that at thrust levels greater than 1×10^{-3} pounds to 2×10^{-3} pounds the input ΔV can generally be considered to be impulsive; at thrust values less than 1×10^{-3} more than 7.2 lb-sec of impulse will probably be required to make the North-South correction. Exact calculations, presently in progress, will be required to evaluate the magnitude of the increase in required impulse. From the results obtained to date, however, it appears that station keeping thrustor will operate at between 1 and 2 mlb, power levels between 25 and 50 watts, and for time periods of the order of 30 to 60 minutes.

The total energy requirement per station keeping pulse is about 25 watt-hours. The batteries required to store 25 watt-hours of energy (assuming 50 percent depth of discharge and 10 watt-hours/lb)[4] weigh about 5 pounds. The batteries can be charged with about 2 watts of solar cells which at 0.25 lb/watt weigh only about 0.50 pound. Thus the station keeping requirement appears quite feasible.

8. Summary of Resistojet Performance Characteristics Required for Satellite Attitude and Orbit Control

The resistojet performance characteristics required for the attitude and orbit control of a 500-lb satellite (see table I) assuming a maximum disturbance torque of 500 dyne-cm, soft limit cycle operation at disturbance torques greater than 50 dyne-cm, and a maximum 5-percent electric power input duty cycle per axis is presented in table IV.

TABLE IV

RESISTOJET PERFORMANCE CHARACTERISTICS REQUIRED FOR SATELLITE ATTITUDE AND ORBIT CONTROL

Characteristics	Attitude Control	Station Keeping
Thrust level, mlb	0.50 to 1.0	1.0 to 2.0
Thrust time, seconds	0.50 to 1.00	1000 to 5000
Impulse bit, lb-sec	0. to to 1.00 $\times 10^{-3}$	1 to 10
Warmup time, seconds	1	--
Power level, watts	10 to 50	25 to 75

The thrustor requirements for attitude control and the requirements for orbit control tend to some extent overlap each other. Only detailed studies will show whether they should be the same or separate thrustors. In the case of the attitude control thrustors by reducing the thrust level and increasing the thrust time, the operational requirements on the propellant control values are minimimized.

B. MEASUREMENT OF ENGINE PROPULSION PERFORMANCE

1. Thrust Measurement

A critical tool in the determination of thrustor performance for satellite attitude control and station keeping is a thrust stand for the accurate determination of the engine thrust-time response. For the present study, as indicated in table IV, the stand must have the capability of detecting thrust levels as low as 10^{-4} pound (0.10 mlb) and a time response at this thrust level of 10×10^{-3} second (10 msec).

The thrust stand designed for this application is based on a simple wire-in-tension techniques and is shown in figure 9. A photograph of the stand is shown in figure 10. The engine system horizontal mounting bracket is supported by four wires in tension. The wires are, in turn, connected to a surrounding aluminum ring which is shock mounted by means of springs. The thrust axis of the engine is vertical; the engine and its propellant tank are located on the mounting bracket.

The entire assembly is located in a transparent bell jar, and the bell jar is evacuated to pressures of 10^{-4} mm of Hg and below by means of a 4-inch diffusion pump. Order-of-magnitude calculations have made it clear that conduction losses can be the predominant energy loss mechanisms (input power $\sim$10 watts) for resistojets operated at a few mm of Hg pressure; thus it is necessary to operate the low-power resistojet in a relatively "hard" vacuum to prevent all the input energy from being conducted away to the surrounding environment.

A simplified analysis of the transient behavior of the thrust stand is based on the behavior of a string when loaded with a mass, M. For the simple analysis the ratio of string to mass weight is assumed to be small; an analysis for finite values of string to mass weight is presented in appendix B.

The equation of motion for a string of length, L, in tension is given by

$$M \frac{d^2y}{dt^2} = -Mg - F - 2T \sin \theta \qquad (15)$$

$$= -Mg - F - 4T \frac{y}{L}$$

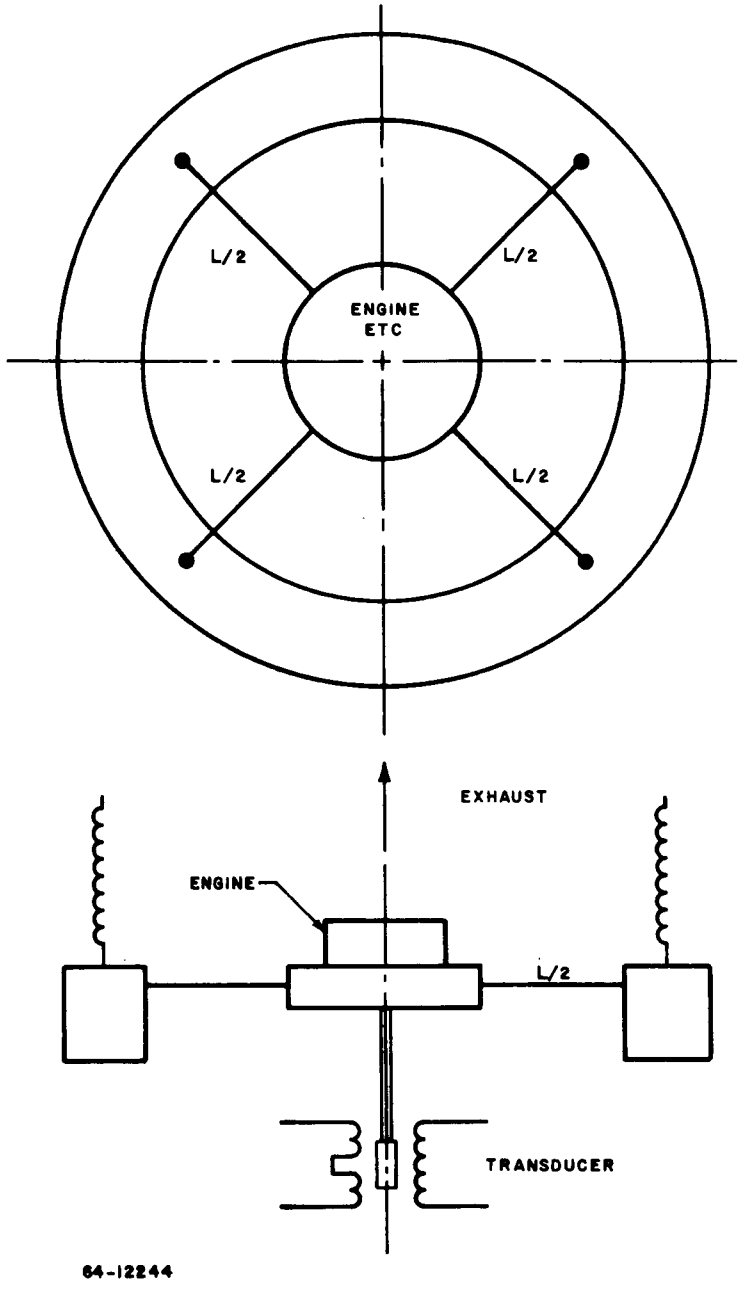

Figure 9 WIRE-IN-TENSION THRUST STAND

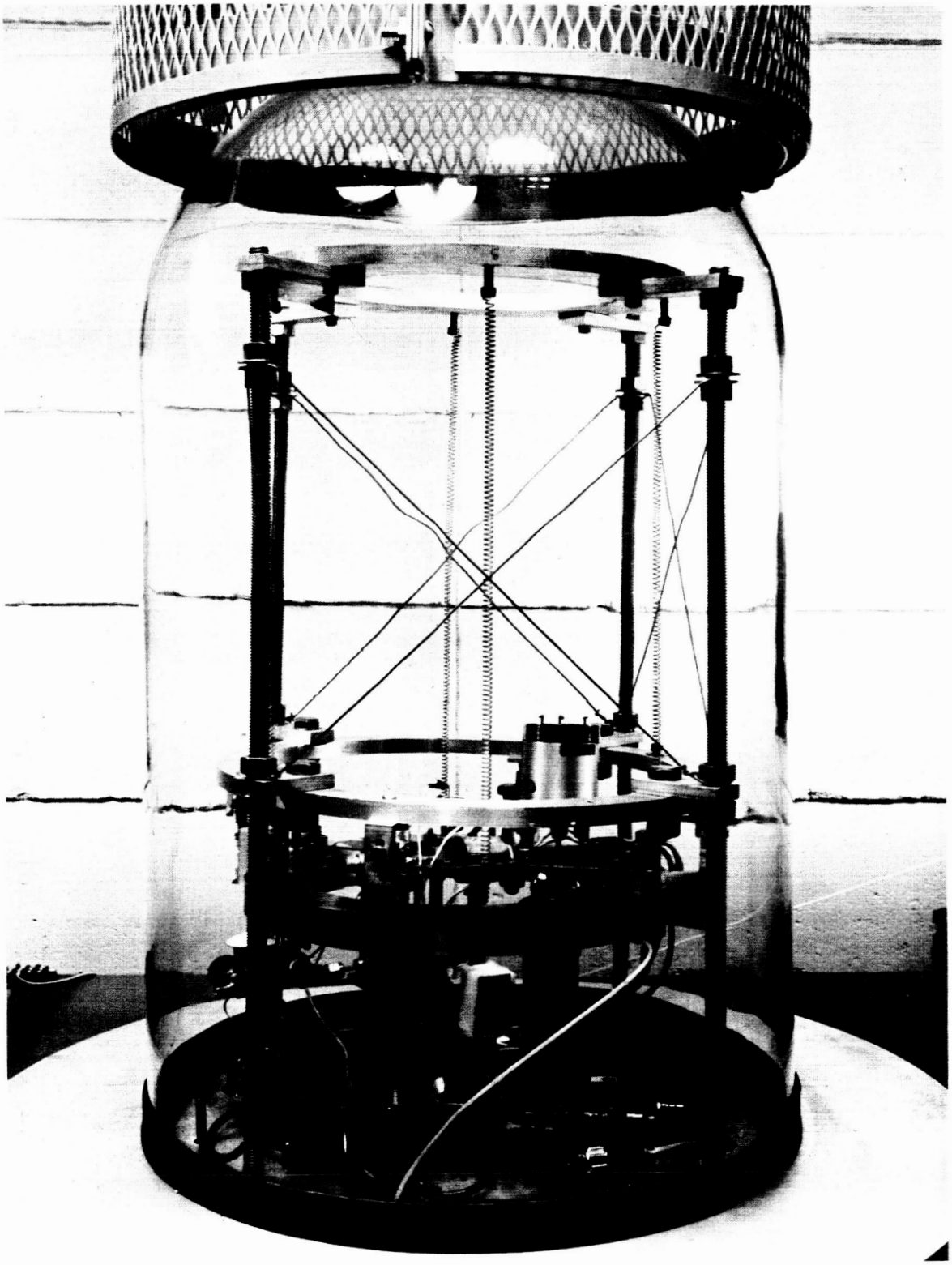

Figure 10 THRUST STAND
P12477-B

where, F is the applied force and y is the displacement.

The solution to this differential equation is

$$y = \frac{MgL}{4T} - \frac{FL}{4T}\left[1 - \cos 2\sqrt{\frac{T}{ML}}\, t\right] \tag{16}$$

The inclusion of damping modifies equation (15) to read

$$\frac{d^2y}{dt^2} + \frac{f}{M}\frac{dy}{dt} + \frac{4T}{ML}\, y = -g - \frac{F}{m} \tag{17}$$

where, $f/M \; dy/dt$ is the damping term.

The displacement is given by

$$y(t) = -\frac{MgL}{4T} - \frac{FL}{4T}\left[1 - \frac{2}{\omega}\sqrt{\frac{T}{ML}}\; e^{-\frac{fT}{2M}} \sin(\omega t + \phi)\right] \tag{18}$$

where

$$\omega^2 \equiv \frac{4T}{ML} - \frac{f^2}{4M^2}$$

and

$$\tan\phi \equiv \frac{2\omega M}{f} .$$

For times long compared with $\frac{2M}{f}$, this decays to the steady position given by

$$y = -\frac{MgL}{4T} - \frac{FL}{4T} \tag{19}$$

as expected.

Figure 11 shows a plot of the two cases: (a) no damping and (b) moderate damping. As can be seen from figure 11, for moderate friction effects which damp the oscillations in just a few cycles, the frequency of oscillation is essentially the same for the damped as for the undamped situation. The actual period for the damped curve shown is

$$Pd = \frac{8}{\sqrt{63}}\, P_u = \frac{8}{\sqrt{63}}\, \pi\sqrt{\frac{ML}{T}} \text{ sec} \tag{20}$$

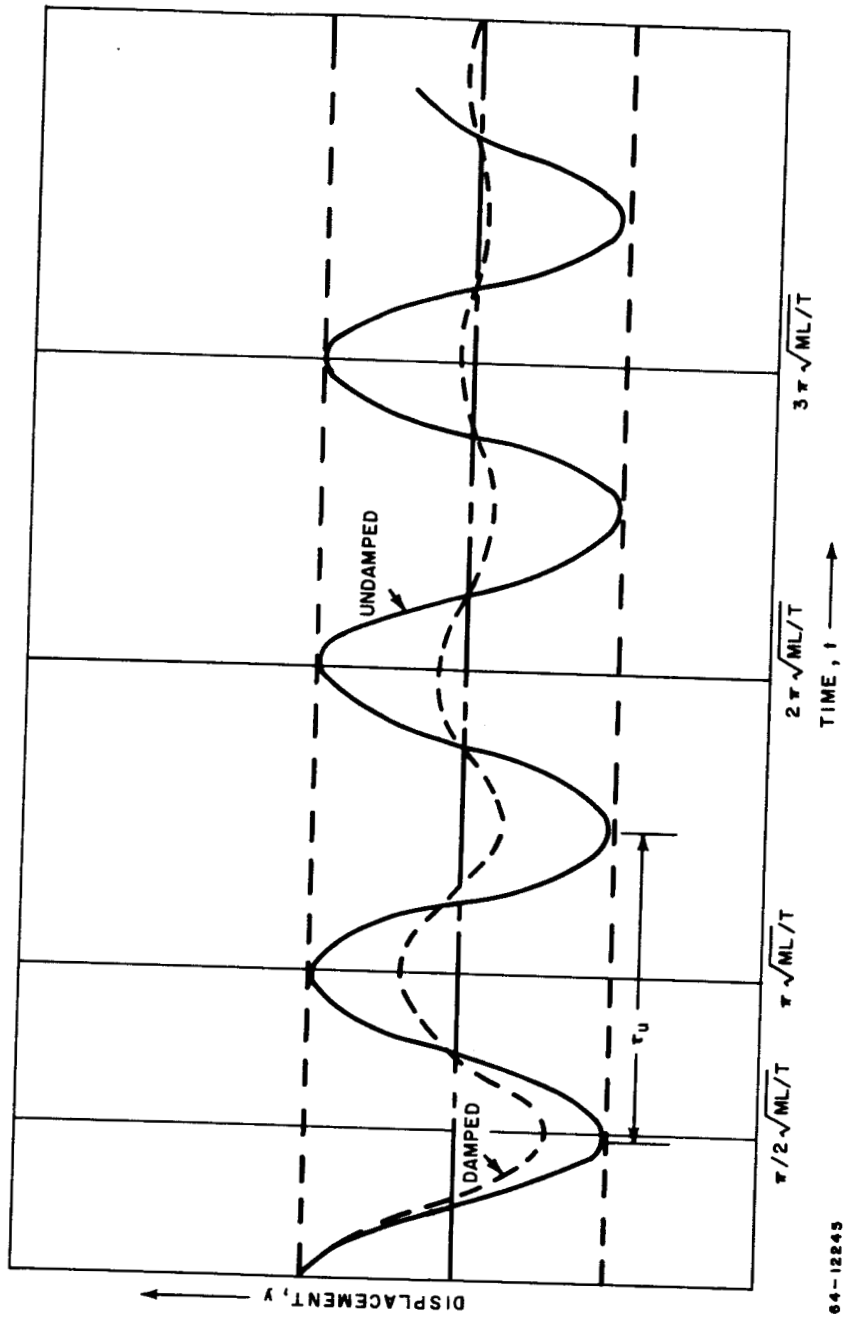

Figure 11 DAMPED AND UNDAMPED THRUST STAND OSCILLATIONS

Thus moderate damping of the thrust stand results in only minor changes in the period of the stand.

In the actual thrust stand, shown in figures 9 and 10, the central support bracket is essentially supported by two strings; the tension term in the above equations must thus be replaced by 2T. The wire weight is about 0.01 pound, and the weight of the engine, propellant storage tank, etc., is about 2 pounds; the condition that wire weight to string weight is much less than unity is therefore satisfied.

The displacement of the engine support as a function of applied thrust is given by

$$y = \frac{FL}{8T} \tag{21}$$

or the engine thrust is given by

$$F = \frac{8T}{yL} \tag{22}$$

For a fixed value of the string tension to length ratio the minimum detectable thrust level is inversely proportional to the displacement, y; similarly, for a fixed detectable displacement, y, the minimum detectable thrust varies directly as the string tension to length ratio. It is noted that the minimum measurable thrust is independent of the mass of the engine system, M. Figure 12 presents curves of minimum measurable displacements of 10^{-6}, 3×10^{-7}, and 10^{-7} inch. The displacement transducer presently installed on the thrust measurement system (Sanborn 581-25-1) has a minimum displacement capability of 3×10^{-7} inch. This value may be decreased to as little as 10^{-7} inch with the installation of a new transducer (Sanborn 595DT-005BM). At the 3×10^{-7} inch displacement level, thrusts of the order of 0.10 mlb can be detected with a string tension to length ratio of about 50 lb/in. The minimum detectable thrust level can be decreased by reducing the T/L ratio; however, as will be shown below there is a corresponding decrease in the thrust stand response characteristics.

The natural frequency of oscillation of the thrust stand is given by

$$\nu = \frac{1}{\pi}\sqrt{\frac{2T}{ML}} \tag{23}$$

and the natural time period is

$$P = \pi\sqrt{\frac{ML}{2T}} \tag{24}$$

The natural frequency of the thrust stand, unlike the minimum detectable thrust level, is a function of the mass, M, of the engine system. Figure 13 presents a plot of natural frequency, ν, as a function of T/L ratio for

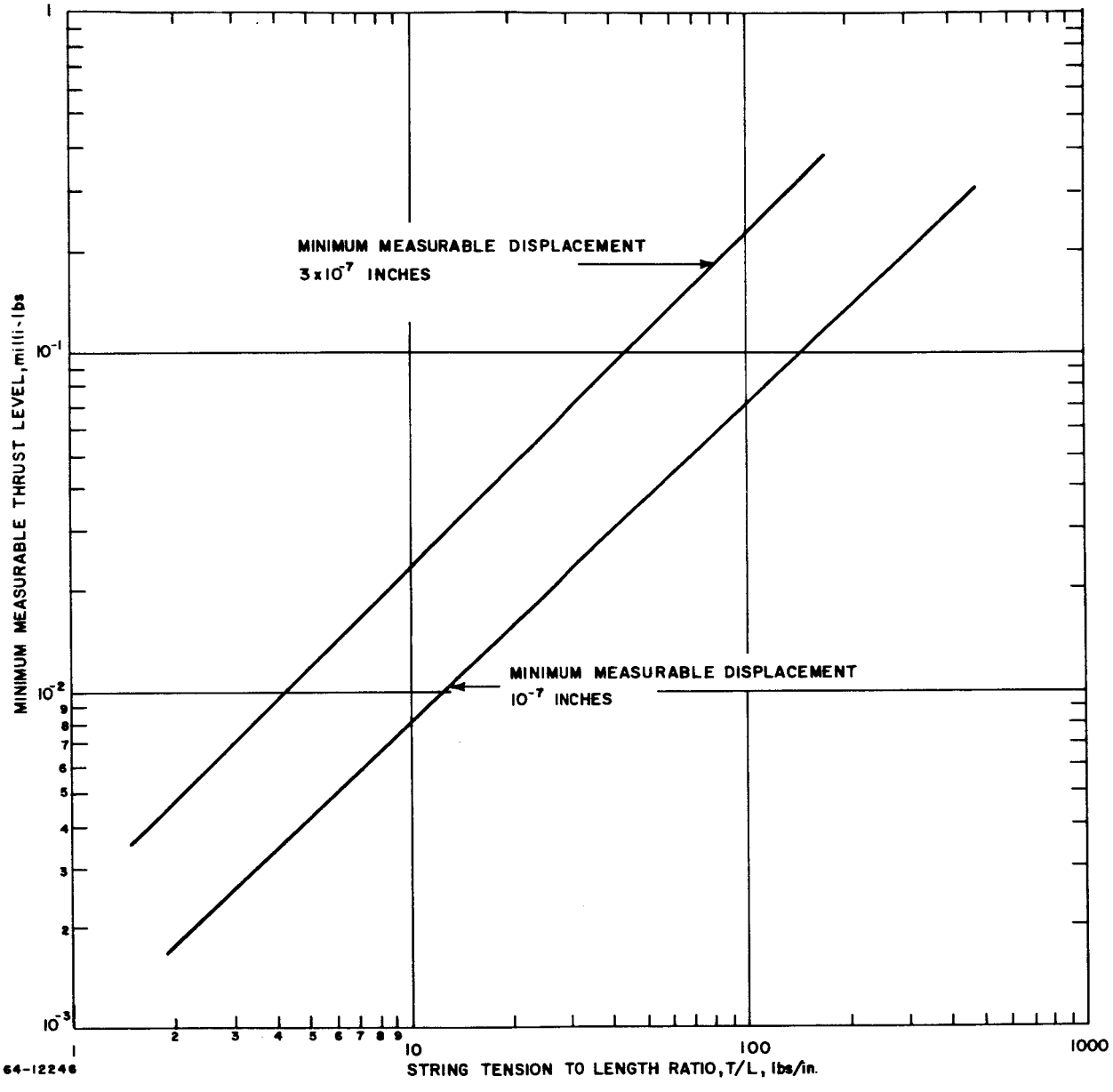

Figure 12 MINIMUM MEASURABLE THRUST VERSUS STRING TENSION-TO-LENGTH RATIO

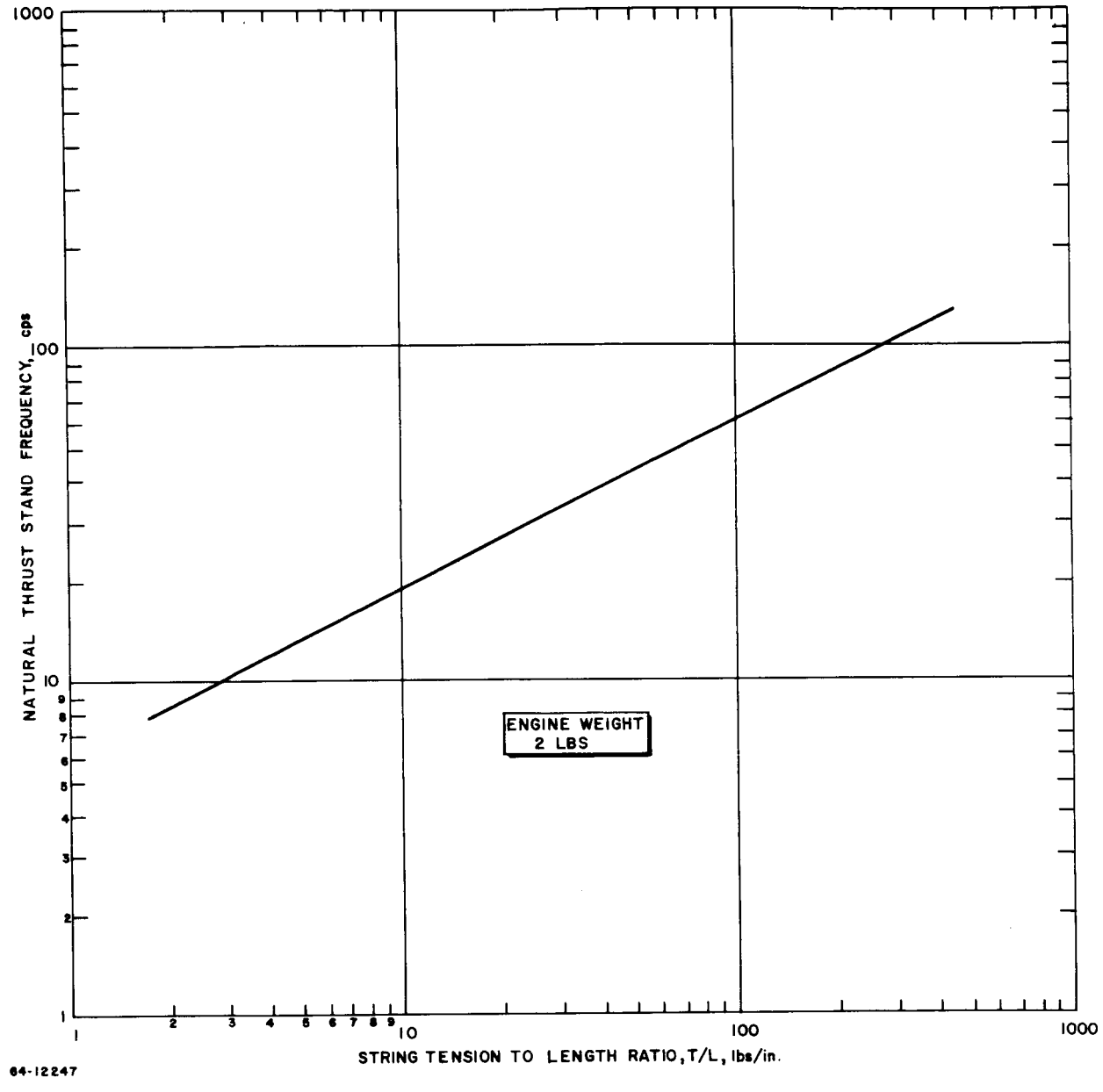

Figure 13 THRUST STAND NATURAL FREQUENCY VERSUS STRING TENSION-TO-LENGTH RATIO

engine system weight of 2 pounds, which is comparable to the actual system weight. The natural frequency setting of the thrust stand for the measurements presented in this report was about 40 cps corresponding to a tension to length ratio of about 40 lb/in. Assuming a minimum detectable displacement of 3×10^{-7} inch this corresponds to a minimum detectable thrust level of 10^{-1} mlb. Estimated values of the natural frequency, time constant, and minimum detectable thrust, as a function of T/L ratio for an engine system weight of 2 pounds and a displacement transducer capable of detecting 3×10^{-7} inch is presented in table V.

TABLE V

FREQUENCY RESPONSE VERSUS MINIMUM DETECTABLE THRUST LEVEL AND STRING TENSION/LENGTH RATIO
(engine mass-2 pounds; minimum displacement, 3×10^{-7} inch)

Tension/Length Ratio (lb/in.)	Natural Frequency Response (cps)	Time Constant (seconds)	Minimum Thrust Level (pounds)
2.5	10	100×10^{-3}	0.006×10^{-3}
10	20	50×10^{-3}	0.024×10^{-3}
40	40	25×10^{-3}	0.10×10^{-3}
160	80	12.5×10^{-3}	0.40×10^{-3}
640	160	6.25×10^{-3}	1.60×10^{-3}
2560	320	3.12×10^{-3}	6.40×10^{-3}
10240	640	6.24×10^{-3}	25.6×10^{-3}

The response of the thrust stand as summarized in table V appears to be satisfactory for measuring the required resistojet performance indicated in table IV. The major present problem with the thrust stand is that of thermal drift during hot engine operation. It is felt that this problem can be alleviated by suitable thermal shielding, and work to this end is presently in progress.

2. Mass Flow Measurement

The propellant flow rates associated with the low-power resistojet thrustor are of the order of 1 to 10 μlb/sec, a range of mass flow which makes direct rate metering difficult. The technique which has been used to determine mass flow rate is based on measuring the pressure rise in a known volume. In brief, the bell jar containing the thrustor and thrust measuring system is evacuated to a value of the order of 10^{-4} mm Hg, and then isolated from the pump. Propellant is then allowed to flow, with a given setting of the

critical metering orifice, for a period of time usually chosen as 100 seconds. The pressure in the bell jar is then measured, after a short wait to allow thermal equilibrium, and the known bell jar volume, pressure rise, and flow time are used to determine the mass flow rate. Typically the pressure rise is of the order of several hundred to several thousand microns, and thus readily measured.

3. Power Measurement

Engine input power is obtained as dc from a set of storage batteries. Current and voltage are measured with precision meters. Control is obtained with rheostats.

C. RESISTOJET DESIGN PHILOSOPHY

There are two basic concepts for the low-power resistojet thrustor. These are thermal storage and fast heatup. In the thermal storage resistojet, thrustor power is continuously supplied to the heater element and only the propellant flow is pulsed. The heat capacity of the thermal storage unit is sufficiently great that the temperature of the heater element remains essentially constant during short propellant pulses. In the fast-heatup resistojet thrustor both the power and propellant flow are pulsed. In contrast to the thermal storage device, the heat capacity of the fast-heatup device is held to a minimum.

The advantages of the thermal storage device include no thermal cycling, minimum time delay between input signal and resulting impulse bit, and constant power input, which reduces system complexity; the main disadvantage of the thermal storage unit is the high average power consumption, and the large resulting system weight. The primary advantage of the fast-heatup unit is low average power consumption; disadvantages include the necessity for frequent thermal cycling and the existence of a delay time between the input signal and the time that the thrustor is at operating temperature.

Experiments have been carried out with both fast-heatup and thermal storage units operated at power levels between 10 and 50 watts. A detailed description of these experiments is presented in the following two sections. Briefly, however, the results are as follows. The prototype thermal storage unit consisted of a composite tungsten-zirconia heater with axial gas flow passages. The heater was surrounded by radiation shields. The unit weighed approximately 10 grams, and at 2000°K had a heat content of 6000 joules. The prototype fast-heatup resistojet consists of a thin-walled, high-temperature metal tube which has a 0.38 mm (15 mil) outside diameter and is 2 cm long. The fast-heatup thrustor weighs approximately 50×10^{-3} grams and has a heat content of only about 30 joules at 1500°K. The minimum power input to maintain the thermal storage unit at an operating temperature of 2000°K was established to be at least of the order of 10 watts. The average power level for the fast-heatup

thrustor operated at a 5-percent duty cycle, which is typical of the 500-pound satellite application, was an order of magnitude lower. Based on these results the experimental effort is presently being concentrated on the design and development of the fast-heatup device.

D. FAST HEATUP RESISTOJET THRUSTOR DEVELOPMENT

1. Thrustor Configuration and Operating Range

The prototype thrustor configuration is presented in figure 14; a photograph of the unit is shown in figure 15. The device simply consists of a heating element, gas valve, and exit nozzle. The prototype heating element consisted of a stainless steel cylindrical tube which had an inside diameter of 0.35 mm, an outside diameter of 0.70 mm, and was 2 cm long. The exit nozzle throat diameter was a nominal 0.10 mm.

The present unit was constructed of stainless steel, which has a limited temperature capability, (1600°K) because of the ready availability of thin-walled tubing. Future units will be constructed of more refractory metals such as tungsten. Radiation shields and other insulation have been eliminated to simplify. It is felt, however, that due to the small size of the unit any required shielding will be minimal. Current is passed through the heating element through electrical connections at the thrustor base and on the exit nozzle.

The range of experimental operating variables used to establish the performance characteristics of the stainless steel fast-heatup resistojet unit are summarized in table VI. The working fluid was ammonia.

TABLE VI

EXPERIMENTAL OPERATING VARIABLES FOR THE FAST-HEATUP THRUSTOR

Variables	Range
Input current	3 to 12 amperes
Input voltage	0.50 to 2.5 volts
Input power	0 to 25 watts
Ammonia flow	1 to 10 x 10^{-6} lb/sec
Chamber pressure	5 to 50 psia
Heating element resistance	0.12 to 0.13 ohms

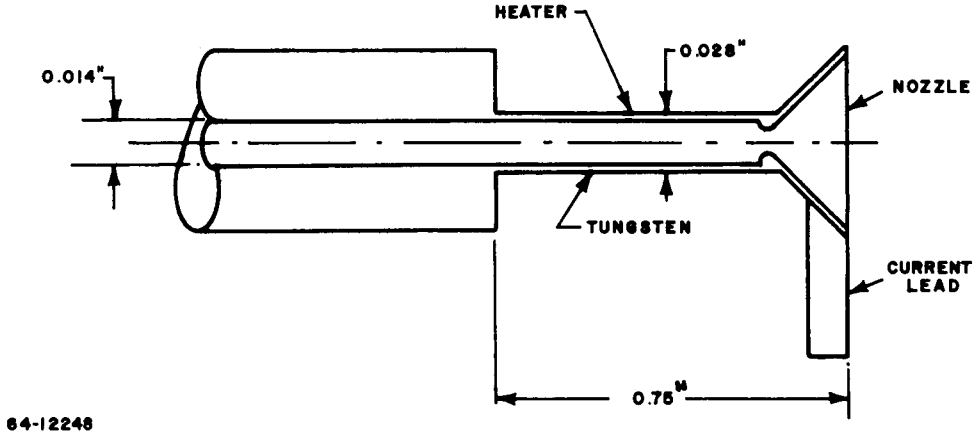

Figure 14 PROTOTYPE, FAST-HEATUP STAINLESS STEEL RESISTOJET

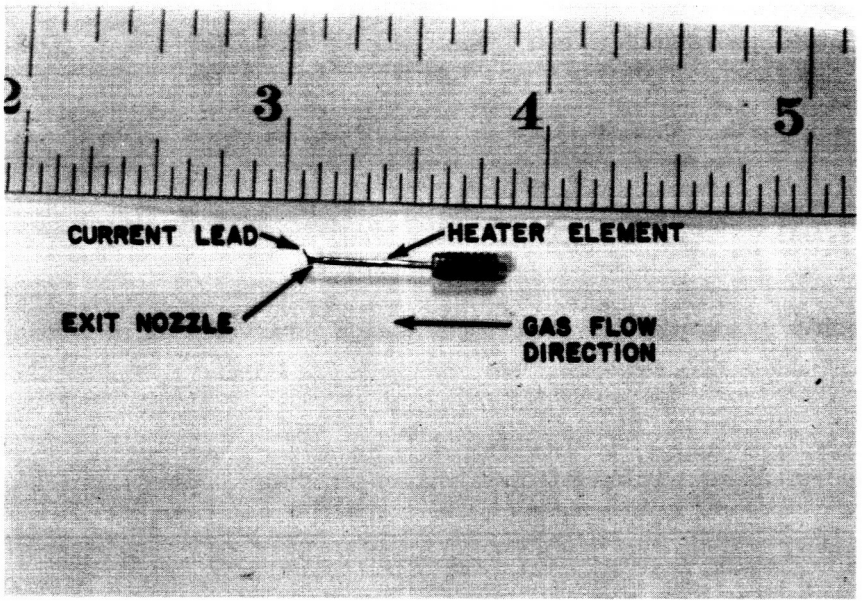

64-13179

Figure 15 FAST-HEATUP RESISTOJET

The resistance of the heating element remained remarkably constant at 0.12 to 0.13 ohm for the currents shown in table VI.

2. Heat Transfer Characteristics of the Fast Heatup Heating Element

The basic question to be answered in the development of the fast-heatup heating element is whether or not the lightweight element (order of milligrams) can provide sufficient surface area to transfer heat to the gas flow. A plot of maximum heater element temperature as recorded with an optical pyrometer as a function of electrical power input to the heater and ammonia flow rate is shown in figure 16. The power required to bring the heater to temperature increases markedly with increase in ammonia flow rate. The additional power must be going into the gas.

Figure 17 indicates engine chamber pressure as a function of heater current for different ammonia flow rates. At zero current the chamber pressure increases directly with flow rate as expected. At a fixed flow rate the chamber pressure increases with current, again indicating a transfer of heat from the heater to the ammonia flow.

From continuity considerations, the resistojet chamber pressure is given by a relation of the form

$$P \sim A_t \sqrt{\frac{T}{m}} \tag{25}$$

where P is the chamber pressure, A_t is the throat area, T is the gas stagnation temperature, and m is the gas molecular weight. The ratio of the chamber pressure when the engine is running hot, P_2, to the chamber pressure when the engine is running cold, P_1, is given by

$$\frac{P_2}{P_1} = \sqrt{\frac{T_2}{T_1}\,\frac{m_1}{m_2}} \tag{26}$$

The temperature-molecular weight ratio, $T_2 m_1 / T_1 m_2$, can be considered as a thermodynamic property of the working fluid. The thermodynamic properties of ammonia are presented in appendix F. Figure 18 presents a curve of gas temperature versus temperature-molecular weight ratio as a function of engine hot-to-cold chamber pressure ratio. Measurement of the ratio of engine chamber pressures for hot and cold operation can thus lead to a reasonable estimate of gas stagnation temperature without knowledge of the engine throat area.

The chamber pressure measurement is made at the entrance to the heater, and the pressure referred to in equation (25) is the pressure at the entrance

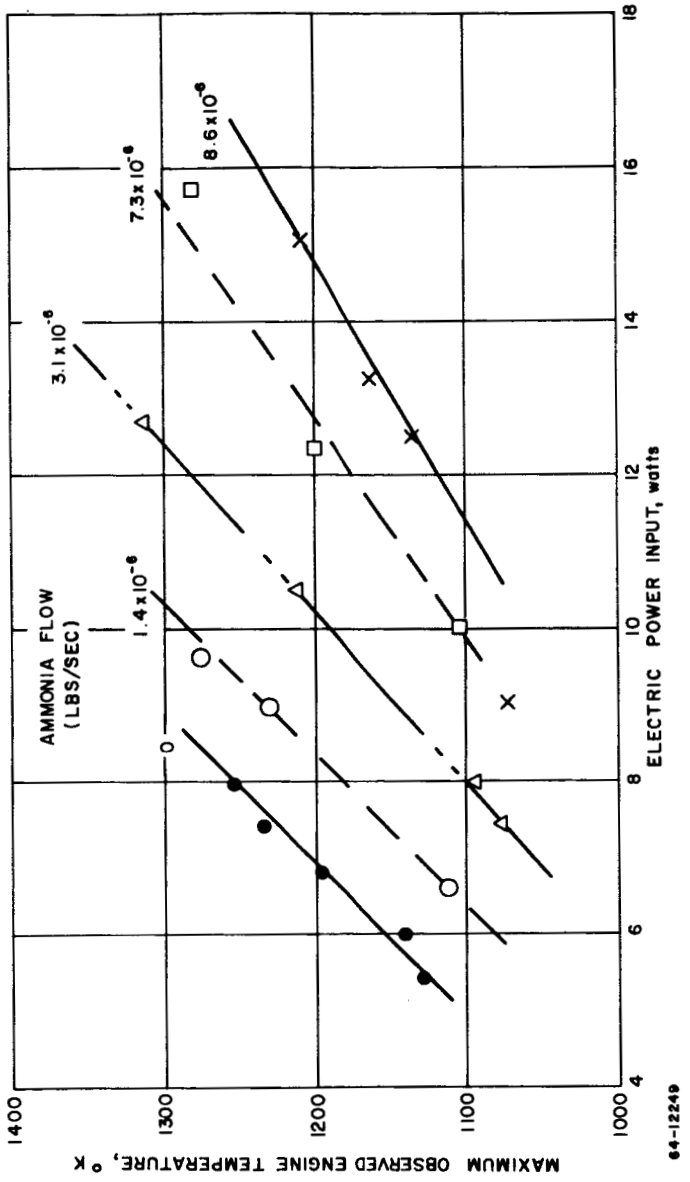

Figure 16 MAXIMUM OBSERVED THRUSTOR TEMPERATURE VERSUS POWER INPUT AND AMMONIA FLOW RATE

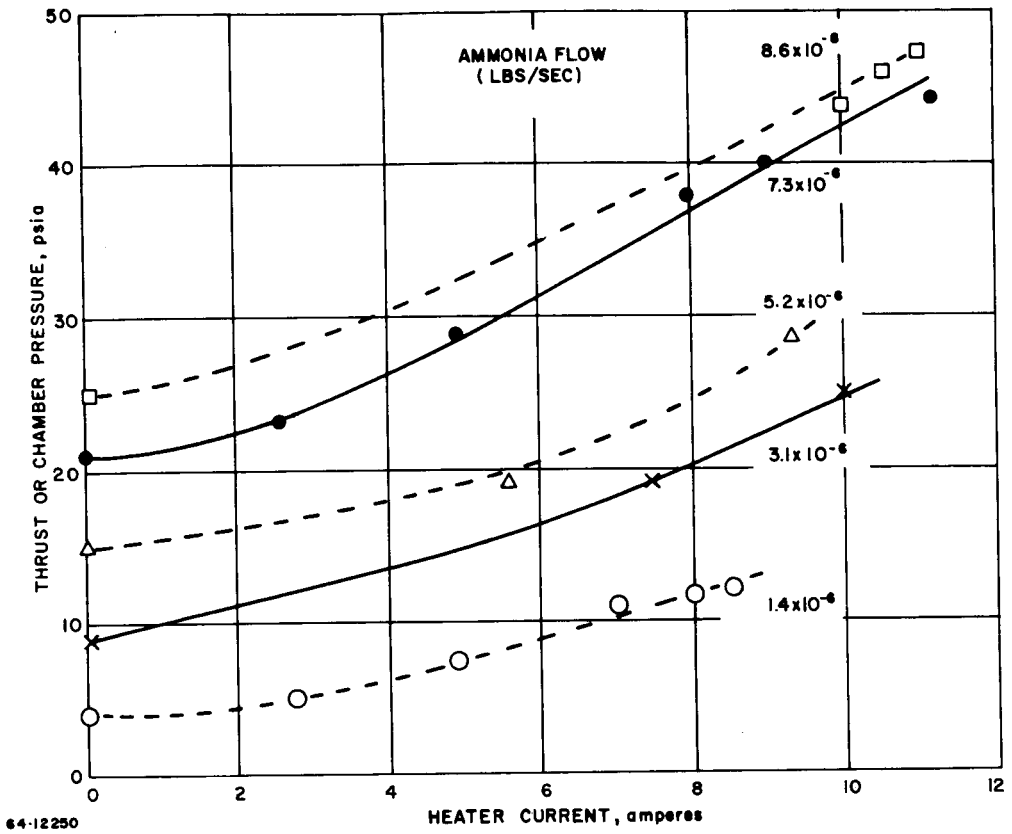

Figure 17 ENGINE CHAMBER PRESSURE VERSUS HEATER CURRENT AND AMMONIA FLOW RATE

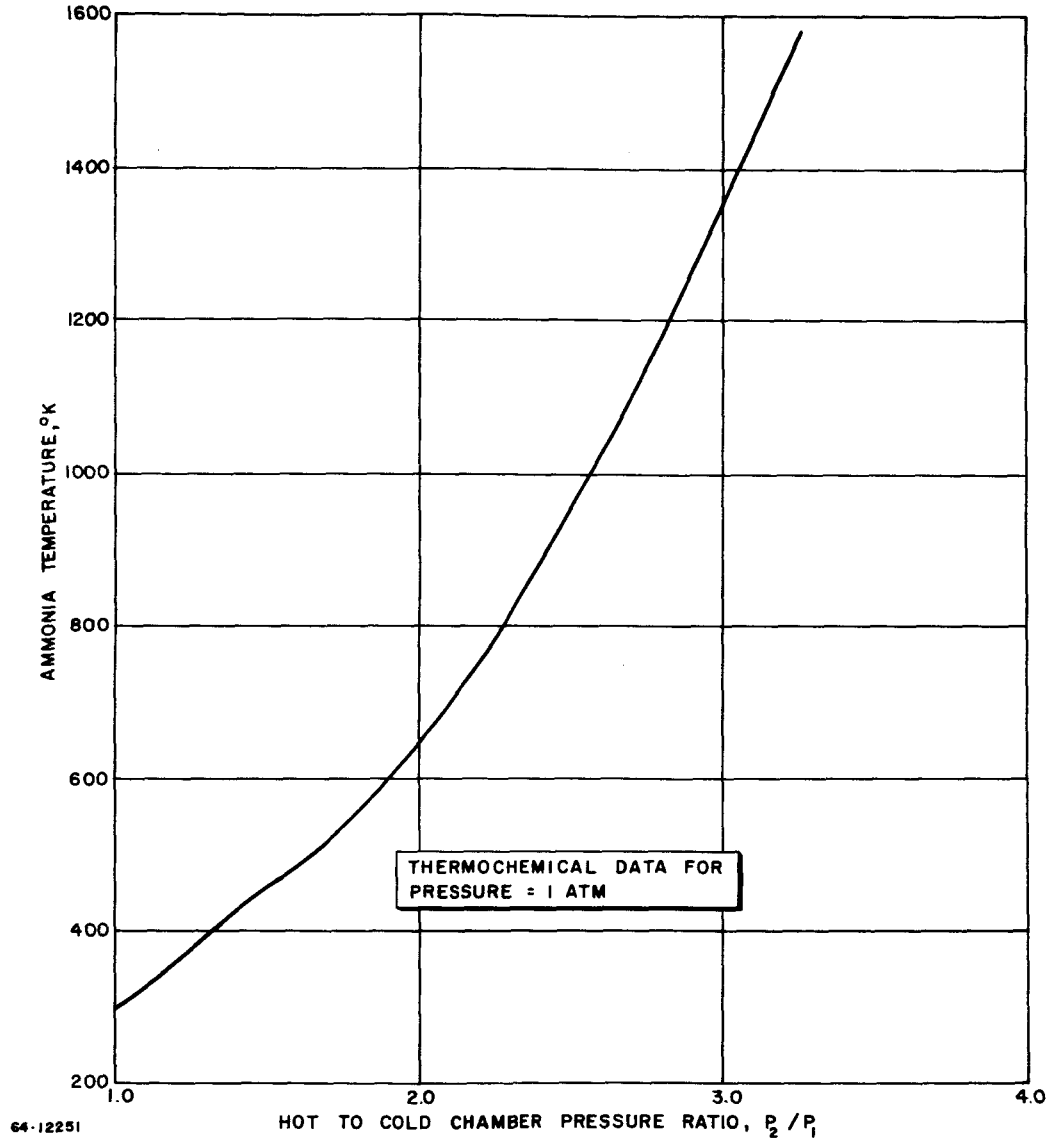

Figure 18 AMMONIA TEMPERATURE-MOLECULAR WEIGHT RATIO VERSUS HOT TO COLD CHAMBER PRESSURE RATIO

to the exit nozzle. The inlet pressure tends to be higher than the nozzle entrance pressure due to frictional pressure drop through the heater. This pressure drop can be as much as 10 percent of the heater inlet pressure; however, since the cold and hot flow frictional pressure drops are of the same order of magnitude, the effect of the pressure drop due to friction on the pressure ratio, P_2/P_1, is relatively small.

Figure 19 shows a curve of gas temperature as estimated from the hot to cold pressure ratio as a function of maximum engine temperature. Superimposed on the experimental results is the ideal curve corresponding to the gas temperature being equal to the engine temperature. At a given engine temperature the gas temperature decreases with increase in mass flow. Physically as the gas flow is increased there is not sufficient heater area to being the gas up to engine temperature.

The heat transfer processes within the heater are essentially laminar. The heat transfer coefficient for fully developed laminar flow within a tube is given by

$$\frac{hD}{k} \approx 4 \qquad (27)$$

where, h is the heat transfer coefficient, D is the tube diameter and k is the thermal conductivity. For example, the heater element has a tube diameter of 3.8×10^{-2} cm, and at 1000°K the thermal conductivity of ammonia is 2.7×10^{-3} watts/cm°K; the film coefficient is thus $h = (4)(2.7 \times 10^{-3})/(3.8 \times 10^{-2}) = 2.8 \times 10^{-1}$ watts/cm^{2}K; at a mean temperature difference between the heater and gas flow of 250°K the heat transfer per unit area would be about 70 watts/cm^2. The total heat transfer per unit heater element length is given by

$$Q_{conv,\,x} \approx \pi D h \, \Delta T = 4\pi k \, \Delta T \, . \qquad (28)$$

At a temperature difference of 250°K and a bulk gas temperature of 1000°K the heat transferred to the gas per unit length of heater is thus approximately 8.5 watts/cm. The observed mean heat transfer values are between 5 and 7 watts/cm at a nominal engine temperature of 1500°K. A reasonable design value appears to be about 5 watts/cm, independent of tube diameter as long as the flow is laminar, and assuming the gas temperature at the end of the heater and the peak heater temperature are nearly equal.

The electric-to-gas power energy conversion efficiency, assuming negligible heat conduction through the ends of the heater element, is given by

$$\epsilon_t = \frac{Q_{conv,\,x}}{Q_{conv,\,x} + \epsilon\sigma T^4 \pi D} = \frac{1}{1 + \dfrac{\epsilon\sigma T^4 \pi D}{Q_{conv,\,x}}} \, . \qquad (29)$$

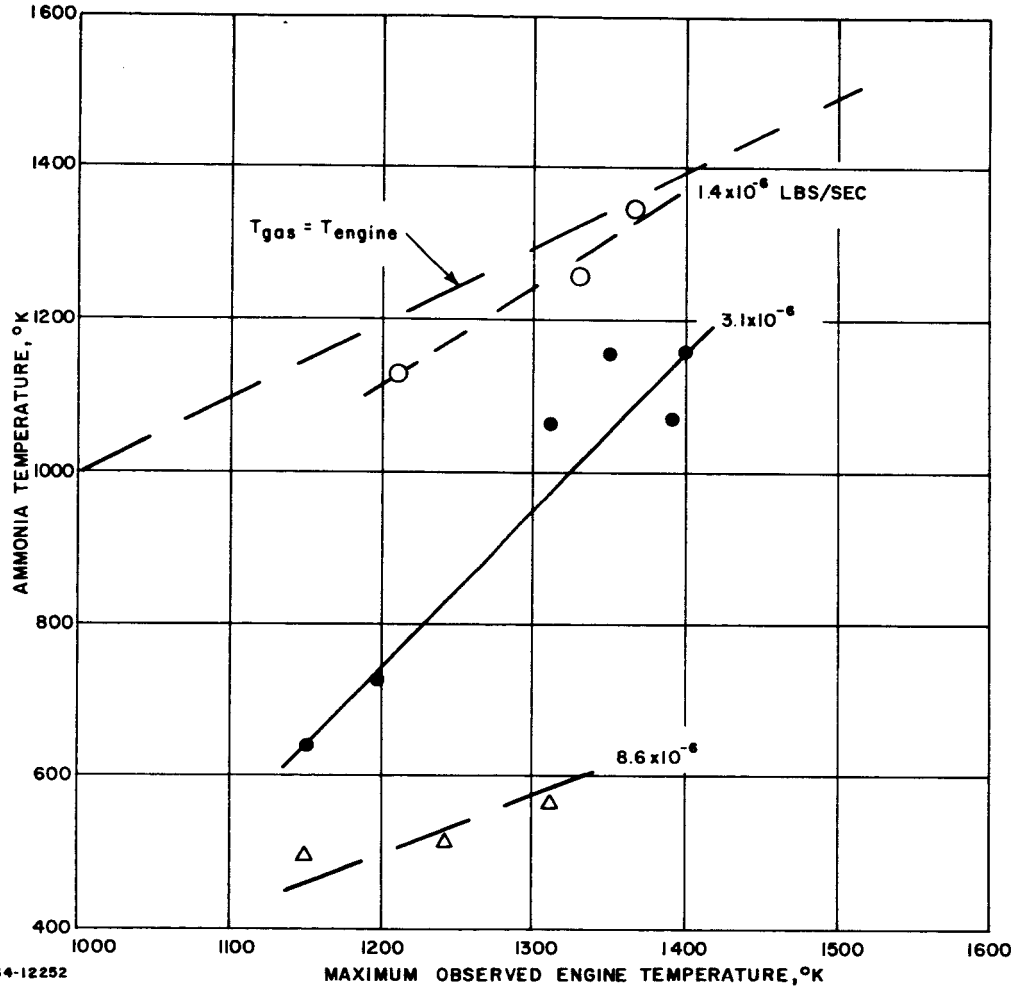

Figure 19 GAS TEMPERATURE VERSUS ENGINE TEMPERATURE AND AMMONIA FLOW RATE

In order to obtain a high thermal efficiency it is necessary that the heater diameter, D, and thus the ratio $\epsilon \sigma T^4 \pi D/Q_{conv,x}$ be held as small as possible. Thus, at a given operating temperature level, the engine diameter should be made as small as possible. At a fixed heater diameter the heater efficiency will fall off with increase in heater temperature.

To summarize, the results to date have indicated that lightweight (order of 10×10^{-3} gram) heater elements can be designed and constructed which have a heat transfer capacity of the order of 5 to 20 watts at ammonia flow rates of the order of 5×10^{-6} lb/sec and electric-to-gas power conversion efficiencies between 50 and 75 percent. Referring to table IV, the required thrust level for an attitude control thrustor is 10^{-3} pound; at a specific impulse of 300 seconds this corresponds to a thrust power of 6.6 watts, or assuming an expansion efficiency of 50 percent a gas power of 13.2 watts. Thus the single pass heat exchanger as described above has the heat transfer capacity necessary for control of a 500-pound satellite.

3. Heater Element Response Time and Cycling Capability

The response time of the heater element can to a first approximation be obtained from an expression of the form

$$T_{heatup} = \frac{M C_p \Delta T}{P_{input}} \qquad (30)$$

The mass of the prototype heater element is about 50×10^{-3} gram, the specific heat is about 0.10 cal/°C gm, the temperature rise about 1000°K, and the heat input about 15 watts or 3.6 cal/sec. The heat capacity of the device is about 5 calories and the heatup time is thus about 1.4 seconds. Decrease in heatup time can of course, be accomplished by reduction in the heater mass. Detailed numerical heat conduction calculations to supplement the above order of magnitude estimates are presented in appendix C.

A remaining important question concerns the ability of the engine structure to survive repeated thermal cycling between quite low temperature characteristic of exposure to the ambient space environment and the relatively high temperature characteristic of thrustor operation. Further, the heater material vapor pressure must be sufficiently low at the operating temperature that evaporation of the material does not reduce heater lifetime below three years. Finally, the heater material must be essentially inert with respect to NH_3, N_2 and H_2.

Of the available refractory metals, tungsten or a tungsten alloy or molybdenum appear most suitable. Tantalum is not inert to hydrogen, and rhenium availability is uncertain. Both tungsten and molybdenum are satisfactory in terms of their inertness and availability.

A series of tests was initiated to investigate the reliability of tungsten and molybdenum wires under repeated cycling. The tests were conducted within a glass chamber which had been evacuated and filled to atmospheric pressure with ammonia. The tests consisted of bringing tungsten and molybdenum wires and ribbons repeatedly to temperatures of approximately 2000°K from room temperature, by passing electrical current through them. Each thermal cycle consisted of approximately 1 second at the high temperature, followed by an interruption of the current for approximately 2 seconds. The entire operation was controlled by timers and relays.

The tungsten wires and ribbons were cycled 100,000 times without failure, and the test was terminated. The molybdenum elements failed characteristically after about 5000 cycles.

The indication of this preliminary test was that grain growth and recrystallization were sufficiently advanced in the molybdenum to cause embrittlement and shock failure. A more precise investigation was then made of these phenomena in the alloy 75 percent tungsten/25 percent rhenium. Previous experience has indicated that these wires may be run at temperatures much higher than 2000 °K for periods at least exceeding 293 hours, in the presence of a hydrogen flow.

Samples of this wire were electrically heated in vacuum for 15, 30, and 60 minutes to a temperature of 2000°C (~2300°K). A second set of samples was heated for equivalent total times with a duty cycle of 30 seconds on - 60 seconds off. Metallographic examination showed no microstructural difference between the two series of wires. Figure 20a is a photomicrograph of one of the first series of wires (continuous heat for 60 minutes), while figure 20b is a photomicrograph of one of the second series of wires (cycled heat for a total of 60 minutes on).

The conclusions of these cycling tests are that:

a. Tungsten or a tungsten alloy such as the 25 percent rhenium alloy should be satisfactory in terms of the thermal cycling requirement. Cycling seems not to affect the microstructure adversely in comparison to steady heating and there is already evidence that the total microstructure change is not sufficient to be damaging.

b. Molybdenum is unsatisfactory.

c. Tungsten is sufficiently inert to NH_3. The remaining tests which will be conducted in the next reporting period involve cycling the actual thrustor configuration to ascertain if the particular geometry in some way causes the reliability to deteriorate.

PLATE 3626 A 250 X

PLATE 3626A B 250X

64-12314

Figure 20 PHOTOMICROGRAPH OF THERMALLY CYCLED TUNGSTEN WIRE

4. Thrustor Propulsion Performance

Due to difficulties of thermal drift with the thrust stand when the engine was running hot, the thrust values for hot flow had to be deduced from the chamber pressure measurements. The procedure was as follows: Simultaneous measurements were made of the engine thrust and chamber pressure over the ammonia flow range from 2 to 10 μlb/sec for cold flow operation. The engine thrust was plotted as a function of chamber pressure; the results are shown in figure 21. As might be expected the cold flow thrust was directly proportional to the chamber pressure.

$$F = C_F A_t P_c \tag{31}$$

where, F is the measured thrust, C_F is the thrust coefficient, A_t is the throat area, and P_c is the chamber pressure. For the hot flow measurements the product of $C_F A_t$ was assumed to be the same as for cold flow; the hot flow thrust was therefore determined directly from the measured chamber pressure and the curve of thrust versus chamber pressure presented in figure 21. Essentially the assumption of a constant $C_F A$ is equivalent to the assumption of a constant nozzle expansion efficiency for hot and cold flow. The validity of the assumption will be checked upon elimination of the thrust stand thermal drift.

A summary of performance results on the resistojet thrustor are presented in table VII. A detailed summary of all the experimental data is presented in appendix E.

A plot of electric-to-thrust power energy conversion efficiency is presented in figure 22. The maximum attainable specific impulse level decreases with increase in ammonia flow rate because the heat transfer area is fixed, and at high flow rates there is not sufficient area to heat up the gas. At a specific impulse of 200 seconds and an engine operating temperature of 1500°K a reasonable design value for the electric-to-thrust power energy conversion efficiency is 25 percent.

E. THERMAL STORAGE THRUSTOR

Initial program emphasis was directed toward development of a thermal storage thrustor. The major advantages of this thrustor are that it avoids both thermal cycling and a control lag between the input signal and the resulting impulse bit, since it is always at operating temperature. The major drawback of this thrustor concept is that power must be continuously supplied, so that the average power consumption can be significant. The purpose of the initial investigations was to determine the feasibility of construction of a thermal storage thrustor, and to evaluate the standby power drain. The conclusions of these investigations are that the

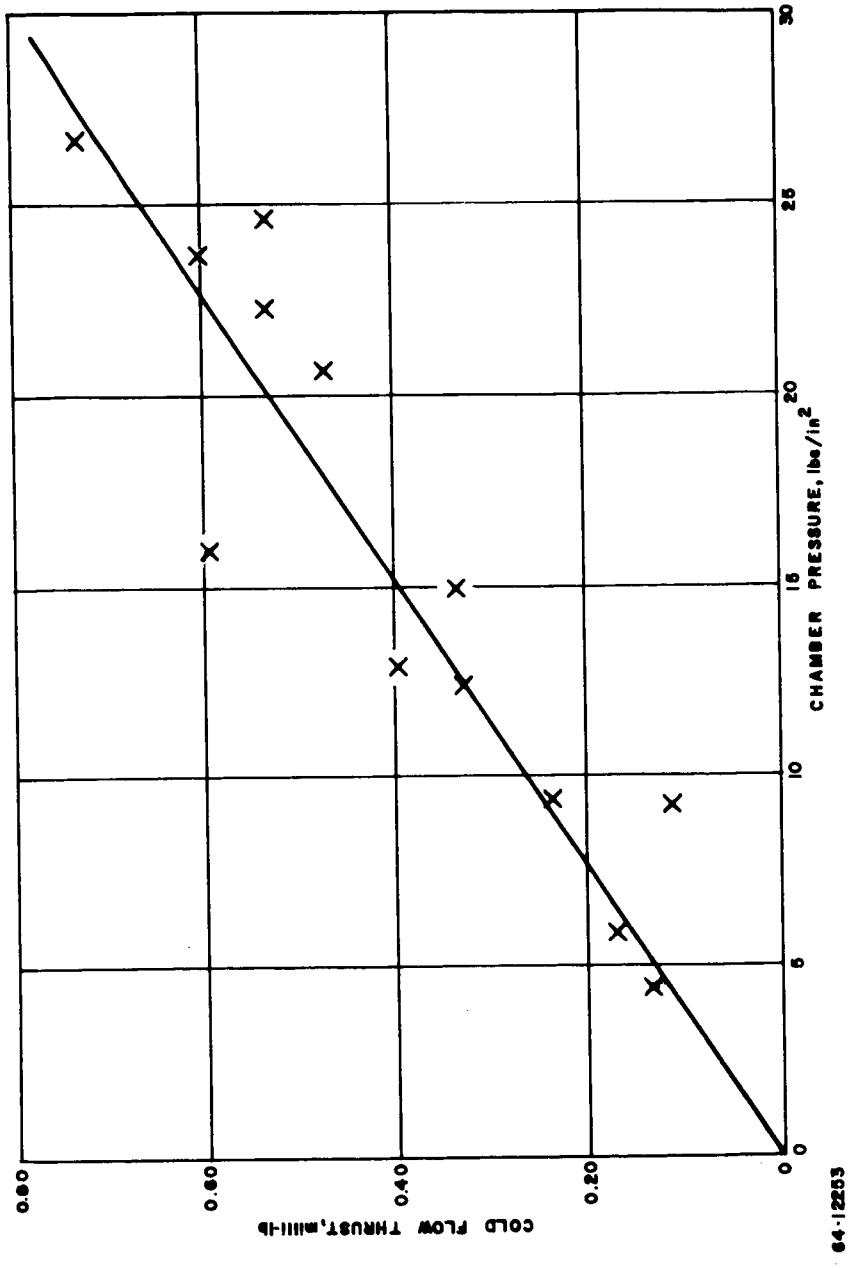

Figure 21 COLD ENGINE THRUST VERSUS CHAMBER PRESSURE

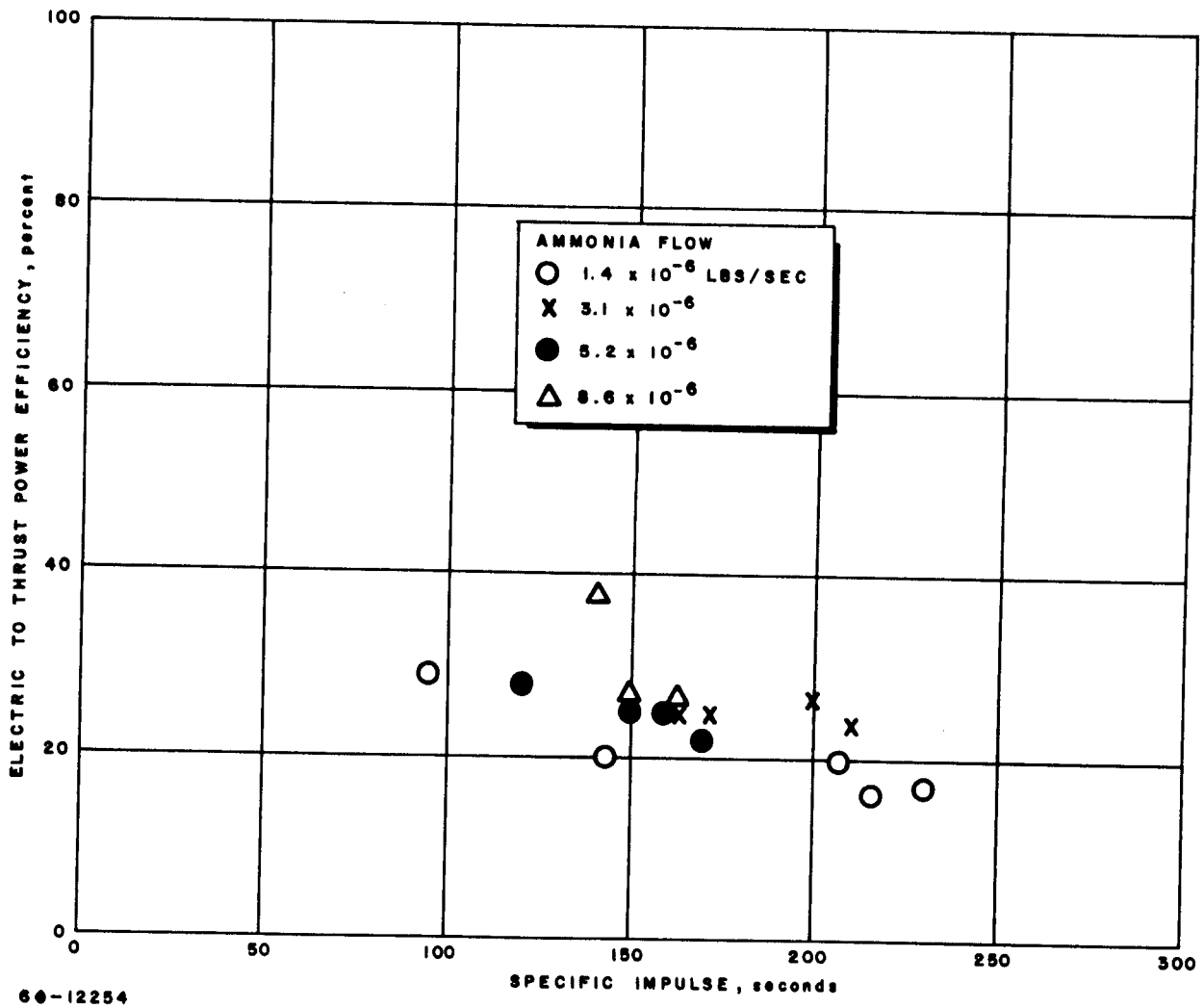

Figure 22 ELECTRIC-TO-THRUST POWER ENERGY CONVERSION EFFICIENCY VERSUS SPECIFIC IMPULSE

TABLE VII

RESISTOJET PROPULSION PERFORMANCE DATA
(stainless steel heater element)

Ammonia Flow (lb/sec)	Power Input (watts)	Thrust (pounds)	Specific Impulse (seconds)	Electric to Thrust Power, Efficiency (percent)
1.4×10^{-6}	---	0.10×10^{-3}	72	---
	1.5	0.13	93	30
	4.7	0.20	143	20
	9.8	0.29	207	20
	13.2	0.30	214	16
	14.3	0.32	228	17
3.1×10^{-6}	---	0.25×10^{-3}	81	---
	11.1	0.50	161	25
	12.3	0.53	171	25
	15.8	0.63	203	27
	18.0	0.66	212	23
	19.2	0.66	212	22
$5.2 \text{ z } 10^{-6}$	---	0.40×10^{-3}	77	---
	6.2	0.50	96	26
	8.8	0.62	119	28
	11.8	0.70	135	27
	14.9	0.82	158	25
	18.0	0.83	160	25
	25.0	0.97	187	23
7.3×10^{-6}	---	0.57×10^{-3}	78	---
	12	1.01	138	39
	18.9	1.07	146	27
	23.6	1.17	160	26
8.6×10^{-6}	---	0.66×10^{-3}	77	---
	14.4	1.11	129	34
	19.0	1.14	133	27
	23.0	1.25	145	26

thrustor construction is feasible, but that the power supply weight requirements are unacceptable for current estimates of solar cell weights (0.25 lb/watt).

1. Thrustor Configuration

The basic thermal storage thrustor configuration is indicated in figure 23. The heat transfer element is a resistance plug made of a composite material of the type discussed below. The thrustor casing is molybdenum. The propellant feed tube is electrically insulated from the resistance plug by boron nitride. During typical operation the thrustor would be surrounded by a large number of concentric cylindrical radiation shields. Appendix D discusses the effectiveness of radiation shields in some detail; the basic conclusion from these results is that the thrustor size is kept small, or the shielding problem becomes extremely difficult. A number of thermal storage thrustors of approximately 1/8-inch diameter were constructed. These thrustors with 10 radiation shields were kept at a temperature of 1500°C with a power input of 30 watts.

The use of a heat exchanger plug is attractive from the point of view of reliability; the design is intrinsically sturdy and resistant to shocks and vibration. However, because of its rather large ratio of cross sectional area to length, the resistance of a plug tends to be extremely low, which makes power handling and conditioning quite difficult problems. Therefore, effort was directed toward development of a high-temperature material with a resistivity order of magnitude higher than that of tungsten or other refractory metals. An additional material requirement was that the heater element be inert with respect to NH_3, N_2, and H_2.

2. Materials

With the assumption that the final thrustor cross sectional area for current flow will be of the order of 10^{-1} cm^2, and that the final length will be of order of 2 cm, the requirement that the overall resistance be of the order of a least 0.1 ohm can be translated to a required resistivity of 10^{-3} to 5×10^{-3} ohm-cm. This is substantially larger than the resistivity of pure tungsten, which is about 5×10^{-5} ohm-cm at 2000°K. The resistivities of refractory carbides, nitrides, and borides are also too small to hold the overall thrustor resistance at an acceptable value. The oxides are insulators at temperatures of the order of 2000°K, and extremely good insulators at room temperature; thus, they cannot be heated to high temperature from lower temperatures by passage of electric current.

As a result of these considerations, attention was focussed on mixtures of refractory metals and metal oxides. Tungsten and molybdenum were the choices for the refractory metal because of their inertness, high-temperature capability, and availability.

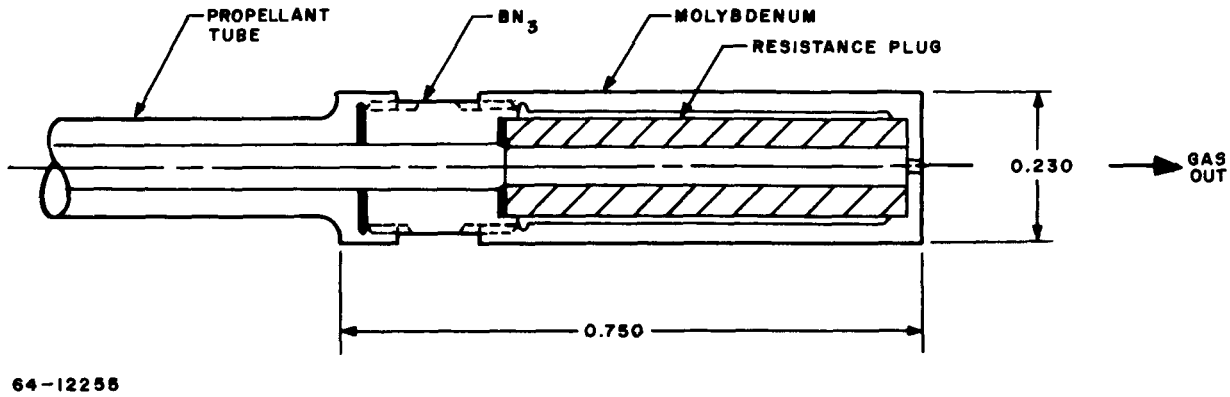

Figure 23 THERMAL STORAGE THRUSTOR CONFIGURATION

The selection of an insulator was based on melting point, evaporation rate, compatibility with molybdenum or tungsten, and inertness to ammonia and/or dissociated ammonia. Many insulators have melting points in excess fo 2000°C, for instance Al_2O_3, MgO, ZrO_2 and ThO_2. Evaporation rates for these materials have been reported by Wolff and Alcock.[5] At 2000°C the evaporation rate of Al_2O_3 is about 2×10^{-6} grams/cm^2-sec, for MgO about 8×10^{-4}, for both ZrO_2 and ThO_2 about 6×10^{-7}. If the oxide particles are of the order of 25 to 50 microns in size, the above evaporation rates indicate that oxide particles at the surface of the heater element will evaporate after 1 to 10 days at 2000°C. However, those particles in the heater interior will not evaporate if no connection to the outer surface exists. This was the case for the samples studied and therefore it is reasonable to assume that any of the four above oxides will be satisfactory for use on the basis of evaporation rate.

The question of compatibility with NH_3, H_2, or N_2 is not as readily treated. In general the oxides are inert to NH_3 and will not be reduced to a measurable extent by H_2 even at 2000°C.[6] These materials are also relatively inert to N_2 although ZrO_2 may form a surface nitride after long exposure times. However, surface reactions are not important as these particles will evaporate soon after engine operation is initiated.

According to a Climax Molybdenum Company publication,[7] molybdenum does not react with Al_2O_3 MgO, ZrO_2 or ThO_2 at 2000,C. Similarly tungsten is compatible with the oxides at this temperature. Al_2O_3 and ZrO_2 were evaluated with molybdenum and tungsten as composite heater materials. At 2000°C, the resistivity of Al_2O_3 is 1×10^4 ohm-cm and that of ZrO_2 is about 1 ohm-cm, thereby a wide spread of resistivities could be studied. MgO has a resistivity intermediate between those of Al_2O_3 and ZrO_2 and was not selected for inital evaluation. ThO_2 is mildly radioactive and therefore not considered for initial studies.

The composite materials studies are described in detail in appendix G. Briefly, composite materials were made by sintering powdered mixtures of the refractory metals and the oxides. The resulting composite slugs were machinable, and could be made with resistance values in the desired range. However, the resistance values "as manufactured" were altered substantially by reheating in a 5- to 50-micron vacuum for a relatively short period of time; this was accompanied by detectable changes in microstructure. Therefore, the stability of the composite materials in terms of electrical resistance is still open to question. Because of the promise of the fast-heatup thrustor these materials studies have been at present deemphasized.

3. Thermal Storage Steady State Power Consumption

The utility of the thermal storage thrustor depends in great measure on the required input power level. Analytical studies were made of the heat losses to be expected from a shielded thermal storage thrustor (see appendix D). Briefly stated, the conclusions are that:

a. For reasonable assupmtions about the thrustor geometry and shield characteristics, the radiative loss will be between 2 and 6 watts/cm length.

b. Lead losses by conduction will be comparable in size to the radiation for a thrustor approximately 2 cm long.

Hence, it seems a realistic assumption that the steady state power requirement for a well-designed thermal storage thrustor will be at least 10 watts. For a 3-axis attitude control and station keeping system on a 500-pound satellite which may involve as many as 12 thrustors, this represents an unacceptable power load.

III. SINGLE-AXIS LABORATORY ATTITUDE CONTROL SYSTEM

A. BACKGROUND

Work is underway on the design, development, and fabrication of a single-axis resistojet attitude control system suitable for operation on the air bearing recently installed in the electric propulsion test facility at the NASA, Lewis Research Center. The attitude control system test bed to be supplied by NASA Lewis will have a moment of inertia of ~ 27 slug-ft^2 which is similar to that of the design satellite, of table I. The test bed will be isolated from the laboratory, and will be completely self-contained. Power will be supplied to the engine from batteries located on the test bed. Communication to and from the test bed will be accomplished by means of a telemetry system. The test will be designed to simulate an actual space mission as far as is possible in the laboratory. An initial interface meeting has been held with NASA Lewis personnel; a preliminary division of responsibility was agreed upon for the different system components. Briefly, Avco RAD will deliver the thrustors, propellant tankage, sensors, control logic, and power conditioning packages; NASA Lewis will supply the engine test bed, battery power supply, command receiver, and telemetry package. A further meeting is planned within the next month to further define the electrical, mechanical, and instrumentation interfaces.

The thrustors for the single-axis thrust system will be similar to those being developed for the attitude and orbit control of the 500-pound satellite. The power input will be of the order of 50 watts, the specific impulse about 275 seconds, and the thrust level about 10^{-3} pound; the working fluid from the viewpoint of storage considerations will be ammonia. The characteristics of the air bearing are still being determined; however, it is presently contemplated that a constant disturbance torque of a few hundred dyne-cm may be applied to the bearing and that the control system will operate in the soft limit cycle.

B. CONTROL SYSTEM DESCRIPTION

A block diagram of the single-axis control system is shown in figure 24. One of the control techniques best suited for the present application is that of Gaylord and Keller.[8] In this type of attitude control system vehicle angular rate is controlled to a very low threshold by the use of time-dependent on-off switching circuits which generate discrete thrust pulses of small but constant time duration. By using a number of switching levels to generate fixed but different thrust impulses, the need for precise rate sensing and rate gyros is eliminated and fuel consumption is minimized.

The attitude sensor can be calibrated to set the desired backup and sector switch locations. Command logic is such that a positive rate will actuate

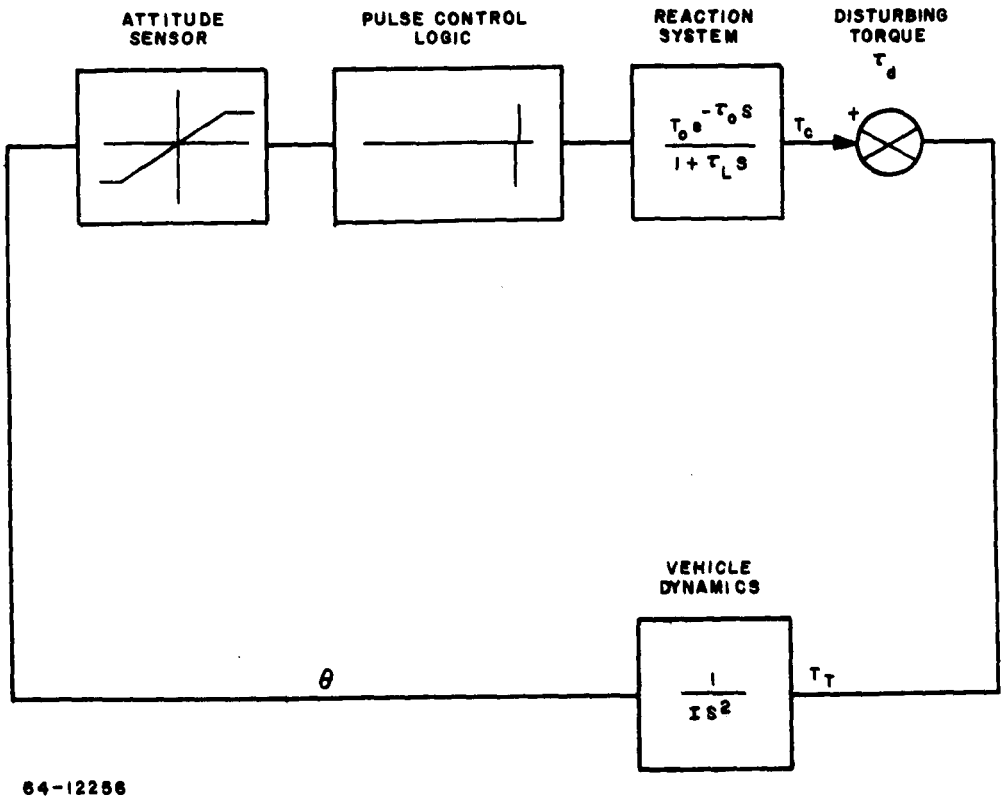

Figure 24 FUNCTIONAL BLOCK DIAGRAM OF THE RESISTOJET SINGLE-AXIS ATTITUDE CONTROL SYSTEM

the negative impulse sector switches, and vice versa. That is, attitude control is provided by pulse torquing the vehicle according to attitude error limits and damping the motion by using phase-plane quadrant information. Attitude error increases in quadrants I and III and only in these quadrants is control action, other than backup required. The pulse torquing logic in quadrants I and III consists of defining a number of switching lines and using a unique jet pulse size for each switching line. Each switch meters a given velocity increment to reduce attitude error in such a manner that a limit cycle can be established within the desired deadband.

C. CONTROL SYSTEM ANALYSIS

The system being analyzed uses a control logic with three pairs of fixed impulse switching lines and a pair for backup. Based on statistical considerations, to ensure meeting the desired accuracy, the first set of switching lines is located at ±0.2 degree. Two more are placed at ±0.5 and ±1 degree. The backup lines are located at ±2 degrees with hysteresis so that torque dropout occurs at 1.96 degrees. The angular rate increments, $\Delta\dot{\theta}_j$ (j = 1, 2, 3) commanded at the three sets of switching lines are based on the following analysis.

$$\Delta\dot{\theta} = \sqrt{4\frac{T_d}{I}\theta} \tag{32}$$

where

T_d = disturbing torque, 500 dyne-cm

I = moment of inertia, 41.2 slug-ft^2

θ = angular position, 0.2 degree

$\dot{\theta}_1$ = 0.00641 deg/sec

To make the probability of a 2-pulse limit cycle near zero $\Delta\dot{\theta}_2$ is selected slightly less than $\Delta\dot{\theta}_1$ so we let $\Delta\dot{\theta}_2$ = 0.006 deg/sec. Similarly, $\Delta\dot{\theta}_3$ must satisfy.

$$\Delta\dot{\theta}_3 < \Delta\dot{\theta}_1 + \Delta\dot{\theta}_2 \tag{33}$$

To locate the backup lines, the following inequality must be satisfied to ensure a convergent trajectory

$$\Delta\dot{\theta}_1 + \Delta\dot{\theta}_2 + \Delta\dot{\theta}_3 > \Delta\dot{\theta}_o - \Delta\dot{\theta}_i \tag{34}$$

where

$\dot{\theta}_i$ = angular rate at which backup switching occurs

$\dot{\theta}_o$ = angular rate at which dropout occurs.

Considering $\Delta \dot{\theta}_i$ to be $\Delta \dot{\theta}_1$, we see that

$$\Delta \dot{\theta}_o < 0.0308 \text{ deg/sec.}$$

The parabolic trajectory in the phase plane is given by

$$\Delta \dot{\theta}_o^2 - \Delta \dot{\theta}_i^2 = -2\alpha(\theta_o - \theta_i) \tag{35}$$

where

$$\alpha = \frac{T_o}{I} = 5.563 \times 10^{-3} \text{ deg/sec}^2 .$$

If there were no delays in obtaining full torque, equation (35) would serve to determine the angle at which torque drops out, θ_o, directly by letting $\theta_i = 2°$. Actually, however, there will be a delay of approximately 1 second before T_o is realized. The incremental change in θ_i is then $\Delta \theta_i = 1 \times 0.00641 = 0.0064°$ so switching occurs at $\theta_i = 2.0064$. Using this value as the initial angle and letting $\dot{\theta}_o = 0.025$ deg/sec, equation (35) gives $\theta_o = 1.98°$, so the backup lines are tentatively set at ±2° and ±1.98°.

These values of fixed-velocity incremental along with the locations of the switching lines are being used in the analog computer simulation. This will allow an investigation of their effects on system performance and a subsequent system optimization.

IV. WEIGHT ESTIMATES FOR A FLYABLE ATTITUDE AND ORBIT CONTROL SYSTEM

Preliminary weight estimates for the attitude control and station keeping system of the 500-pound satellite described in table I are presented below. These weight estimates will be continually revised as the program proceeds and new information becomes available.

A. ASSUMPTIONS

1. Constant disturbance torque of 500 dyne-cm

2. Soft limit cycle

3. Three-year mission

4. Attitude control impulse requirement (soft cycle)

Single-axis	585 lb-sec/year
Single-axis (3 years)	1755 lb-sec
Three-axis (3 years)	5265 lb-sec

5. Station keeping impulse requirement (minimum)

1 year	2640 lb-sec
3 years	7920 lb-sec

B. ENGINE PERFORMANCE

1. Thrust	10^{-3} pound
2. Specific impulse	263 seconds
3. Power input	35 watts
4. Peak operating temperature (no gas flow)	2400°K
5. Peak Temperature (gas flow)	2000°K
6. Overall efficiency (electric to thrust)	16 percent

7.	Thrustor Mass	50×10^{-3} gram
8.	Attitude control duty cycle Station keeping duty cycle	5 percent 10 percent

C. SYSTEM WEIGHT FOR 12 THRUSTORS

		Weight (pounds)
1.	Ammonia	50
2.	Tankage	5
3.	Controls	6
4.	Valves	6
5.	Solar Power Supply	9
6.	Structure	5
7.	Miscellaneous	5
8.	Total System	86

It is stressed that the preceding weight estimates are preliminary; however, it is interesting to note that a control engine having a specific impulse of 75 seconds, which is about the state of the art at thrust levels of the order of 10^{-3} pound, would require nearly 175 pounds of propellant for the above mission. Thus, although many questions remain unanswered the fast-heatup resistojet hold some promise for attitude and orbit control of satellites in the 500 to 1000-pound class.

V. DIRECTION FOR FUTURE RESEARCH AND DEVELOPMENT

During the next quarter, effort will be directed to the following areas:

A. THRUST MEASUREMENT SYSTEM

A series of cooled baffles will be introduced into the thrust stand vacuum chamber in an attempt to eliminate the thermal drift of the string-in-tension thrust stand when the engine is running hot. A larger diffusion pump will be installed on the thrust stand vacuum system in order to obtain tank pressures of the order of 10^{-4} mm of Hg during semicontinuous engine operation. A new displacement transducer with a sensitivity of 10^{-7} inch will be used on the thrust stand in order to reduce the value of minimum measurable thrust.

B. RESISTOJET THRUSTOR DEVELOPMENT

Work will be continued on the 5-to 50-watt fast-heatup resistojet thrustor using ammonia as the working fluid. Work on the thermal storage thrustor concept will be deemphasized. Engine propulsion performance measurements will be continued to verify the existing engine heat transfer concepts. Engines will be fabricated from tungsten in order to increase the normal operating temperature from the 1500°K characteristic of stainless steel to the 2000° to 2500°K characteristic of tungsten. The prototypes were made of stainless steel because of both its availability and machinability. By going to the higher tungsten operating temperatures the nominal engine specific impulse range should be increased from the present 200 seconds to close to 275 or even 300 seconds. An experimental study will carried out on the shape of the impulse bit and an investigation made of the effect of engine volume and valve characteristics on the thrustor response time. Finally, experiments will be continued to determine the thermal cycling capability of potential heater materials.

C. SINGLE AXIS ATTITUDE CONTROL SYSTEM

Work will be continued on the design and development of a single-axis attitude control system to be evaluated on the air bearing at the NASA Lewis Electric Propulsion Test Facility. A breadboard-control logic package will be constructed and evaluated on an analog computer. Thermal, mechanical, and electrical design studies will be carried out and fabrication started on the single axis attitude control system to be delivered for evaluation at NASA Lewis. Preliminary schedules call for the control system, including thrustors, propellant tankage, control logic and power conditioning packages, and instrumentation to be delivered in January or February, 1965. Schedules and the thermal, mechanical, and electrical interfaces with NASA Lewis will be firmly established during the next quarter.

D. ENGINE PROPULSION PERFORMANCE REQUIREMENTS

Effort will be continued on the establishment of the propulsion performance required of the attitude control and station keeping system for the 500-pound satellite. In particular, studies will be carried out on the effect of impulse height, width, and frequency on the total impulse requirements for satellite station keeping. This work will be continuation of the studies performed by J. H. Molitor with emphasis in the propulsion characteristics of resistojet rather than ion engines.

E. DESIGN OF A THREE-AXIS PROTOTYPE ATTITUDE CONTROL AND STATION KEEPING SYSTEM

The weight estimates for the design satellite control syste will be continually revised as new engine performance and system weight data becomes available. Preliminary layouts and design studies will be initiated with the purpose of verifying the compatibility of the fast-heatup resistojet attitude control system with a 500-pound satellite.

VI. REFERENCES

1. Boucher, R. A. J. Spacecraft and Rockets, 1, 164 (1964).

2. Molitor, J. H. and M. H. Kaplan, J. Spacecraft and Rockets, 1, 557 (1964).

3. Molitor, J. H., J. Spacecraft and Rockets, 1, 170 (1964).

4. Cybulski, R., Private Communication, (September 1964).

5. Wolff, E. G., and C. B. Alcock, Trans. Brit. Ceram. Soc. 61, 667 (1962).

6. Vasilos, T., Avco RAD, Private Communication (September 1964).

7. Nair, F. B. and J. Z. Briggs, Corrosion Resistance of Molybdenum and Molybdenum Base Alloys. Climax Molybdenum Co. Detroit, Michgan (1964).

8. Gayloard, R. S. and W. N. Keller, Guidance and Control, Progress in Astronautics and Rocketry, Academic Press, 8, (1962).

APPENDIXES

A. STATION KEEPING REQUIREMENTS

B. THRUST STAND

C. HEATUP TIME FOR FAST HEATUP THRUSTOR

D. HEAT LOSS FROM A THERMAL STORAGE THRUSTOR

E. THRUSTOR PERFORMANCE DATA

F. THERMODYNAMIC PROPERTIES OF AMMONIA

G. COMPOSITE MATERIALS FOR THERMAL STORAGE THRUSTORS

APPENDIX A

STATION KEEPING REQUIREMENTS

The orbit of the synchronous satellite is subject to perturbations which will cause apparent angular motion of the satellite in the sky. Perturbations exist which will produce apparent motion in longitude (East-West motion) and latitude (North-South motion.) To maintain the satellite position within prescribed error limits (± 0.1 degree) a "station-keeping" system must be employed to deliver corrective thrusts.

Requirements on the corrective thrust have been discussed in references 1 and 2; the values reported in these references have been used in the discussion given earlier in this report. Work is currently underway at Avco RAD to extend the results of Boucher and Molitor to higher thrust levels, so that impulse requirements may be established for a wider range of possible thrust sequences.

An existing Avco RAD digital computer code (program 1546) is being used to solve the satellite equations of motion. This computer code allows insertion of arbitrary thrust sequences. Included as subroutines in the equations of motion are the important perturbations on the satellite orbit. The equations of motion are integrated using the "generalized variational method".[3]

The following perturbations are available as subroutines for use with program 1546:

1. The first three Earth oblateness terms

2. Triaxiality of the Earth

3. Gravitation attraction of sun, moon, Jupiter, Venus (ephemeris data for the period 1960 to 1980 are available on magnetic tape)

4. Solar radiation pressure.

Up to the present time the computer program has been used to evaluate the relative importance of the various perturbations by exploring their effect on the satellite position singly, with no corrective torque application. Results which have been obtained are summarized in figures 25 through 28. Figures 25 and 26 give, as a function of time, the variations in satellite latitude and altitude owing to lunar gravitational attraction. Figures 27 and 28 show the variation in satellite longitude owing to oblateness and triaxiality, respectively.

During the next reporting period this initial study will be completed, and the effects of various corrective thrust levels and thrusting schedules will be evaluated.

References

1. Boucher, R. A., J. Spacecraft and Rockets, 1, 164 (1964).

2. Molitor, J. H., J. Spacecraft and Rockets, 1, 170 (1964).

3. Battin, R., Astronautical Guidance, McGraw - Hill (1964).

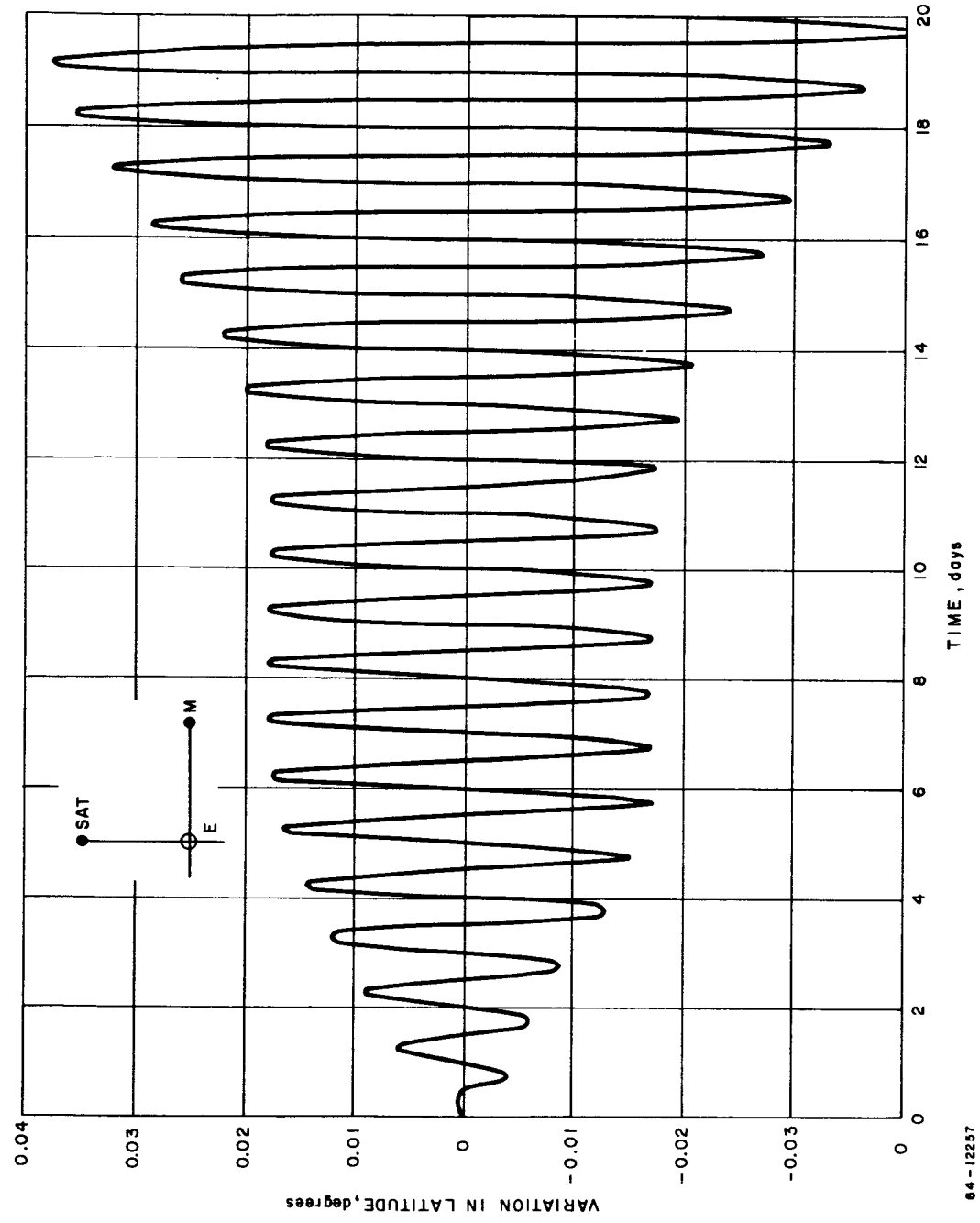

Figure 25 VARIATION IN LATITUDE DUE TO LUNAR GRAVITATIONAL ATTRACTION

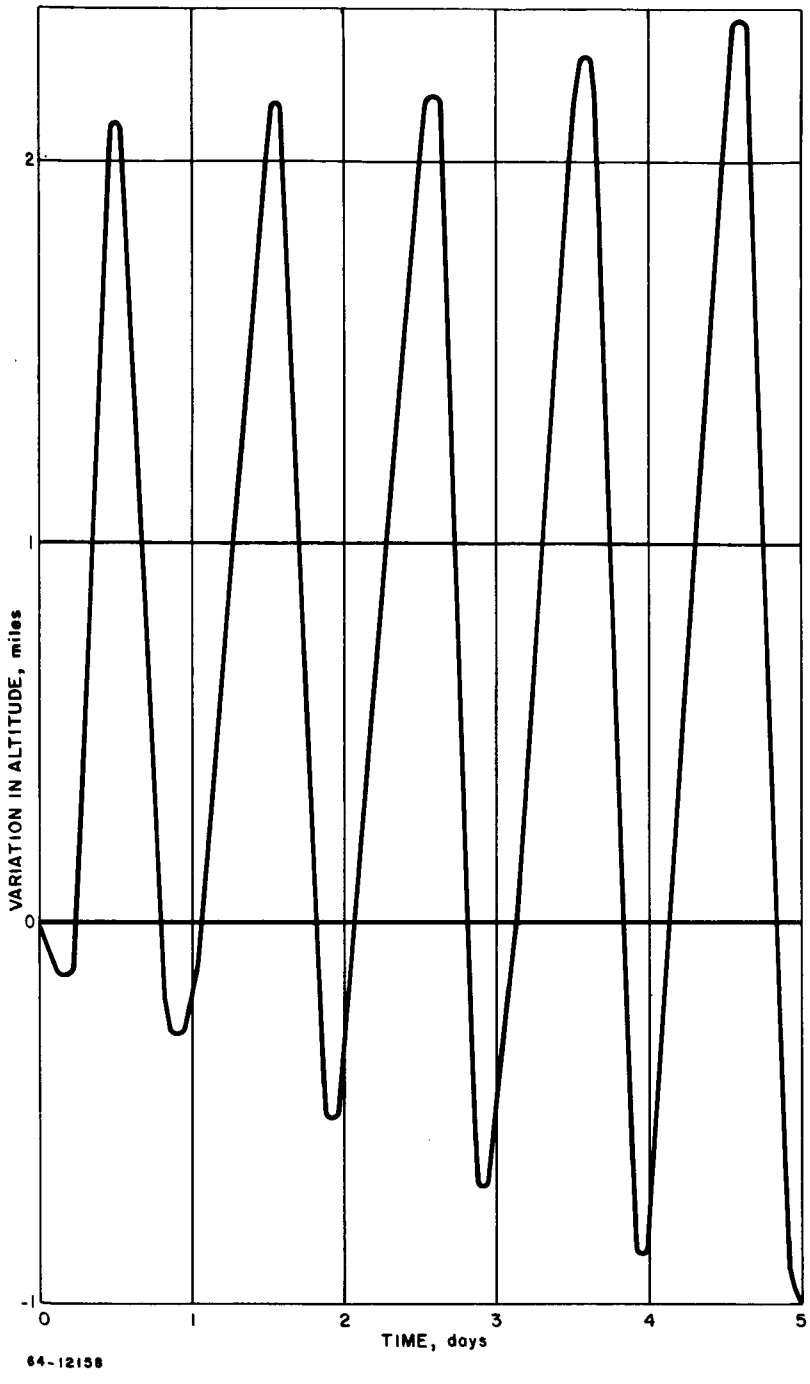

Figure 26 VARIATION IN ALTITUDE DUE TO LUNAR GRAVITATIONAL ATTRACTION

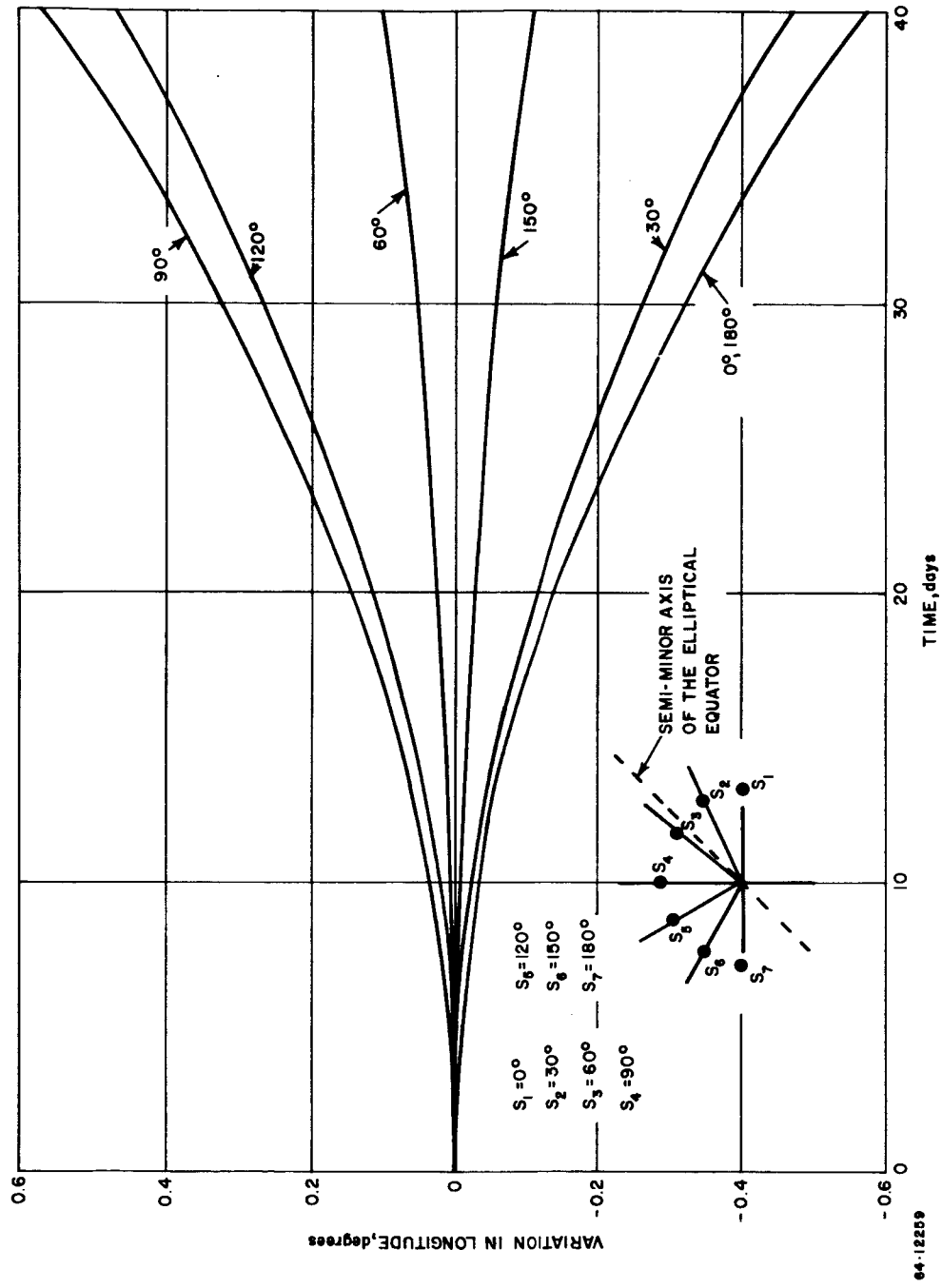

Figure 27 VARIATION IN LONGITUDE DUE TO EARTH OBLATENESS

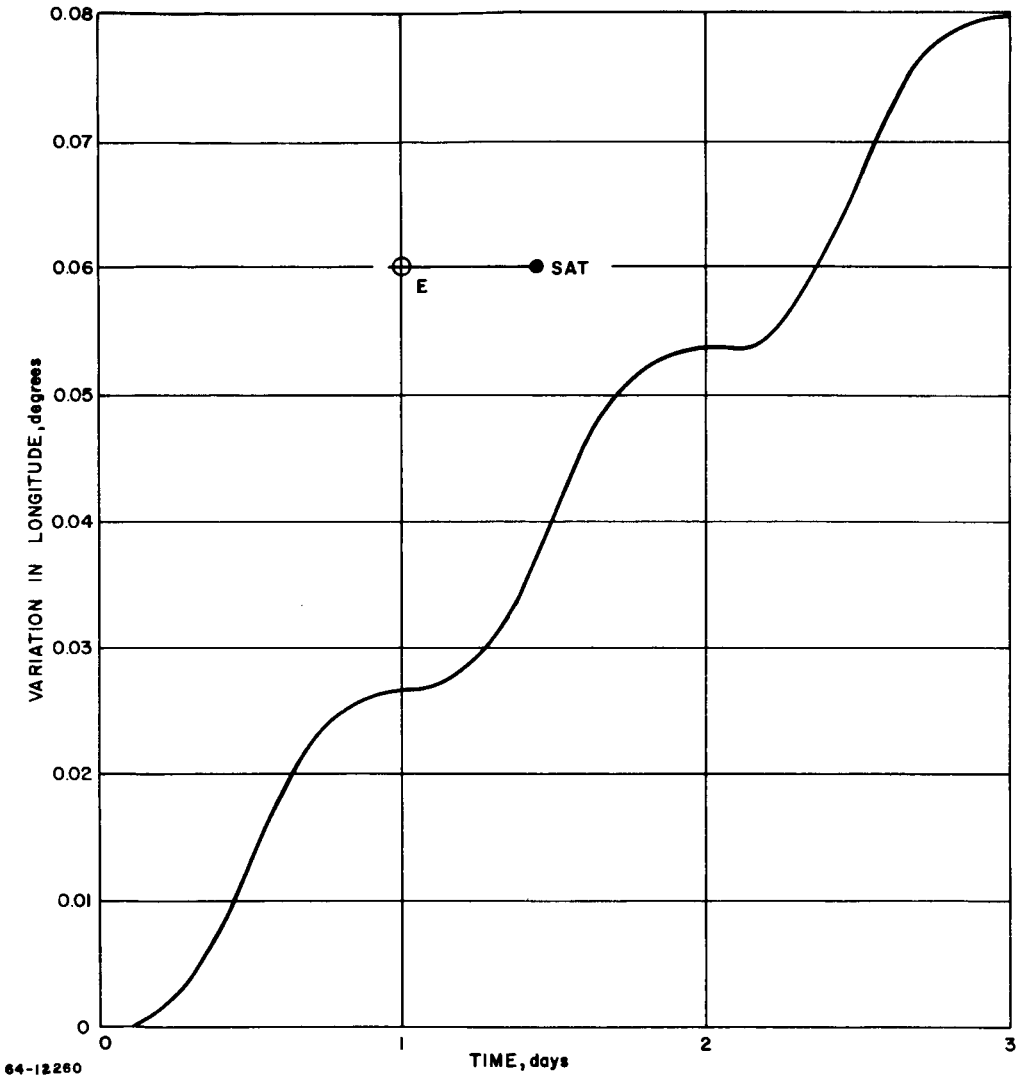

Figure 28 VARIATION IN LONGITUDE DUE TO TRIAXIALITY

APPENDIX B

THRUST STAND SYSTEM

In order to measure performance of thrustors operating in the millipound thrust range in the pulsed mode, the thrust measurement system depicted in figure 9 has been employed. Basically, the thrust stand consists of a central horizontal ring suspended by four wires in tension from a massive concentric ring. The thrustor and propellant supply are mounted on the central ring, aligned so that the thrust direction is vertical. Application of thrust causes the central ring to move until the vertical component of the wire tension exactly balances the applied thrust. The response time of the thrust stand is related to the natural frequency of vibration of the light central ring, which is in turn controlable through adjustment of the tension in the supporting wires. The displacement of the central ring, which is proportional to the applied thrust, is measured by a linear differential transformer. The massive support ring is suspended on long, fairly soft springs to provide seismic isolation.

To solve the equation of motion for the thrust stand; the thrust stand is simplified to the case of a string of mass per unit length, ρ, under a tension T, stretched between two fixed supports separated by a distance L, and loaded at its center with a mass M. (See figure 29.) A force (thrust) F is instantaneously applied at the center $X = \xi = \frac{L}{2}$ and the ensuing motion, for constant force, is governed by the differential equation:

$$[\rho + M\delta(x - \xi)] \frac{\partial^2 y}{\partial t^2} + f \frac{\partial y}{\partial t} = T \frac{\partial^2 y}{\partial x^2} - \rho g - (Mg + F)\delta(x - \xi) \tag{36a}$$

where the thrust is assumed to be directed in the negative direction (down). The displacement of each point on the string, $y(x,t)$, is fully determined by the boundary and initial conditions, viz:

$$y(0, t) = 0 \qquad y(L, t) = 0 \tag{36b}$$

$$\frac{\partial y(x, 0)}{\partial t} = 0 \qquad y(x, 0) = v(x) \ . \tag{36c}$$

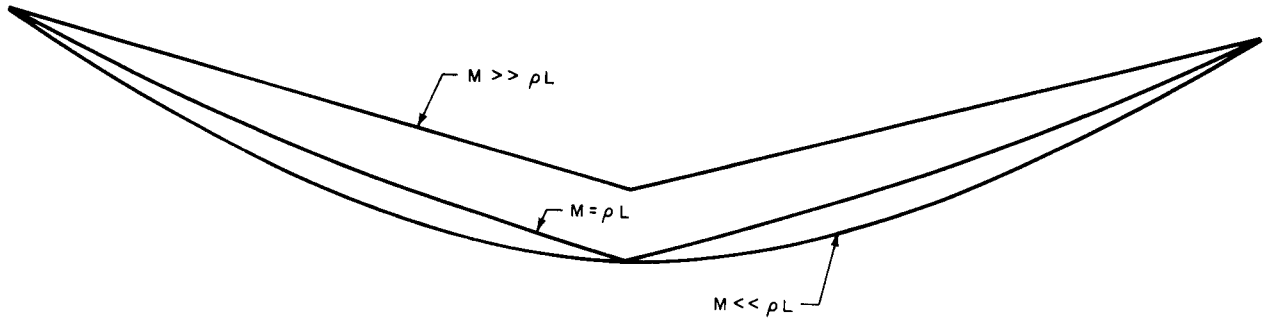

64-12261

Figure 29 SIMPLIFIED SCHEMATIC OF WIRE-IN TENSION THRUST STAND

The conditions (36b) fix the end points of the string, the first of the conditions (36c) is the stipulation that the string is at rest when the thrust is applied, and the last condition states that before the thrust is applied the string's shape is given by some function $v(x)$.

Before the application of the thrust, the steady state shape of the string is given by the solution of equation (36a), with F set equal to zero, and with the time dependence removed, i.e.,

$$T \frac{\partial^2 v}{\partial x^2} = \rho g + Mg\, \delta(x - \xi) \; ; \quad v(0) = v(L) = 0 \quad . \tag{37}$$

After the thrust has been applied, the string will come to rest in a new position, and its steady state orientation is given by the solution of (36a) with the time dependence removed, viz:

$$T \frac{\partial^2 \omega}{\partial x^2} = \rho g + (Mg + F)\, \delta(x - \xi) \; ; \quad \omega(0) = \omega(L) = 0 \; . \tag{38}$$

It is clear from the above, that the steady state position of the string at a time long after the thrust has been applied is given by the solution for the position found for the time immediately before the thrust has been applied, with the addition of the thrust force to the gravitational force, i. e., $Mg \rightarrow Mg + F$.

The solution of equation (37) is given by

$$v(x) = -\frac{\rho g}{2T}\, x(L - x) - \frac{Mg}{2T} \begin{cases} v & x < \frac{L}{2} \\ (L - x) & x > \frac{L}{2} \end{cases} \tag{39}$$

This is plotted in figure 30 for the three cases where the fixed central weight is respectively much greater than, equal to, and much less than the total weight of the string. It is readily seen that the shape is that of a parabola, and that for the practical cases ($Mg >> \rho g L$) the shape approaches that of a triangle.

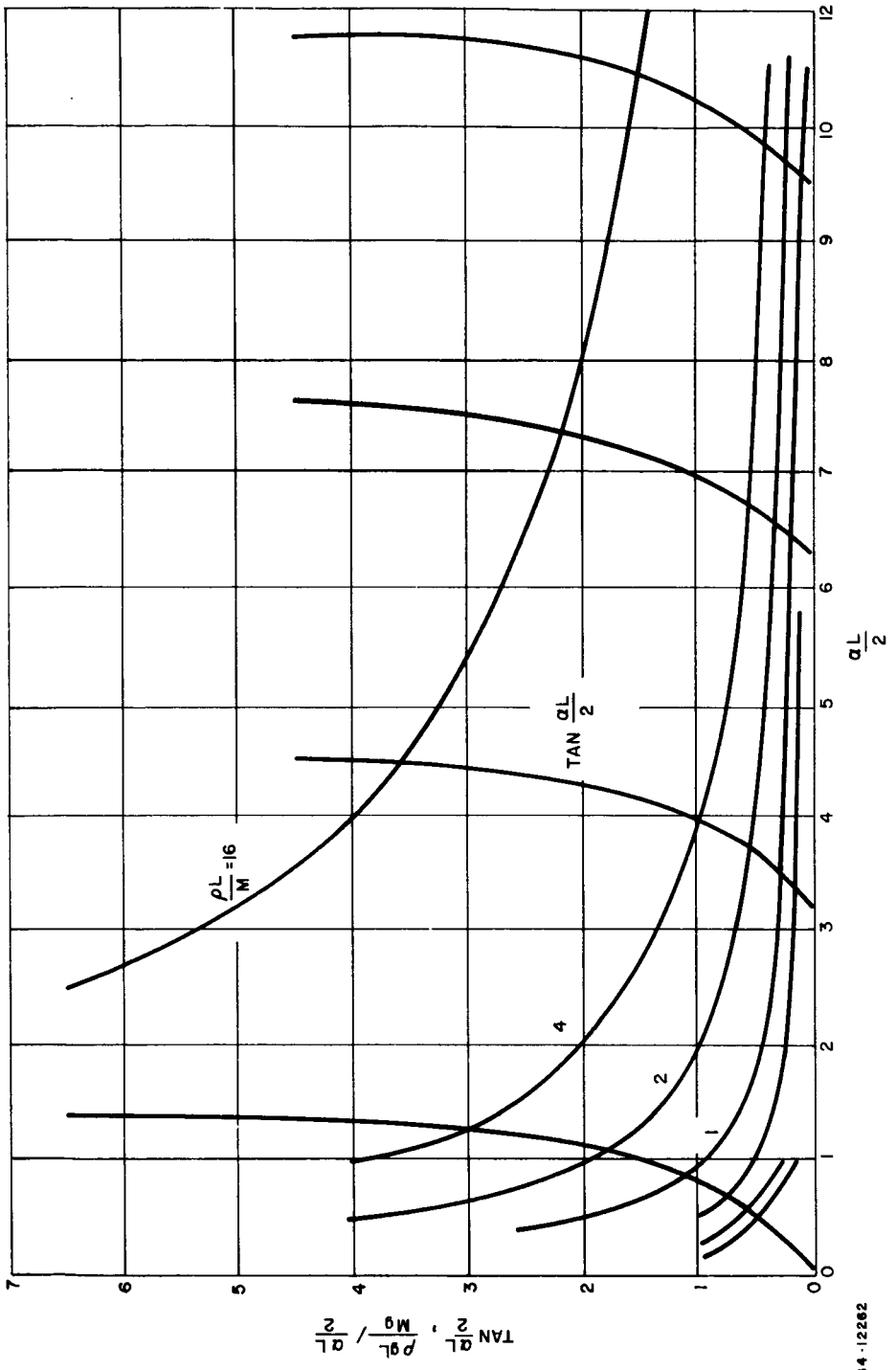

Figure 30 STRING CONTOUR FOR VARIOUS RATIOS OF ENGINE WEIGHT TO STRING WEIGHT

The steady state solution of equation (38) is simply

$$\omega(x) = -\frac{\rho g}{2T}\, x(L-x) - \frac{Mg+F}{2T} \begin{cases} x & x < \frac{L}{2} \\ (L-x) & x > \frac{L}{2} \end{cases} \tag{40}$$

and is obtained from the solution of equation (37) by the replacement of Mg by the sum of the "external" forces, $Mg + F$.

Of greatest interest is the position of the string midpoint. Before the application of the thrust, this is simply

$$v\left(\frac{L}{2}\right) = -\frac{L}{4T}\left\{Mg + \frac{\rho g L}{2}\right\} \tag{41}$$

a long time after the application of a step thrust it becomes

$$\omega\left(\frac{L}{2}\right) = -\frac{L}{4T}\left\{Mg + \frac{\rho g L}{2} + F\right\} \tag{42}$$

Hence, the new position of the string center is just lower by an amount $\frac{FL}{4T}$; this is linearly dependent upon the magnitude of the thrust level and the string length, and inversely proportional to the tension. It is independent of both the string weight per unit length and the weight of the central mass. This is important since for the measurement of the thrust levels without regard to response time of the system, no limitation on engine weight is required.

In order to consider the transient response of the thrust stand, it is convenient to first solve the problem with the assumption of no damping forces, i.e., f in equation (36a) is zero. The displacement of any point on the string is then given by

$$y(x, t) = \omega(x) + \phi(x, t) \tag{43}$$

where $\omega(x)$ is given above (equation 40) and $\phi(x, t)$ is given by

$$\phi(x, t) = \frac{F\rho^2 L^3}{4MT} \sum C^2_m \left(\frac{2}{\alpha_n L}\right)^3 \cos\left(\frac{\alpha_n L}{2}\right) \cos\left(\sqrt{\rho/T}\,\alpha_n t\right) \sin \alpha_n x \tag{44a}$$

for points on the string to the left of center, and

$$\phi(x, t) = \frac{F \rho^2 L^3}{4MT} \sum C_n^2 \left(\frac{2}{\alpha_n L}\right)^3 \cos\left(\frac{\alpha_n L}{2}\right) \cos\left(\sqrt{\rho/T}\ \alpha_n t\right) \sin \alpha_n (L - x) \tag{44b}$$

for points to the right of center. C_n and α_n are defined by the relations

$$C_n = \left(\frac{\rho L}{2} + \frac{2M\rho^2}{\alpha_n^2 M^2 + 4\rho^2}\right)^{-1/2} \tag{45a}$$

and

$$\left(\frac{\alpha_n L}{2}\right) \tan\left(\frac{\alpha_n L}{2}\right) = \frac{\rho L}{M} \tag{45b}$$

In particular, the position of the center of the string is given by

$$y\left(\frac{L}{2}, t\right) = -\frac{L}{4T}\left[Mg + \frac{\rho g L}{2} + F\right] + \tag{46}$$

$$+ \frac{F \rho L^2}{4T} \sum_{n=0}^{\infty} C_n^2 \left(\frac{2}{\alpha_n L}\right)^2 \sin^2\left(\frac{\alpha_n L}{2}\right) \cos \sqrt{\rho/T}\ \alpha_n t$$

Figure 31 shows plots of $\frac{\rho g L}{Mg} / \frac{\alpha L}{2}$ and $\tan \frac{\alpha L}{2}$, both against $\frac{\alpha L}{2}$, and with the ratio $\frac{\rho g L}{Mg}$ as a parameter. The intersections of the tangent curves with the hyperbolas are the values of $\frac{\alpha_n L}{2}$ which satisfy equation (45b) for the parameter values of the ratio of string weight to mass weight to mass weight, $\frac{\rho g L}{Mg}$.

For limitingly small relative weight of the central mass, $Mg << \rho g L$, the values of $\frac{\alpha_n L}{2}$ approach the values $\frac{2n + 1}{2}\pi$. The series of equation (46) may then be summed analytically and yields

$$y\left(\frac{L}{2}, t\right)_{M \to 0} = -\frac{\rho g L^2}{8T} - \frac{FL}{2T} g(t) \tag{47}$$

where $q(t)$ is shown plotted in figure 32. The curve of figure 33 then represents the position of the center of the string as a function of time. It is seen to be periodic with a period given by

$$\tau = 2L \sqrt{\rho/T}\ .$$

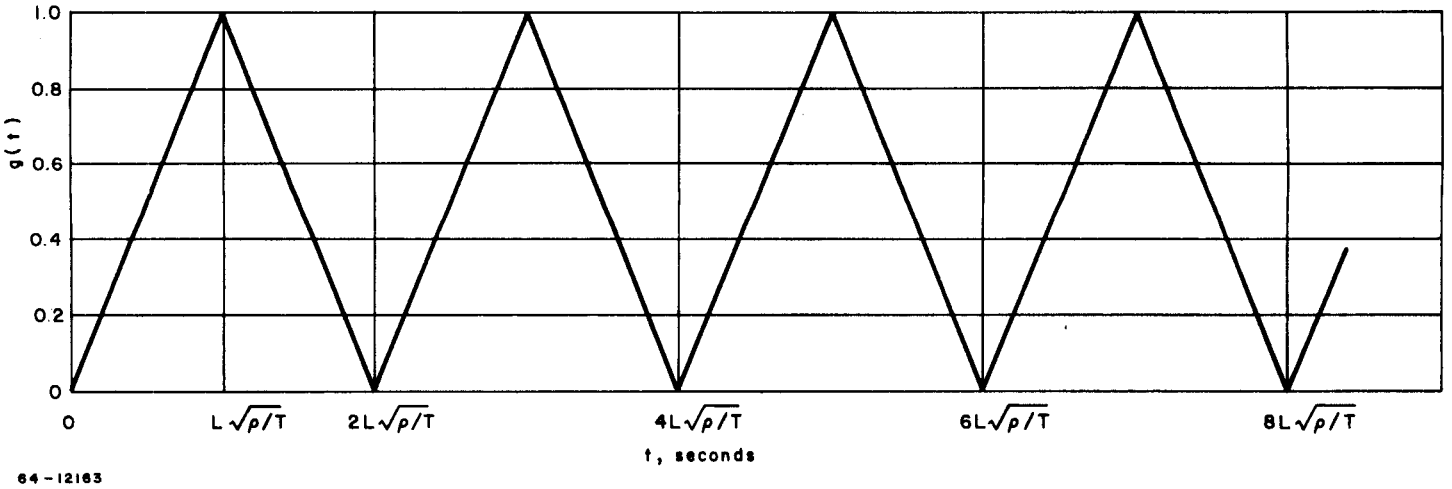

Figure 31 STRING VIBRATIONAL MODE CHARACTERISTICS

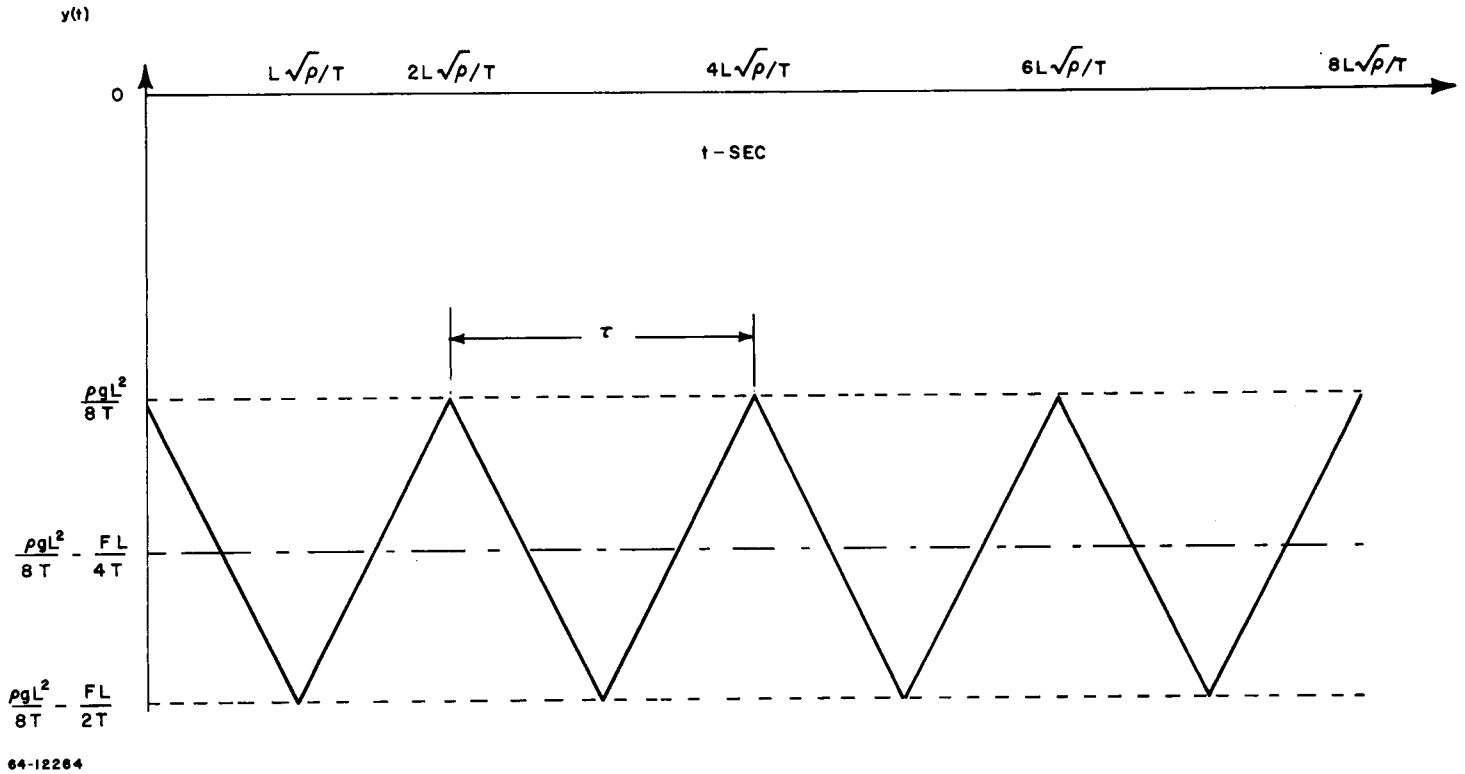

Figure 32 FUNCTION TO DETERMINE STRING VIBRATIONAL AMPLITUDE

The average position is given by

$$\bar{y}\left(\frac{L}{2}, t\right)_{M \to 0} = -\frac{\rho g L^2}{8T} - \frac{FL}{4T} \quad . \tag{48}$$

This is indeed the value of the steady state position in the limit of small M, as seen from equation 42. The effect of damping upon the system should be to reduce the magnitude of the oscillation as time goes on and the steady state position should then be just the average value of the position as shown in equation 42.

In the more practical case, it is the string's weight which is small compared with the weight of the engine and engine mounting, i.e., $Mg >> \rho g L$.

For this case, the introduction of the substitutions

$$R \equiv \frac{L}{M}\rho$$

and

$$X_n \equiv \frac{\alpha_n L}{2}$$

reduces equation (11) to

$$y\left(\frac{L}{2}, t\right)_{\rho L \to 0} = -\frac{(Mg + F)L}{4T}$$

$$+ \frac{FL}{2T} \frac{R^2}{X_1^2 (R^2 + R + X_1^2)} \left[\cos \frac{2}{L}\sqrt{T/\rho}\, X_1 t + \sum_{n=2}^{\infty} \left(\frac{X_1}{X_n}\right)^2 \left(\frac{R^2 + R + X_1^2}{R^2 + R + X_n^2}\right) \cos \frac{2}{L}\sqrt{T/\rho}\, X_n t\right]. \tag{49}$$

It is seen from figure 31 that

$$X_n \approx X_{n-1} + \pi \quad .$$

Moreover, for $\frac{\rho L}{M} << 1$,

$$\tan X_1 \approx X_1 \quad \text{and} \quad X_1 \approx \sqrt{R} \quad .$$

These approximations lead to the final results for the position of the center of a string of negligible weight,

$$y\left(\frac{L}{2}, t\right)_{\rho \to 0} = -\frac{MgL}{4T} - \frac{FL}{4T}\left[1 - \cos\sqrt{\frac{4T}{ML}}\, t\right] \quad . \tag{50}$$

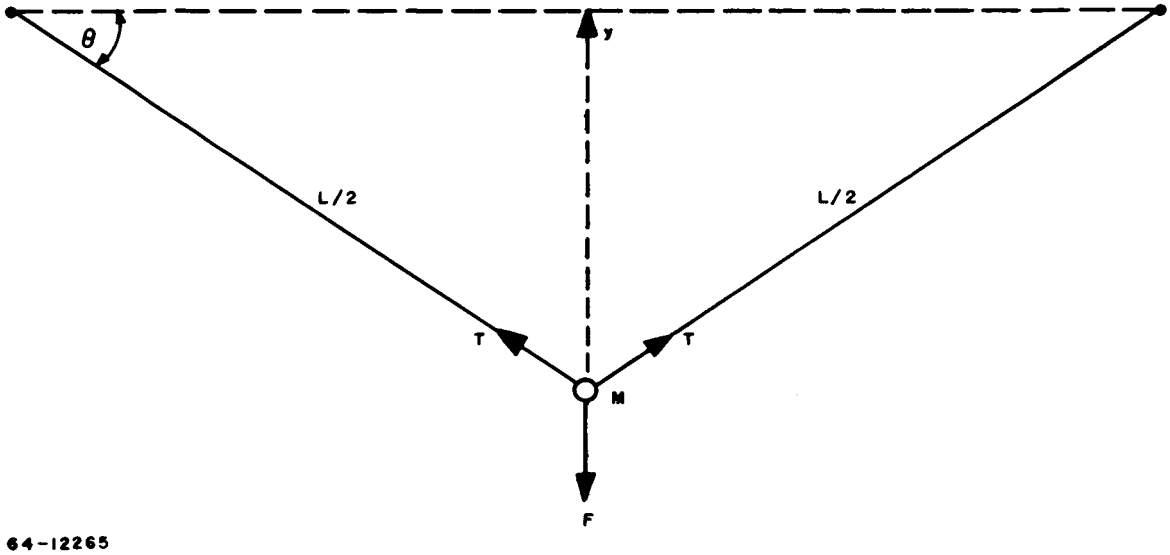

Figure 33 STRING CENTER POSITION VERSUS TIME

To test the limits of validity of the above for larger values of the ratio $R = \frac{\rho L}{M}$, substitution of $R = 1$ yields:

$$y\left(\frac{L}{2}, t\right)_{\rho L = M} = -\frac{MgL}{4T} - \frac{FL}{4T}\left[1 - 1.02 \cos\left(0.85 \sqrt{\frac{4T}{ML}}\, t\right)\right].$$

It is thus clear that for a practical thrust stand, the relation (50) is valid to very high order of precision.

APPENDIX C

HEATUP TIME FOR FAST HEATUP THRUSTOR

In order to determine more exactly the transient heating characteristic of the heatup thrustor, an existing digital computer program has been utilized. The program solves for temperature as a function of time and position given the geometry, power input, material properties as a function of temperature, and boundary conditions. Conductive and radiative heat transfer are accounted for.

The idealized thrustor for which the transient heating calculations were made is drawn in figure 34. It consists of a heater tube made of tungsten with the dimensions 1.9 cm length (0.75 inch), 0.28 mm inner diameter (0.011 inch), and 0.38 mm outer diameter (0.015 inch). At one end, this tube is attached to a stainless steel tube with the dimensions 2.54 cm length (1.0 inch), 1.52 mm inner diameter (0.060 inch), and 3.13 mm outer diameter (0.125 inch). The other end of the tungsten tube terminates in a flat tungsten power lead, with the dimensions 3.8 mm length (0.15 inch), 2.54 mm width (0.10 inch), and 0.128 mm thickness (0.005 inch).

Power is supplied to this thrustor at a constant rate, which can be adjusted to various levels to perform parametric studies. The boundary conditions employed are that: (1) the base of the large stainless steel tube (the end furthest removed from the thrustor) is maintained at 300°K, as is the end of the flat power lead, (2) each exposed surface radiates an amount of power consistent with its temperature and emissivity.

Results of this analysis are given in figures 35, 36, and 37. Figure 35 shows, as a function of input power, the final steady state temperature distribution over the chosen geometry. At each power level the thrustor assembly temperature reaches a peak near the center of the thin-walled tungsten tube and falls off at each end. Neither the stainless steel mounting cylinder nor the power lead are themselves appreciably heated. A power input of 20 watts brings the thrustor to a temperature of the order of 2500°K in steady state, with no gas flow.

Figure 36 shows the transient temperature rise at the center of the tungsten tube. Even with a power input of only 10 watts the warmup time is below 1 second, while 20 watts it is of the order of one-half second, and one-quarter second at 40 watts of input power.

Finally, for a power level of 40 watts, figure 37 shows the temperature distribution as a function of time. From figure 37 it can be seen that the general shape of the temperature distribution varies little with time.

It can be concluded from this analysis, that, with an input power of 20 watts, with losses both by conduction and radiation, the thrustor will reach operating temperature in less than one second. Since the dominating loss mechanism at the higher temperatures is radiation, and since a thrustor twice as long will radiate twice as much, essentially, the conclusions can be simply scaled within a limited range of thrustor sizes. Hence, it appears reasonable to assume that a thrustor x centimeters long will require a power 10 x watts to reach steady state temperature in about one-half second, and that the steady state temperature will be approximately 2500°K, for values of x which do not depart too much from 2 cm.

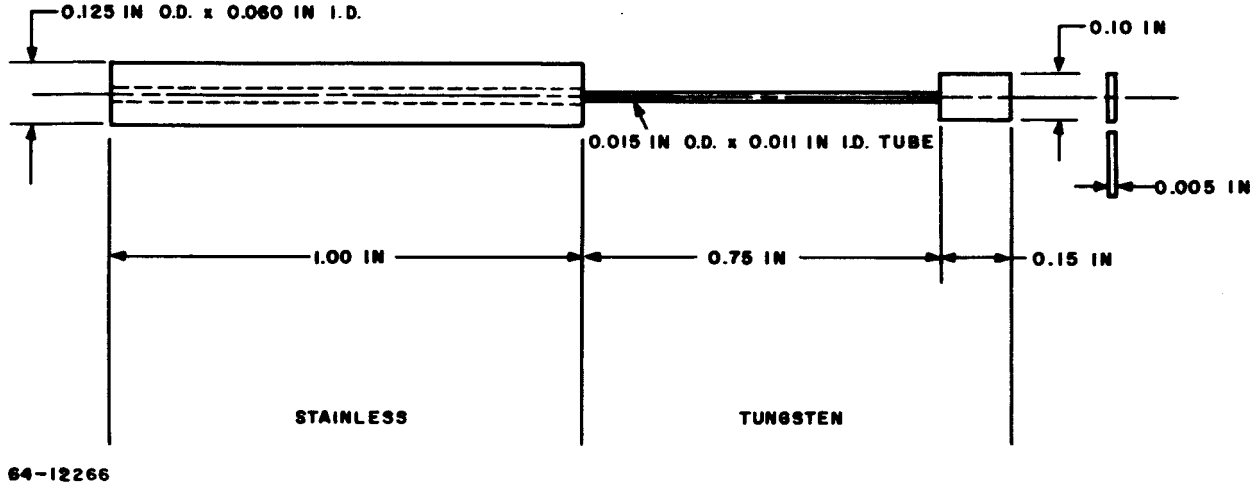

Figure 34 MODEL FOR HEAT TRANSFER ANALYSIS

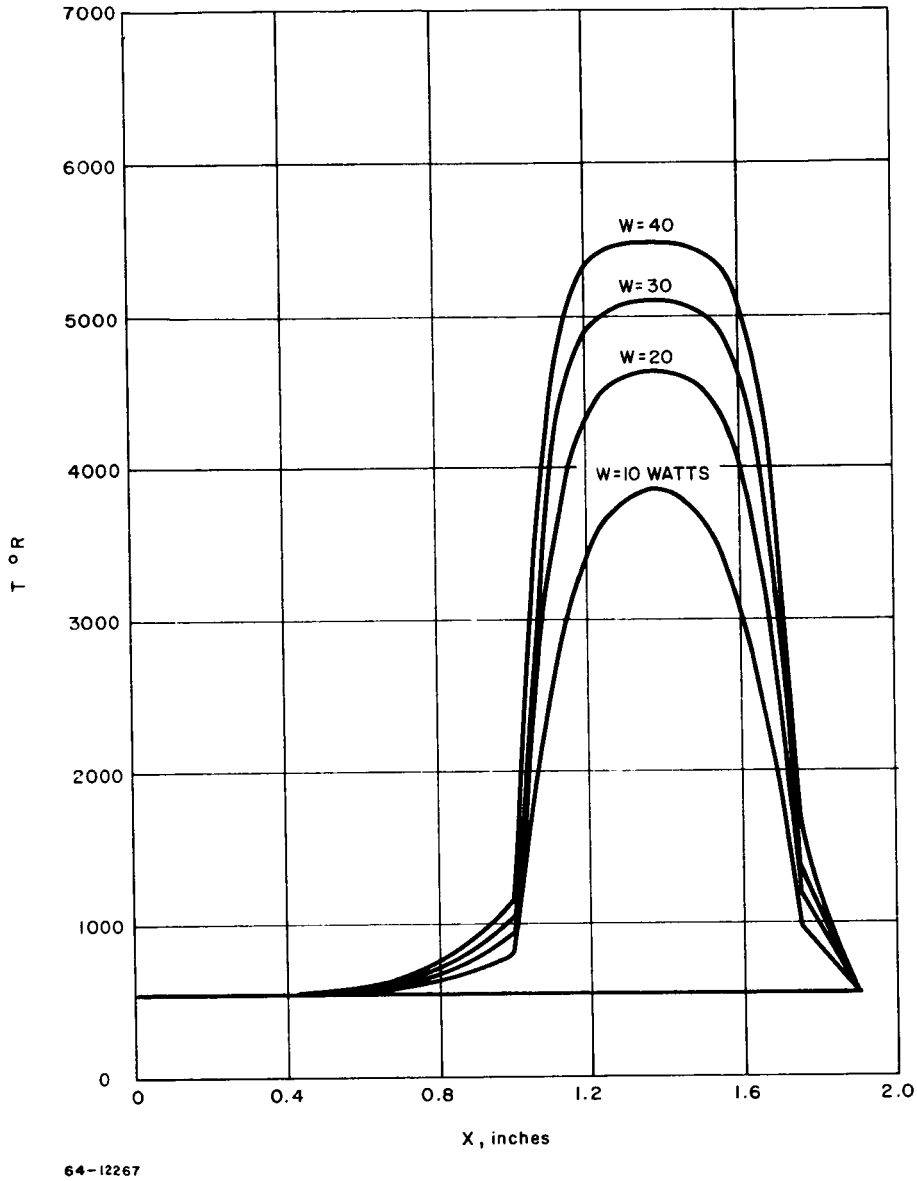

Figure 35 TEMPERATURE DISTRIBUTION AFTER 5 SECONDS

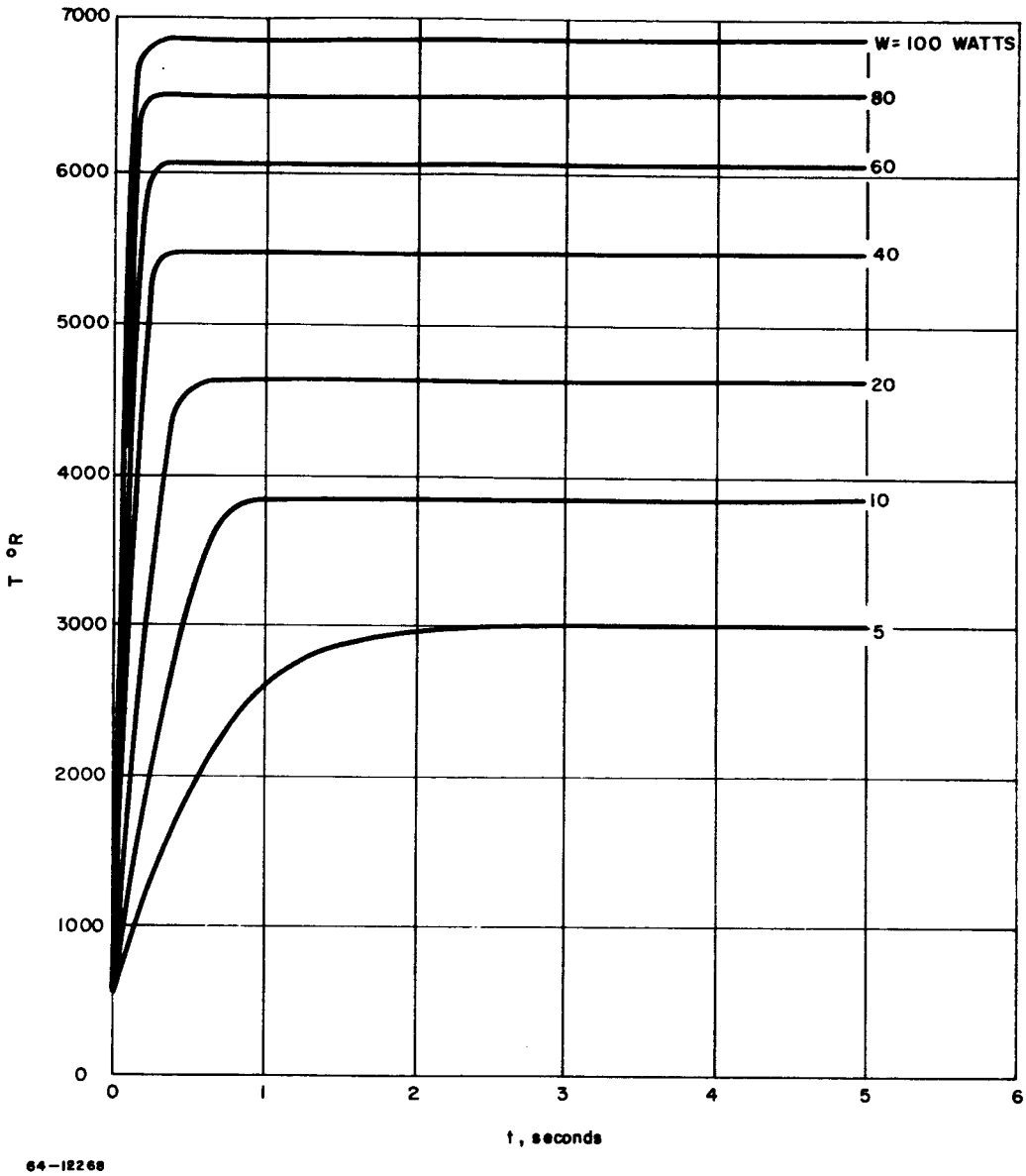

Figure 36 MAXIMUM THRUSTOR TEMPERATURE VERSUS TIME FOR DIFFERENT POWER INPUT LEVELS

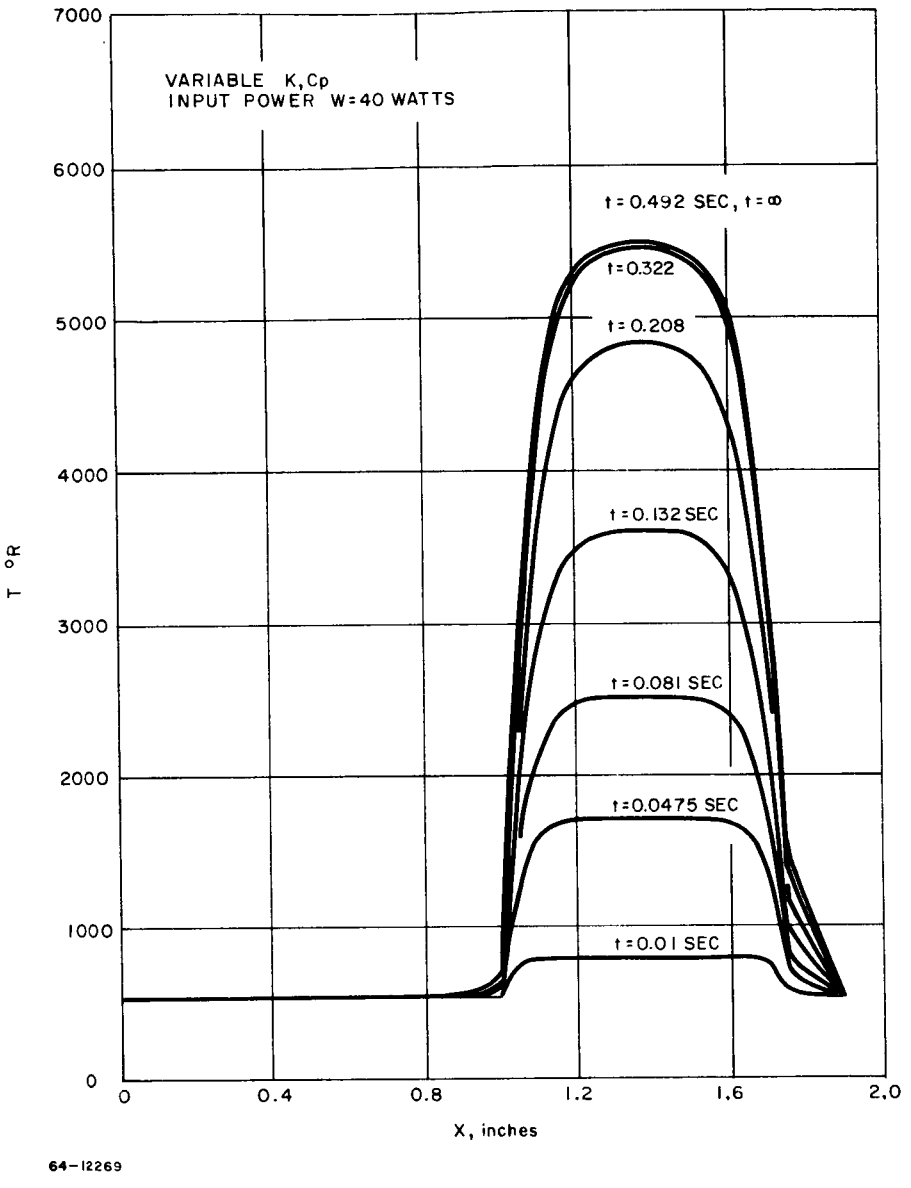

Figure 37 THRUSTOR TEMPERATURE DISTRIBUTION VERSUS TIME AT INPUT POWER OF 40 WATTS

APPENDIX D

HEAT LOSS FROM A THERMAL STORAGE THRUSTOR

Estimates have been made of the standby power loss associated with a thermal storage thrustor. The thermal storage thrustor is defined as one which is continuously supplied with electrical power. In the steady state, with no gas flow, the input power level equals exactly the power loss. Reduction of losses therefore directly reduces the required input power. It is assumed that the thrustor heat capacity greatly exceeds the heat capacity of the total propellant mass heated by the thrustor during a thrust pulse, and that the average over a long time of the power absorbed by the propellant is small compared to the input power level. Under these conditions the power requirements for the thrustor are determined by the standby conditions, and the propellant flow can actually be treated as a small perturbation on these standby conditions.

There are two principal loss modes associated with the thermal storage thrustor; these are radiation and conduction along the input power leads and propellant supply tube. These are treated separately below. Calculations are made for the thrustor as indicated schematically in figure 23.

Radiation Loss

For a body surrounded by a radiation shield, it is shown in reference 1 that the heat lost by radiation from the body is given by

$$Q = \frac{A_o \sigma}{\frac{1}{\epsilon_o} + \frac{A_o}{A_1}\left(\frac{1}{\epsilon_1} - 1\right)} \left(T_o^4 - T_1^4\right) \qquad (51)$$

where Q is the heat loss in watts/cm^2-^{o}K^4, A_o is the body surface area, σ is 5.67 X 10^{-12}, A_1 is the shield surface area, ϵ_o and ϵ_1 are the body and shield emissivities, respectively, and T_o and T_1 are the body and shield temperatures, respectively. For the thrustor of figure 23 it is a useful approximation to neglect end effects, and to evaluate the power radiated per unit length of the cylindrical thrustor body. Equation (51) can be written

$$Q^1 \equiv \frac{Q}{L} = \frac{2\pi r_o \sigma}{\frac{1}{\epsilon_o} + \frac{r_o}{r_1}\left(\frac{1}{\epsilon_1} - 1\right)} \left(T_o^4 - T_1^4\right) \qquad (52)$$

[1] Eckert, E. R. G., and R. M. Drake, Jr., Heat and Mass Transfer, p. 405, McGraw-Hill, New York (1959).

where r_o and r_1 are, respectively, the radii of the thrustor and the shield. In the event that the emissivities of the body and the shield are equal, equation (52) can be further simplified:

$$Q' = \frac{2\pi\epsilon\sigma}{\frac{1}{r_o} + (1-\epsilon)\frac{1}{r_1}} (T_o^4 - T_1^4) \ . \tag{53}$$

If now there are N such concentric shields, and if Q' and the geometry are fixed, there are N + 1 unknown temperatures T_i for a given heat flux. Equation (53) can be used to relate the temperature of the thrustor to that of the first shield, the temperature of the first shield to that of the second, etc., yielding N equations. The N + 1st comes from the radiation between the N^{th} shield and the surrounding space. This system of equations can then be solved for T_o in terms of the heat flux, the geometry, and the emissivity. The solution is

$$T_o^4 = \frac{Q'}{2\pi\epsilon\sigma} \left[\frac{1}{r_o} + (2-\epsilon) \sum_{n=1}^{N} \frac{1}{r_n} \right] \ . \tag{54}$$

Solutions to equation (54) have been obtained using a digital computer, and the results are presented below. Some physical insight can be gained, however, by considering a special case. If the shields are equally spaced by distance δ, and if the number of shields is large so that the sum can be replaced by an integra, equation (54) becomes:

$$T_o^4 = \frac{Q'}{2\pi\epsilon\sigma} \left[\frac{1}{r_o} + \frac{2-\epsilon}{\delta} \ln \frac{r_o + N\delta}{r_o + \delta} \right] \tag{55}$$

It is clear from equation (55) that, for a given T_o, Q' is reduced as ϵ, r_o, and/or δ are reduced; Q' is also reduced as N increases, but only logarithmically. Therefore, the number of shields which can be usefully employed is subject to diminishing returns.

Figure 38 shows the radiation per unit length in watts/cm as a function of number of radiation shields. The assumptions of this calculation are that the thrustor outer wall temperature is 2000°K, the thrustor radius is 0.5 cm, and the emissivity is 0.3. The shield separation, δ, is taken as a parameter and curves are plotted in figure 26 for values of δ of 0.01, 0.05, and 0.1 cm. The shield thickness is assumed small compared to δ.

If the radiation loss is to be kept below about 2 watts/cm, which is imperative if the thrustor overall standby heat loss is to be kept of the order of 10 watts, then the number of shields required is seen to exceed 30 even with the rather optimistic value of 0.01 cm for δ. If the shield separation is as much as milli-

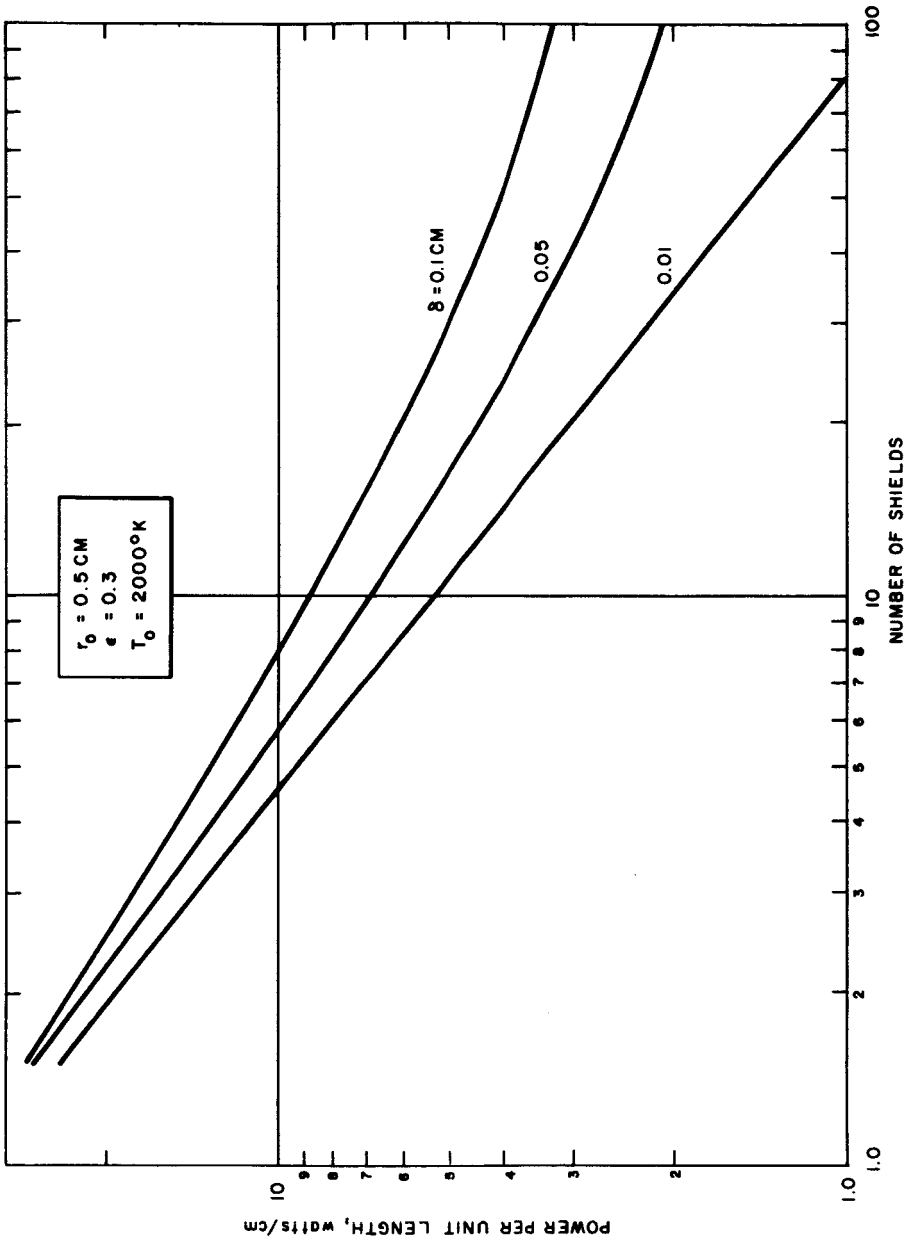

Figure 38 HEAT RADIATED PER UNIT LENGTH VERSUS NUMBER OF SHIELDS, $\epsilon = 0.3$

meter, even 100 shields are not sufficient to keep Q' below 2 watts/cm.

If the emissivity is decreased to 0.1, the situation is greatly improved. Figure 39 indicates that only 15 shields would be required at the quite reasonable spacing of 1 mm, if this emissivity can be obtained, to limit the loss per unit length by radiation to 2 watts/cm.

The effects of emissivity and shield separation are shown again in figure 40, drawn for a total of 20 shields with a thrustor temperature of 2000°K and radius of 0.5 cm. The indication of this figure is that the emissivity must not exceed ~0.2 if Q' is to be kept below 2 watts/cm with shield separation distances of the order of one-half millimeter. Figure 41 shows the effect of heater diameter on the required number of shields.

This analysis has not accounted for radiation from the ends of the thrustor; however, it is thought that proper design can keep this loss smaller than the loss through the sides for a thrustor with a length-to-diameter ratio greater than 2; if the thrustor can be made with a length to diameter ratio of the order of 8 or 10, this loss can be made very small.

2. Conduction Loss

The conduction loss has been estimated from the results of the computer program reported in appendix C. Briefly, the steady state temperature distribution obtained from the computer was used to estimate the temperature gradient at the end of the thrustor section, and this was in turn used with the thermal conductivity and the known cross sectional area to evaluate the heat loss. For a 10-watt input power level, which corresponds to a central temperature of 2000°K, the calculated conduction loss was 2.9 watts into the stainless steel holder and 2.7 watts into the tungsten power lead, for a total of 5.6 watts. It is anticipated that the larger thermal storage thrustor would have a larger lead loss than the very small fast heatup unit, so that these estimates may serve as lower limit values.

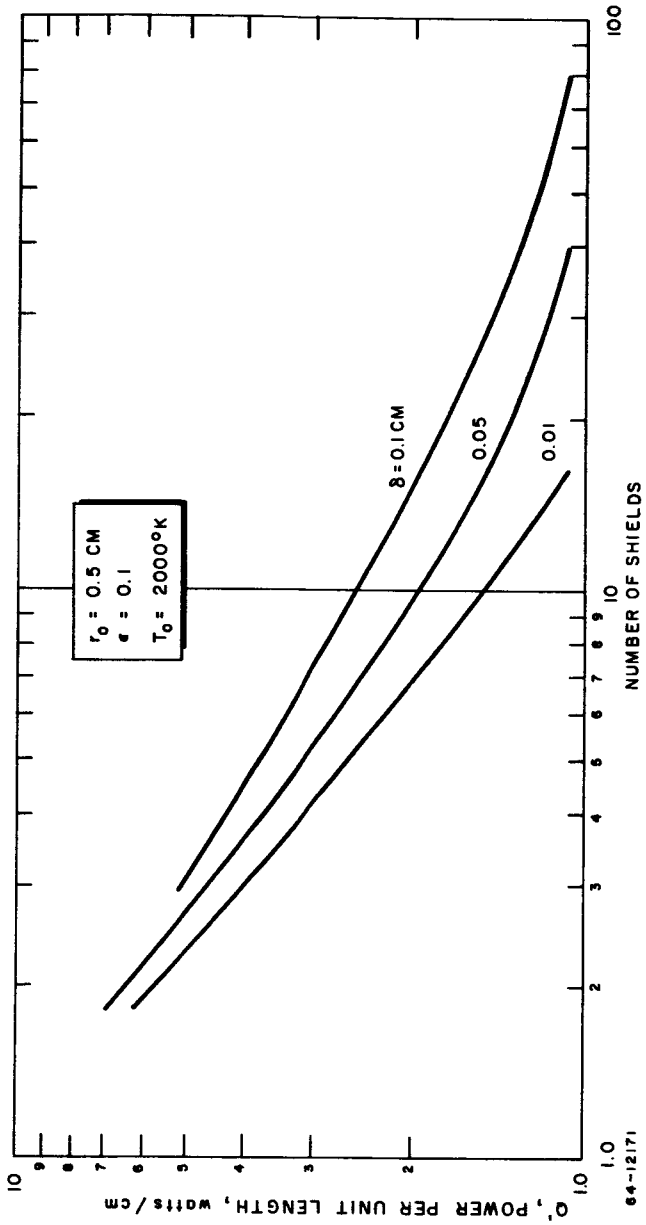

Figure 39 HEAT RADIATED PER UNIT LENGTH VERSUS NUMBER OF SHIELDS, $\epsilon = 0.1$

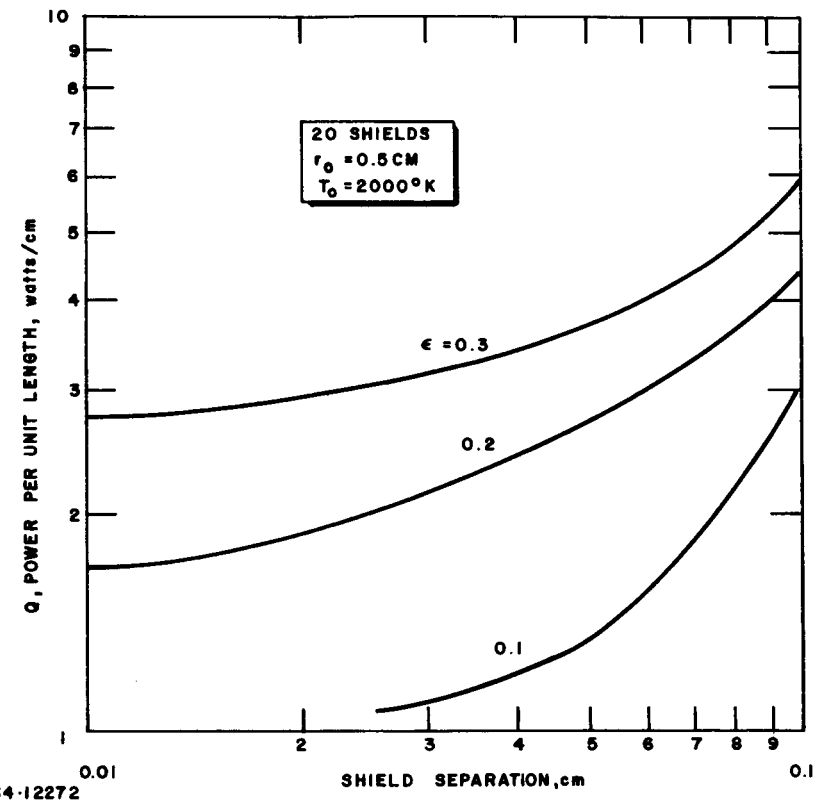

Figure 40 HEAT RADIATED PER UNIT LENGTH VERSUS SHIELD SEPARATION

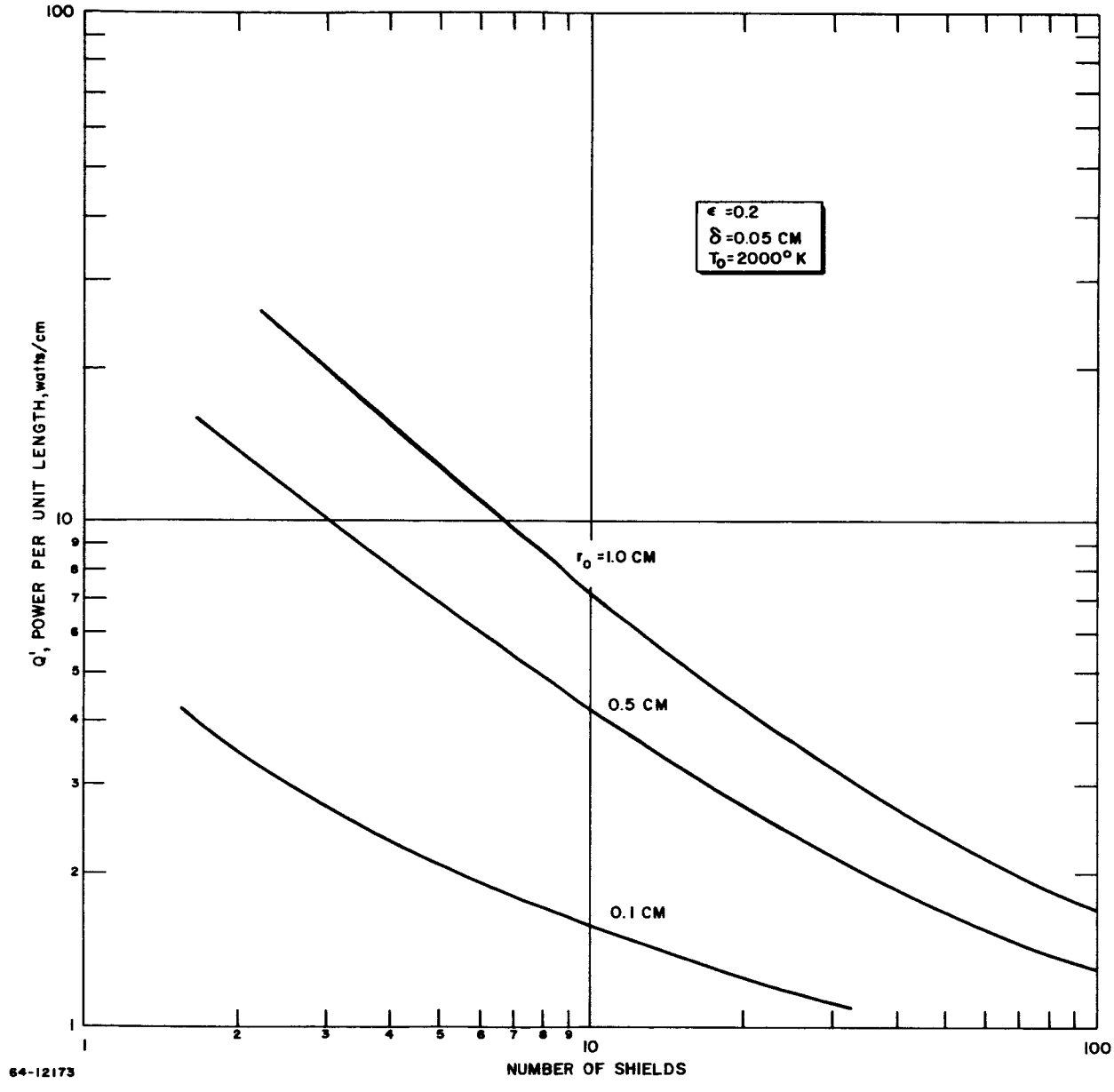

Figure 41 HEAT RADIATED PER UNIT LENGTH VERSUS NUMBER OF SHIELDS AND THRUSTOR RADIUS

APPENDIX E

THRUSTOR PERFORMANCE DATA

Tables VIII through XII summarize thrustor performance data at five different ammonia flow rates. The data are determined as follows:

Mass Flow Rate:	measured by a positive displacement technique, as summarized in the main body of this report.
Supply Current:	measured with a precision DC ammeter.
Supply Voltage:	measured with a precision DC voltmeter near the battery power supply terminals, so that lead voltage drops are included.
Supply Power:	calculated as the product of supply current and supply voltage.
Lead Losses:	measured as a function of current by replacing the thrustor with an essentially zero resistance slug.
Heater Power:	calculated as the difference of supply power and the lead loss measured for the appropriate supply current level.
Chamber Pressure:	measured with a piezoelectric pressure transducer, calibrated against a standard pressure gauge.
Thrust:	measured, for cold ammonia flow, with the thrust stand. Calculated, for hot ammonia flow, from the chamber pressure and the value of $C_F A_t$ measured for cold ammonia flow.
Specific Impulse:	calculated from the ratio of thrust to mass flow rate.
Thrust Power:	calculated from the thrust and specific impulse.
Overall Electrical Efficiency:	calculated from the ratio of thrust power to the heater power.
Overall Total Efficiency:	calculated from the ratio of thrust power to the sum of heater power plus power in the cold gas flow.

Engine Temperature:	measured with an optical pyrometer.
Gas Temperature:	calculated from the enthalpy, which is in turn calculated from the hot-to cold chamber pressure ratio.
Gas Power:	calculated from the mass flow rate and the computed gas enthalpy.
Thermal Efficiency:	calculated from the ratio of (gas power minus cold gas power) to heater power.

TABLE VIII

ENGINE PROPULSION PERFORMANCE AT AN AMMONIA FLOW RATE OF 1.4×10^{-6} lb/sec

Run Number	Ammonia Flow (lb/sec)	Supply Current (amperes)	Supply Voltage (volts)	Supply Power (watts)	Lead Losses (watts)	Heater Power (watts)	Chamber Pressure (psia)	Thrust (pounds)
1	1.4×10^{-6}						4.0	0.10×10^{-3}
2	1.4×10^{-6}	2.8	0.52	1.5	0.55	0.90	5.0	0.13×10^{-3}
3	1.4×10^{-6}	4.9	0.95	4.7	1.6	3.1	7.5	0.20×10^{-3}
4	1.4×10^{-6}	7.0	1.40	9.8	3.2	6.6	11.0	0.29×10^{-3}
5	1.4×10^{-6}	8.0	1.65	13.2	4.2	9.0	11.5	0.30×10^{-3}
6	1.4×10^{-6}	8.5	1.68	14.3	4.7	9.6	12.0	0.32×10^{-3}

Run Number	Specific Impulse (seconds)	Thrust Power (watts)	Overall Electrical Efficiency (percent)	Overall Total Efficiency (percent)	Engine Temperature (°K)	Gas Temp. (°K)	Gas Power (watts)	Thermal Efficiency (percent)
1	72	0.16		40		300	0.40	
2	93	0.26	29	20		380	1.12	86
3	143	0.62	20	18		560	2.42	70
4	207	1.31	20	19	1220	1130	3.96	57
5	214	1.40	16	15	1330	1260	4.22	47
6	228	1.59	17	16	1370	1360	4.46	45

TABLE IX

ENGINE PROPULSION PERFORMANCE AT AN AMMONIA FLOW RATE OF 3.1×10^{-6} lb/sec.

Run Number	Ammonia Flow (lb/sec)	Supply Current (amperes)	Supply Voltage (volts)	Supply Power (watts)	Lead Losses (watts)	Heater Power (watts)	Chamber Pressure (psia)	Thrust (pounds)
1	3.1×10^{-6}						9.0	0.25×10^{-3}
2	3.1×10^{-6}	7.5	1.40	11.1	3.7	7.4	19.0	0.50×10^{-3}
3	3.1×10^{-6}	8.0	1.54	12.3	4.25	8.0	20.0	0.53×10^{-3}
4	3.1×10^{-6}	9.0	1.75	15.8	5.3	10.5	24.0	0.63×10^{-3}
5	3.1×10^{-6}	9.5	1.85	18.0	5.9	12.1	25.0	0.66×10^{-3}
6	3.1×10^{-6}	9.8	1.85	18.1	6.3	11.8	24.0	0.63×10^{-3}
7	3.1×10^{-6}	10.0	1.92	19.2	6.5	12.7	25.0	0.66×10^{-3}

Run Number	Specific Impulse (seconds)	Thrust Power (watts)	Overall Electrical Efficiency (percent)	Overall Total Efficiency (percent)	Engine Temperature (^{o}K)	Gas Temperature (^{o}K)	Gas Power (watts)	Thermal Efficiency (percent)
1	81	0.43		49		300	0.88	
2	161	1.76	24	21	1150	640	6.20	75
3	171	1.98	25	22	1190	730	6.82	77
4	203	2.79	27	25	1310	1070	8.48	74
5	212	3.05	25	23	1350	1160	8.90	69
6	203	2.79	24	22	1380	1070	8.50	67
7	212	3.05	24	22	1420	1160	8.90	66

TABLE X

ENGINE PROPULSION PERFORMANCE AT AN AMMONIA FLOW RATE OF 5.2×10^{-6} lb/sec

Run Number	Ammonia Flow (lb/sec)	Supply Current (amperes)	Supply Voltage (volts)	Supply Power (watts)	Lead Losses (watts)	Heater Power (watts)	Chamber Pressure (psia)	Thrust (pounds)
1	5.2×10^{-6}						15	0.40×10^{-3}
2	5.2×10^{-6}	6.8	1.30	8.8	3.0	5.8	23.5	0.62×10^{-3}
3	5.2×10^{-6}	8.0	1.40	11.2	4.2	7.0	29.0	0.76×10^{-3}
4	5.2×10^{-6}	9.0	1.65	14.9	5.3	9.9	31.0	0.82×10^{-3}
5	5.2×10^{-6}	9.5	1.65	15.7	5.9	9.8	31.0	0.82×10^{-3}
6	5.2×10^{-6}	10.0	1.80	18.0	6.5	11.5	31.5	0.83×10^{-3}
7	5.2×10^{-6}	10.5	1.85	19.4	7.0	12.4	33.0	0.87×10^{-3}
8	5.2×10^{-6}	11.5	2.20	25.3	8.4	16.9	36.5	0.97×10^{-3}

Run Number	Specific Impulse (seconds)	Thrust Power (watts)	Overall Electrical Efficiency (percent)	Overall Total Efficiency (percent)	Engine Temperature (^{o}K)	Gas Temperature (^{o}K)	Gas Power (watts)	Thermal Efficiency (percent)
1	77	0.67		46		300	1.47	
2	119	1.61	28	22		470	6.60	91
3	146	2.42	35	28		590	9.40	91
4	158	2.82	29	25		645	10.3	91
5	158	2.82	29	25	1210	645	10.3	
6	160	2.90	25	22		670	10.7	
7	168	3.18	25	23	1300	730	11.4	
8	187	3.96	23	22	1410	870	12.7	

TABLE XI

ENGINE PROPULSION PERFORMANCE AT AN AMMONIA FLOW RATE OF 7.3×10^{-6} lb/sec

Run Number	Ammonia Flow (lb/sec)	Supply Current (amperes)	Supply Voltage (volts)	Supply Power (watts)	Lead Looses (watts)	Heater Power (watts)	Chamber Pressure (psia)	Thrust (pounds)
1	7.3×10^{-6}						21	0.57×10^{-3}
2	7.3×10^{-6}	2.6	0.50	1.3	0.5	0.80	23	0.61×10^{-3}
3	7.3×10^{-6}	4.9	0.92	4.5	1.6	2.90	29	0.77×10^{-3}
4	7.3×10^{-6}	8.0	1.50	12.0	4.2	7.80	38	1.01×10^{-3}
5	7.3×10^{-6}	9.0	1.70	15.3	5.3	10.0	40	1.06×10^{-3}
6	7.3×10^{-6}	10.0	1.89	18.9	6.5	12.4	40.5	1.07×10^{-3}
7	7.3×10^{-6}	11.2	2.10	23.6	7.9	15.7	44	1.17×10^{-3}

Run Number	Specific Impulse (seconds)	Thrust Power (watts)	Overall Electrical Efficiency (percent)	Overall Total Efficiency (percent)	Engine Temperature (°K)	Gas Temperature (°K)	Gas Power (watts)	Thermal Efficiency* (percent)
1	78	0.96		46		300	2.1	
2	84	1.12		39		330	3.6	126
3	105	1.76	61	36		430	7.6	130
4	138	3.06	39	31		540	11.9	120
5	145	3.35	34	28	1100	590	13.0	108
6	146	3.40	27	24	1200	590	13.0	90
7	160	4.09	26	26	1280	670	15.0	85

*The recorded thermal efficiencies of greater than 100 percent are associated with the temperature region from 300° to 500°K. In this temperature region because of ammonia dissociation the enthalpy is an extremely sensitive function of temperature and hence of the hot-to-cold flow pressure ratio. An uncertainty of 10 percent in this pressure ratio would result in an uncertainty by a factor of 2 in the gas enthalpy, and hence in the thermal efficiency. For comparison, for gas temperatures of approximately 800°K a 10 percent uncertainty in the pressure ratio results in an uncertainty in the enthalpy of only about 12 percent.

TABLE XII

ENGINE PROPULSION PERFORMANCE AT AN AMMONIA FLOW RATE OF 8.6×10^{-6} lb/sec

Run Number	Ammonia Flow (lb/sec)	Supply Current (amperes)	Supply Voltage (volts)	Supply Power (watts)	Lead Losses (watts)	Heater Power (watts)	Chamber Pressure (psia)	Thrust (pounds)
1	8.6×10^{-6}						25	0.66×10^{-3}
2	8.6×10^{-6}	9.0	1.6	14.4	5.3	9.1	42	1.11×10^{-3}
3	8.6×10^{-6}	10.0	1.9	19.0	6.5	12.5	43	1.14×10^{-3}
4	8.6×10^{-6}	10.6	1.92	20.4	7.1	13.3	46	1.22×10^{-3}
5	8.6×10^{-6}	11.2	2.05	23.0	7.9	15.1	47	1.25×10^{-3}

Run Number	Specific Impulse (seconds)	Thrust Power (watts)	Overall Electrical Efficiency (percent)	Overall Total Efficiency (percent)	Engine Temperature (°K)	Gas Temperature (°K)	Gas Power (watts)	Thermal Efficiency (percent)
1	77	1.1		44		300	2.5	
2	129	3.1	34	27	1150	500	12.4	107*
3	133	3.3	26	22	1240	520	12.9	86
4	142	3.8	28	24	1260	560	14.6	93
5	145	4.0	26	22	1310	575	15.0	85

*See note to table XI.

APPENDIX F

PROPERTIES OF AMMONIA

Properties of ammonia have been determined as a function of temperature to 3000°K for pressures of 1 and 2 atmospheres, and are shown in tables XIII and XIV. The calculation was based on standard techniques of thermodynamics, without consideration of kinetics.

TABLE XIII

PROPERTIES OF AMMONIA

	p = 1 atmosphere			p = 2 atmosphere		
T (°K)	h (cal/gm)	I_{sp}, f (seconds)	M (grams)	h (cal/gm)	I_{sp}, f (seconds)	M (grams)
500	841	182	9.27	768	178	9.81
600	1019	205	8.63	1002	204	8.73
700	1117	223	8.54	1112	223	8.57
800	1203	239	8.52	1202	239	8.53
900	1289	254	8.52	1288	254	8.52
1000	1375	268	8.52	1374	268	8.52
1100	1462	282	8.52	1462	282	8.52
1200	1550	295	8.52	1550	295	8.52
1300	1639	308	8.52	1639	308	8.52
1400	1730	321	8.52	1730	321	8.52
1500	1822	333	8.52	1822	333	8.52
1600	1914	345	8.52	1914	345	8.52
1700	2009	357	8.52	2008	357	8.52
1800	2105	368	8.52	2104	368	8.52
1900	2202	379	8.51	2202	379	8.51
2000	2304	390	8.51	2302	390	8.51
2100	2410	401	8.50	2405	401	8.51
2200	2522	412	8.50	2513	411	8.50
2300	2644	422	8.4	2628	422	8.49
2400	2778	432	8.46	2753	432	8.48
2500	2930	443	8.42	2890	443	8.45
2600	3105	453	8.38	3043	453	8.42
2700	3310	463	8.31	3218	463	8.37
2800	3550	474	8.23	3418	473	8.31
2900	3835	484	8.12	3651	483	8.23
3000	4173	495	7.98	3922	494	8.13

TABLE XIV

PRESSURE RATIO AS A FUNCTION OF TEMPERATURE
FOR CONSTANT MASS FLOW

$T_{cold} = 300°K$

T	$\sqrt{T/300}$	$\sqrt{17/M}$	P_2/P_{cold}
300	1	1	1
500	1.29	1.31	1.69
600	1.41	1.4	1.97
700	1.52	1.41	2.14
800	1.63	1.41	2.30
900	1.73	↓	2.44
1000	1.82	↓	2.57
1100	1.91	↓	2.70
1200	2	↓	2.83
1300	2.08	↓	2.94
1400	2.16	↓	3.06
1500	2.24	↓	3.17

Note: $\frac{P_2}{P_{cold}} = \sqrt{\frac{17T}{300M}}$

APPENDIX G

COMPOSITE MATERIALS FOR THERMAL STORAGE THRUSTORS

The composites were produced by cold pressing mixed metal-metal oxide powders and sintering the compacts to a high density. Based on previous experience, 1-micron size tungsten power[1] and 2-micron molybdenum powder[2] were selected for starting materials as they sintered readily to high densities at 1750°C. The Al_2O_3 and ZrO_2 powders were -325 mesh size. A typical microstructure of a 31 weight percent Mo - 69 weight percent ZrO_2 mixture after sintering is shown in figure 42.

Figure 43 shows the microstructure of a 50 weight percent Mo - 50 weight percent Al_2O_3 following sintering. The sintering cycle used for all compacts, after the cold pressing operation, was to insert the compacts slowly into a hydrogen atmosphere furnace set at 1000°C. Slow insertion at 1000°C prevented the compacts from failing by thermal shock. They were held at this temperature for 30 minutes to "pre-sinter", or increase the strength, the compacts before raising the temperature for final sintering. Final sintering was accomplished by raising the temperature to 1750°C and holding the compacts for 120 minutes at this temperature. This schedule gave usable samples of metal-metal oxide mixtures for machining into heater elements.

Several compositions of ZrO_2 and Mo or W have been tested to determine their resistence at room temperature. For each composition a resistance range was found rather than a single resistance as might be expected. This probably results from inhomogeneities in the microstructure resulting from inadequate mixing or differences in the oxide particle size. The room temperature resistance change with composition is shown in figure 44. The most apparent fact from these curves is the large change in resistance with small alterations in composition. The 50 percent Mo - 50 percent Al_2O_3 mixture had a resistance of about 10 ohms but Al_2O_3 was dropped for ZrO_2, as ZrO_2 melts at a much higher temperature.

Several of the specimens were heated to 1500°C (optical temperature) in a vacuum of 5 to 50 microns. In all cases at 1500°C the resistance dropped to 0.2 to 0.1 ohms from a room temperature value of about 15 ohms. However, after cooling to room temperature, the resistance remained at 0.2 to 0.1 ohms indicating that a permanent change had occurred during the vacuum heating cycle. Figure 45 shows the microstructure of the 31 percent Mo - 69 percent ZrO_2 sample after heating. The change in microstructure is quite apparent by the rounding of the ZrO_2 particles, by the presence of a "phase" within the particles, and by the absence of ZrO_2 in a portion of the Mo. X-ray diffraction data identified ZrO_2 and Mo as the constituents of these areas with no other phases present. Since the time and temperature of heating in vacuum were

less than those for sintering in hydrogen, the change in microstructure must be caused by the vacuum atmosphere. Two possible reactions may have occurred but cannot be positively identified as the cause of the change. First, molybdenum oxidizes to a limited extent in a 5-to 50-micron vacuum and this may have altered the metal-metal oxide interface to the extent shown in figure 45. Secondly, minor impurities in the oxides may cause reactions in vacuum not found in hydrogen, and thus effect the microstructure after vacuum heating. It is possible that the volume of these impuities or impurity compounds is not sufficient to be detected by X-ray techniques.

References

1. T. Vasilos and J. T. Smith, J. Appl. Phys. 35, 1, p. 215 (January 1964).

2. J. T. Smith, J. Appl. Phys. to be published December 1964.

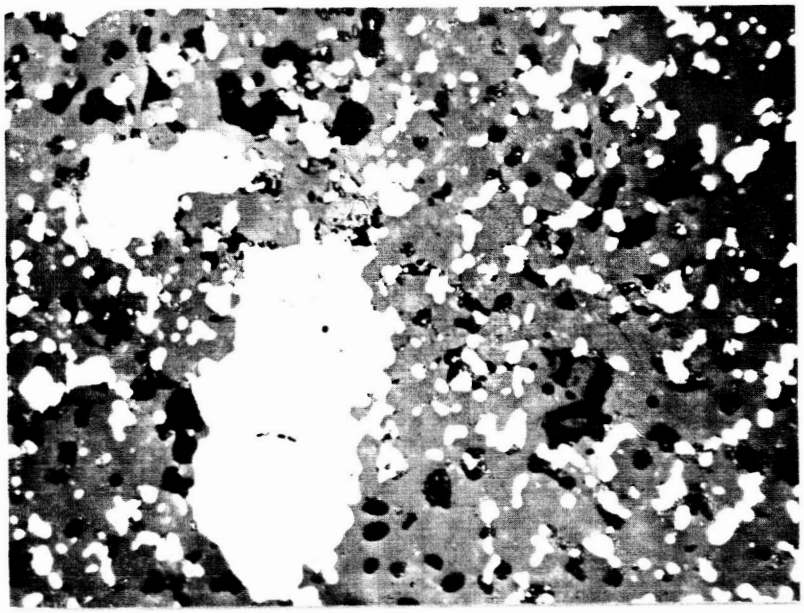

PLATE 3624C 500X

Figure 42 MICROSTRUCTURE 31% Mo, 69% $Zr0_2$ AFTER SINTERING

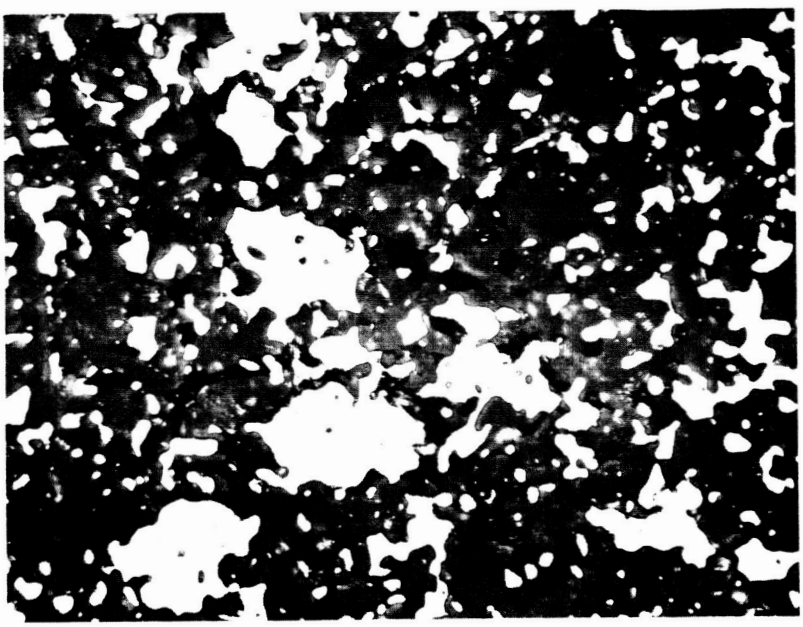

PLATE 3624 500X

64-12315

Figure 43 MICROSTRUCTURE 50% Mo, 50% Al_20_3 AFTER SINTERING

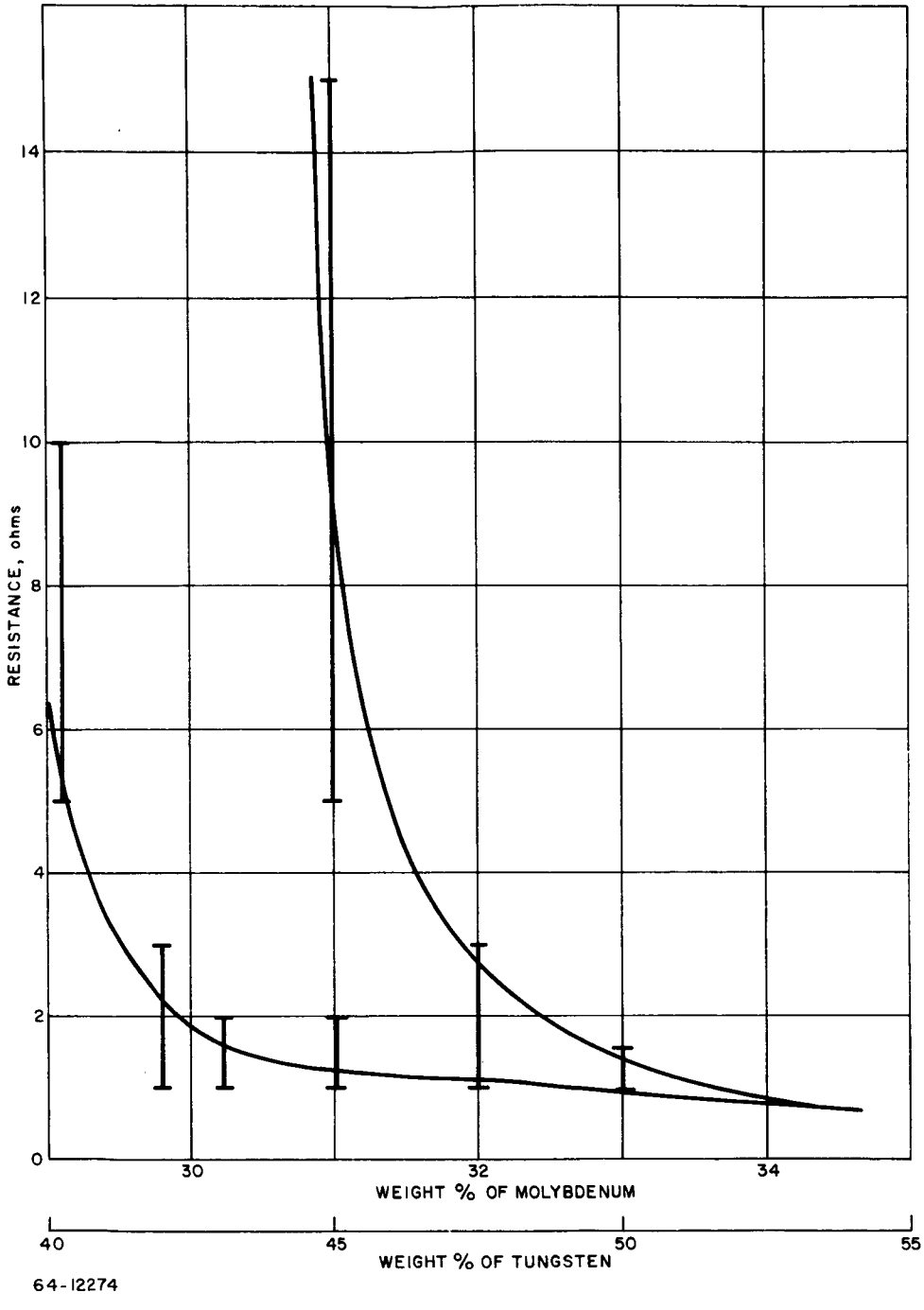

Figure 44 SLUG RESISTANCE VERSUS COMPOSITION

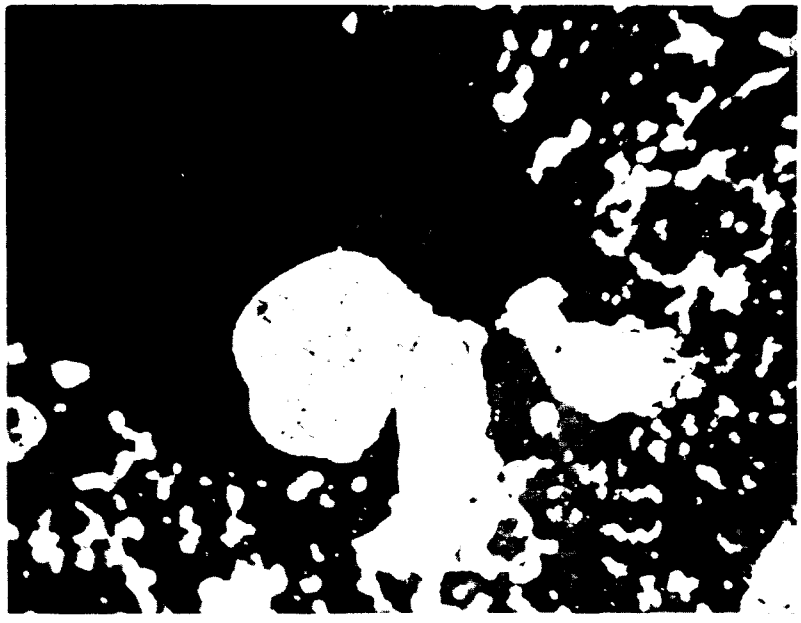

PLATE 3624D 500 X

Figure 45 MICROSTRUCTURE 31% Mo, 69% Z_rO_2 AFTER HEATING

64-12316

DISTRIBUTION

Addressee	No. of Copies
NASA-Lewis Research Center 21000 Brookpark Road Cleveland, Ohio 44135	
Attention: J. H. Childs	1
R. J. Rulis	3
H. Gold	1
R. Cybulski	1
NASA Headquarters FOB - 10B 600 Independence Avenue, Northwest Washington, D. C. 20546	
Attention: RNT/J. Lazar	1
RNT/J. Mullen	1
NASA-Lewis Research Center 21000 Brookpark Road Cleveland, Ohio 44135	
Attention: J. H. DeFord	1
H. R. Hunczak	2
J. Jack	1
N. Musial	1
Reports Control Office	1
Technology Utilization Office	1
Library	1
NASA Scientific and Technical Information Facility Box 5700 Bethesda, Maryland 20014	
Attention: RQT-2448/NASA Representative	6
NASA Marshall Space Flight Center Huntsville, Alabama 35812	
Attention: Library	1
R-RP-DIR/G. Heller/Bldg. 4481	1
R-RP-DIR/Dr. E. Stuhlinger	1
R-RP-T/W. Jones/Bldg. 4488	1
MS-T/Dan Gates/Bldg. 4488	1
NASA-Ames Research Center Moffett Field, California 94035	
Attention: Library	1
DR. G. Goodwin	1

DISTRIBUTION (Cont'd)

Addressee	No. of Copies
NASA Goddard Space Flight Center Bldg. 6 Greenbelt, Maryland 20771 Attention: W. Isley/Code 623	1
Commander Aeronautical Systems Division Wright-Patterson AFB, Ohio 45433 Attention: AFAPL (APIE)/R. Supp AFAPL (APIE)/P. Lindquist	 1 1
Aeronautical Systems Division Wright-Patterson Air Force Base, Ohio 45433 Attention: ASRMPE/F. L. 'Hommendieu	1
Electro-Optical Systems, Inc. 125 North Vinedo Avenue Pasadena, California Attention: Dr. R. Buhler Dr. J. Teem	 1 1
General Electric Company Electric Space Propulsion Projects Evandale, Ohio Attention: Dr. M. L. Bromberg	1
Marquardt Corporation 16555 Saticoy Street Van Nuys, California Attention: R. Page	1
Gianinni Scientific Corporation 3839 South Main Street Santa Ana, California Attention: Adriano Ducati	1
Gianinni Scientific Corporation 3839 South Main Street Santa Ana, California Attention: Dr. Gabriel Gianinni	1

DISTRIBUTION (Cont'd)

Addressee	No. of Copies
Jet Propulsion Laboratory Pasadena, California 91103 Attention: G. Robillard	1
Thrust Systems Company 1641 Monrovia Costa Mesa, California Attention: W. Stoner	1
Ling-Temco-Vought, Inc. Advanced Systems, Astronautic Division Box 6267 Dallas, Texas 75222 Attention: F. T. Esenwein	1
Air Products and Chemicals, Inc. P.O. Box 538 Allentown, Pennsylvania 18101 Attention: R. Barclay	1
Arthur D. Little, Inc. Acorn Park Cambridge, Massachusetts 02140 Attention: A. Fowle	1
Beech Aircraft P.O. Box 631 Boulder, Colorado Attention: J. Bell	1
Garrett Corporation/Air Research 9851 Sepulveda Blvd. Los Angeles, California 90045 Attention: R. Fischer	1
TAPCO 7209 Platt Avenue Cleveland, Ohio 44104 Attention: Dr. P. Lawlor	1

DISTRIBUTION (Concl'd)

Addressee	No. of Copies
NASA-Langley Research Center Langley Station Hampton, Virginia Attention: Mike Ellis, MS 160	1
Jet Propulsion Laboratory California Institute of Technology 4800 Oak Grove Drive Pasadena, California Attention: John W. Stearns, Jr. MS 125-224	1
Dr. J. Lundholm Fairchild Aircraft Washington, D.C.	1
Central Files	1
Research Library (+ 1 reproducible)	25